Soil-Structure Interaction for Integral Bridges and Culverts

Esra Bayoğlu Flener

Department of Civil and Architectural Engineering
Structural Design and Bridge Division
Royal Institute of Technology
SE-100 44 Stockholm, Sweden

TRITA-BKN. Bulletin 74, 2004
ISSN 1103-4270
ISRN KTH/BKN/B--74--SE

Licentiate Thesis

Abstract

A thorough state of the art on the soil-structure-interaction issues of integral bridges and culverts is provided, focusing on the earth pressure behind integral-bridge abutments. The procedure of the Swedish design code for estimating the earth pressure response to integral bridge abutment movement is found to be conservative compared to the one of the British code and to some recent experimental studies.

The influence of soil stiffness and different ways of acquiring this parameter are discussed. Upon comparison of several methods for the determination of the elasticity modulus of soil, it can be concluded that the E_s values of Duncan et al.'s SCI method are much more conservative than the E_t values by Duncan et al.'s hyperbolic equation and Pettersson et al.'s Method 2. Also, there are significant differences between that Method 2 and Lehane et al.'s and Lade et al.'s methods.

The results of the bending moment calculations done on three culverts with different height-to-span ratios suggest that live-load moments are very sensitive to the stiffness of the backfill soil. The bending moments due to live loads are also sensitive to cover depths. For low covers, the moments are much more sensitive to changes in cover depth. This demonstrates how and when arching effects actually take place. The moment calculations for a typical slab-frame bridge reveal that the moments at the abutment front are reduced significantly as the soil stiffness changes from very low to high. The effect of change of the parameter in the passive soil-response formula of the Swedish bridge design code on moments is also significant.

Keywords: Soil-structure interaction, integral bridges, culverts, elasticity modulus of soil, lateral earth pressure.

Acknowledgements

I hereby express my gratitude to my advisor, Prof. Håkan Sundquist, for giving me the opportunity to do this research at KTH, as well as for his expertise, support, and understanding throughout the development of this thesis. My research was financed by study grants supported from funds by ViaCon AB and Vägverket (the Swedish Road Administration), which I hereby gratefully acknowledge.

I very much appreciated the perceptive comments made on a draft of part of this thesis and a report of mine by Dr Raid Karoumi and Lars Pettersson (Skanska AB).

Extra thanks go to Gerard James and Abraham Getachew for supporting me against the numerous software packages that incessantly fought with me during the elaboration of this thesis.

My infinite thanks for many common laughs and tears, meals and drinks, walks and cross-country ski trips go to my dear friends Lütfi Ay (now back at Skanska AB) and Michael Quilligan (now at Mott MacDonald, London, UK), as well as Oxana Samoteeva and Samer Sawalha (Department of Energy Technology).

Last, but not least, I thank my husband Pierre, for his endless support and patience, and our daughter Deniz Isabelle, for all the sunshine in our life.

Esra Bayoğlu Flener

Stockholm, February 2004

Contents

Abstract i

Acknowledgements iii

List of Symbols ix

List of Figures xv

List of Tables xix

1 Introduction 1

1.1 Background 1

1.2 Aims and Scope 2

1.3 Structure of the Thesis 2

2 Literature Review 5

2.1 Soil-Structure-Interaction for Integral Bridges 5

2.1.1 Types of Integral Bridge Abutments 6

2.1.2 Advantages of Integral Bridges 8

2.1.3 Problems and Limitations Concerning Integral Bridges 9

2.1.4 Integral Bridge Applications in Sweden 10

2.1.5 Integral Bridge Applications Around the World 10

2.1.6 Geotechnical Aspects 13

2.1.7 Overview of the Research on Integral Bridges 20

2.1.8 General Design Considerations for Integral Bridges 25

2.1.9 Earth Pressure Distribution in the Design of Integral Bridges . 27

2.2 Soil-Structure-Interaction for Culverts 37
2.2.1 Types of Culverts 37
2.2.2 Overview on the Research on Buried Structures 38
2.2.3 Design of Culverts 47
2.3 Analysis of Soil-Structure Interaction 50
2.3.1 Earth Pressure Theory 51
2.3.2 Limited Analysis 51
2.3.3 Characteristics 51
2.3.4 Limit Equilibrium 51
2.3.5 Elasticity Theory 51
2.3.6 The Finite Element Method (FEM) 52
2.3.7 The Boundary Element Method (BEM) 52
2.3.8 Combined FEM and BEM 52
2.4 Soil Modelling 53

3 Stiffness Characteristics for Soil-Structure Interaction 55

3.1 Definitions 55
3.2 Methods for the Determination of the Elasticity Modulus 57
3.2.1 History 57
3.2.2 Hyperbolic Stress-Strain Model by Duncan et al. 59
3.2.3 Secant Modulus for the SCI Method by Duncan et al. 61
3.2.4 Secant Modulus by Pettersson et al. (Method 1) 62
3.2.5 Tangent Modulus by Pettersson et al. (Method 2) 62
3.2.6 Secant Modulus According to Lehane et al. (Method 3) 64
3.2.7 Elasticity Modulus According to Lade et al. (Method 4) . . . 65
3.3 Comparisons and Discussion of Methods 67
3.3.1 Comparison of Duncan's E_s Curves with Pettersson et al.'s Method 1 68
3.3.2 Comparison of Methods 1 and 2 of Pettersson et al. 68
3.3.3 Comparison of Pettersson et al.'s Method 2, Lehane et al.'s Method, and Lade et al.'s Method 70

4 The Effect of Soil Stiffness on the Design of Culverts and Integral Bridges **73**

4.1 Maximum Bending Moment for Culverts 73

4.1.1 The SCI Method 74

4.1.2 Geometry and Material Parameters 74

4.1.3 Calculations 74

4.1.4 Results and Comparisons 75

4.2 Maximum Bending Moment for Slab-Frame Bridges 81

4.2.1 Geometry and Parameters 81

4.2.2 Calculations 83

4.2.3 Results and Comparisons 87

5 Conclusions **91**

5.1 Conclusions from the Literature Review 91

5.2 Conclusions about the Stiffness Characteristics of Soil 92

5.3 Conclusions about the Effect of Soil Stiffness on the Design of Culverts and Integral Bridges 92

5.3.1 Soil Stiffness in the Design of Culverts 92

5.3.2 Soil Stiffness in the Design of Integral Bridges 93

5.4 Further Research 93

Bibliography **95**

A Evaluation of the Secant Modulus - Tangent Modulus Relationship **103**

A.1 Definitions 103

A.2 Derivation of the Relation E_t/E_s 103

A.3 Further Simplifications 104

B Passive Earth Pressure Response Proposal – Simple Elastic Approach **105**

B.1 Assumptions 105

B.2 Equations Used 105

B.3 Calculation Steps 106
B.4 Numerical Example 107

List of symbols

β stress exponent (by Duncan), page 64

β_f factor depending on the W/L_f ratio, page 83

β_r ratio of wall deflection to wall height, page 27

ΔM moment due to live load in metal box culverts, page 50

ΔP horizontal soil reaction pressure on piles and walls, page 27

Δx horizontal deflection of the pipe, page 40

δ horizontal displacement at the top of the abutment wall, page 15

δ_w coefficient of wall friction, page 18

δ_{100} deformation due to triangular soil reaction pressure where $\Delta P = 100$ and reaction force, page 86

$\delta_{\Delta P}$ deformation due to triangular soil reaction pressure in slab-frame bridge calculations, page 86

δ_{frame} final deformation of the frame in slab-frame bridge calculations, page 85

δ_{H_b} deformation due to the brake force in slab-frame bridge calculations, page 85

$\delta_{R_{100}}$ deformation due to support reaction force at the top of the abutment wall, page 86

γ shear strain in the backfill soil, page 15

γ_c unit weight of concrete, page 82

γ_r factor for characterizing the rotational deformation property of foundations, page 83

γ_s unit weight of soil, page 16

λ dimensionless material constant for elasticity modulus , page 67

μ_1 arching factor, page 41

ν Poisson's ratio, page 23

ϕ angle of internal friction, page 16

ψ slope of the earth pressure variation, page 31

ρ_d dry density of soil, page 62

ρ_w density of water, page 62

σ_0 confining pressure, page 57

σ_1 vertical stress in triaxial test, normal pressure, page 58

σ_3 lateral stress, chamber pressure, page 58

σ_v effective overburden pressure before loading, page 57

θ rotation of the abutment wall about its foundation, page 32

ε normal strain, page 58

B bulk modulus of soil, page 56

C stiffness factor used for reaction pressure calculation, page 27

c soil cohesion, page 16

C_1 stiffness factor used for reaction pressure calculation, page 27

C_c coefficient of curvature, page 57

C_u uniformity coefficient, page 57

d deformation at the foundation surface, page 53

D_1 deflection lag factor, page 40

D_p diameter of the pipe, page 40

D_s depth below approach slab, page 16

d_{10} effective size of soil material, page 57

E modulus of elasticity, Young's modulus , page 55

e void ratio, page 23

E' the modulus of soil reaction in the Iowa deflection formula, page 40

E_c elasticity modulus of concrete, page 82

E_i initial tangent modulus, page 56

E_k settlement modulus given by geotechnical investigations, page 83

E_p modulus of elasticity of the pipe material, page 40

e_p modulus of passive resistance, page 40

E_s secant modulus of elasticity, page 23

E_t tangent modulus of elasticity, page 56

E_{st} elasticity modulus of the culvert, page 49

$F(e)$ normalizing function for shear stiffness, page 23

G shear modulus, page 23

G_s specific gravity of soil, page 62

H rise / distance between top of the culvert and level of the largest span, page 41

H_a height of abutment, page 15

H_b horizontal brake force for slab-frame bridge calculations, page 85

h_c depth of soil cover over the culvert, page 40

H_e height of the end-screen, page 27

I_1 first stress invariant, page 65

I_D relative density, page 64

I_p moment of inertia of the pipe, page 40

I_{st} moment of inertia of the culvert, page 49

J_2 second deviatoric stress, page 65

K lateral earth pressure coefficient, page 13

k factor depending on stiffness and Poisson's ratio/modulus of subgrade reaction, page 44

K^* uniform earth pressure coefficient , page 24

K^*_{alt} uniform earth pressure coefficient, page 31

K_0 at rest earth pressure coefficient, page 16

K_a active earth pressure coefficient, page 28

K_B bedding constant, page 40

K_p passive earth pressure coefficient, page 16

k_{θ_k} characteristic bending deformation modulus of the soil depending on foundation size, page 83

K_{M1} moment coefficient for culvert (SCI Method), page 49

K_{M2} moment coefficient for culvert (SCI Method), page 49

K_{M3} moment coefficient for culvert (SCI Method), page 49

K_{p1} ring compression coefficient for backfill, page 41

K_{p2} ring compression coefficient for cover, page 41

K_{p3} ring compression coefficient for live load, page 48

L length of bridge, page 82

L_f length of the foundation, page 83

LL live load, page 48

M total bending moment due to backfill and live load, page 49

m experimentally obtained modulus number, page 58

M_1 maximum bending moment for culverts at cover-depth=0, page 49

M_s constrained modulus for soil, page 44

M_T sum of the haunch and crown moments due to backfill and cover in metal box culverts, page 50

M_{LL} maximum bending moment for culverts due to traffic load (SCI), page 75

M_{soil} maximum bending moment for culverts due to soil load (SCI), page 75

N dimensionless material constant for elasticity modulus, page 65

n experimentally obtained stress exponent (by Janbu), page 58

N_f flexibility number of the culvert, page 49

P uniform ring compression pressure, page 40

p pressure at the soil surface, page 53

p' mean effective stress, page 21

P_0 earth pressure at rest, page 27

P_p maximum passive pressure, page 16

p_t uniformly distributed load due to traffic, page 82

p_a atmospheric pressure, page 23

q equivalent live load, page 40

q_o uniformly distributed load due to own weight of the bridge, page 82

q_p uniformly distributed load due to pavement of the bridge, page 82

r mean radius of the pipe, page 40

R_B moment reduction factor for culverts (SCI Method), page 49

R_f failure ratio, page 60

R_L moment reduction factor for culverts (SCI Method), page 49

R_T top radius of the crown, page 41

R_{100} support reaction force at both ends of the abutment wall, page 86

RP degree of compaction, page 56

S diameter/span of the culvert, page 41

S_{ar} arching coefficient (reduction factor for surcharge), page 64

T ring compression load, maximum thrust per m length of the pipe, page 40

t slab thickness of the slab-frame bridge, page 82

T_c coefficient of thermal expansion for concrete, page 82

W width of the foundation, page 83

W_c vertical load of soil per unit length of the pipe, page 40

List of Figures

2.1 BA 42 classification of integral bridge abutments (redrawn from [6]): (a)(b) frame abutments, (c) embedded abutment, (d) bank pad abutment, (e)(f) end screen abutments. Backfill soil is shown as hatched in the figures. 7

2.2 A typical integral abutment reinforcement detail 11

2.3 A typical link slab application together with an end-screen 11

2.4 Soil behaviour to shear strain relationship (after Ishihara [44]) 15

2.5 Shear strain due to abutment rotation (after Card et al. [19]) 16

2.6 Prediction of the coefficient of earth pressures (K) for different wall rotations (redrawn from the US Department of Navy 1986 "Soil Mechanics Foundations and Earth Structures" as reported by Thomson [89]) 19

2.7 Design earth pressures on slab frame bridges (according to the Swedish Bridge Code Bro 2002) 28

2.8 Design earth pressure distribution for frame abutment (according to BA 42/96) 29

2.9 Design earth pressure distributions for full height embedded wall abutments (from BA 42/96) 29

2.10 Design earth pressure distributions behind abutments (from Sandford [74]) 31

2.11 Comparison of design earth pressure distributions behind abutments from different sources 34

2.12 A presentation of the wall rotation about its base and the soil pressure distribution behind the integral bridge abutments 36

2.13 Some types of culvert profiles (after Pettersson et al. [72]). H = rise, h_c = cover height, R_T = radius of the crown and S = span 39

2.14 Value names used for buried pipe culverts. H is the rise, h_c is the cover height, $R_T$is the radius of the crown, and S is the span of the culvert 41

3.1 Hyperbolic representation of stress-strain relationship (from [103]) . . 58

3.2 Approximate secant modulus for various types of backfill soil (to be used in the SCI method), redrawn from Duncan [27] 61

3.3 Secant modulus versus dry density of backfill soil, after Lehane et al. [56] 66

3.4 Comparison of Duncan's E_s curves with the formulation in Pettersson et al.'s Method 1. Only the curves for GW, GP, SW, and SP type of soils were compared 68

3.5 Elasticity modulus versus depth of soil cover. Comparison of Methods 1 and 2 of Pettersson et al. (Note that Method 1 calculates the secant modulus and Method 2 calculates the tangent modulus.) . . . 69

3.6 Elasticity modulus versus depth of soil. Comparison of Method 2 of Pettersson et al., Lehane et al.'s Method (Method 3) and Lade et al.'s Method (Method 4) 70

4.1 SCI design bending moments versus relative compaction for a depth of cover of 0.5 m for 3 different culverts. (Unit weights are calculated by Equation 4.1 with an optimum unit weight of 21 kN/m^3.) 76

4.2 SCI design bending moments versus depth of cover for culvert 1 . . . 78

4.3 SCI design bending moments versus depth of cover for culvert 2 . . . 79

4.4 SCI design bending moments versus depth of cover for culvert 3 . . . 80

4.5 A typical slab-frame bridge 81

4.6 Angle changes and value names for the moments and forces in the frame for the analysis of a slab-frame bridge: (i) representation of the loads, (ii) deformations under loading with no lateral freedom of the joints, (iii) deformations due to the lateral movement and foundation rotations, and (iv) section moments 84

4.7 Braking load and corresponding soil reaction forces for the analysis of a slab-frame bridge according to braking 86

4.8 Change in moments with change in soil stiffness, which is expressed as the settlement modulus E_k 89

4.9 Change in moments with change in the parameter C in the ΔP formula 90

B.1 Calculation of the earth pressure distribution behind the abutment due to wall rotation, for a 3 m wide earth fill 108

B.2 Calculation of the earth pressure distribution behind the abutment due to wall translation, for a 3 m wide earth fill 108

B.3 Lateral earth pressure response to rotation of the wall; each curve is for a different backfill width 109

B.4 Total lateral earth pressure distributions due to rotation of the wall . 109

List of Tables

2.1 Summary of abutment rotations and recorded earth pressures (after Card et al. [19]) 17

2.2 Influence of shear strain on soil behavior and lateral earth pressure coefficient values (after Card and Carder 1993) 17

2.3 Passive earth pressure coefficients (K_p) depending on abutment inclinations and internal friction angles 18

2.4 Lateral earth pressure coefficients of different material (from Bro 2002) 28

2.5 Lateral earth pressure coefficients to be used in the design of integral bridges (recommendations by Springman et al. [79]) 32

2.6 Parameters used in the numerical example 33

2.7 Experimental K values obtained for different wall deflections (rotation about the base) 35

2.8 Equations for the maximum thrust (T) according to different sources (after Vaslestad [92]) 41

3.1 Particle size classification of soils 56

3.2 Classification according to the Unified Soil Classification System . . . 57

3.3 Some typical values for modulus of elasticity from different sources . . 59

3.4 Recommended hyperbolic parameters by Duncan et al. [31] 64

3.5 Value range of the parameters used in Equation 3.23 (after Lade et al. [54]) 67

3.6 Soil parameters chosen for comparison of the methods for calculating elasticity modulus 67

4.1 Geometry and material parameters used for moment calculations of steel culverts (using the SCI method) 75

4.2 Comparison of the results of the moment calculations according to the SCI method 77

4.3 Material parameters, geometry and loading conditions used for the slab-frame bridge problem 82

4.4 Settlement modulus values used in calculations for slab-frame bridges 83

4.5 Summary of the calculations and moments at the abutment front for medium and high stiffness levels 87

4.6 Summary of the calculations and moments at the abutment front for low and very low stiffness levels 88

B.1 Parameters used in the numerical example 107

Chapter 1

Introduction

1.1 Background

Soil-structure interaction has been of interest for many decades. It encompasses the general phenomena involved in the behaviour of structures while interacting with the soil medium in response to the loading imposed on the system. These phenomena include the indeterminate effects of the interaction between a structure and the soil. This indeterminacy is the result of the distribution and magnitude of the earth pressure varying with the amount and type of deflection of the structure. The pressure distribution on the structure depends on many combined factors that make the phenomena quite complicated. The major difficulty is that soil has variable properties; in other words, soil is neither homogeneous nor elastic.

With the aid of computers, it is nowadays possible to achieve very accurate results by using mathematical methods, which are based on soil information obtained by sophisticated sampling and analytical techniques. But their accuracy is limited by the initial assumptions and the mathematical representation of the material properties used in the model.

With the increasing size and usage of buried structures, the soil-structure-interaction topic gains more and more importance. Among the structures that are most subjected to soil-structure-interaction problems are buried structures such as metal and concrete culverts. Especially metal culvert bridges, due to their flexible nature, go through interaction during construction and in service. As the popularity and demand for such structures increase, the need for more accurate analysis and design will naturally increase. Increasing span lengths make it even more challenging for engineers.

Another type of structure that needs attention is the integral bridge.[1] Due to their rapid construction, low costs, and high durability with minimal maintenance, integral bridges are more and more built instead of bridges with expansion joints. Their popularity increases the need for larger spans and total lengths, which may increase

[1]For a definition, see Section 2.1.

soil-structure-interaction problems such as the lateral movement of abutments towards and away from the backfill soil. The amount of passive pressure generated behind the abutment wall is the main concern, as well as the effects of the iterative wall displacement due to thermal expansion and contraction of the bridge slab.

1.2 Aims and Scope

The first aim of this thesis is to provide a thorough literature review of the state of the art on the soil-structure interaction of integral bridges and culverts. Secondly, the influence of soil parameters on the design of such structures, as well as the historical development and different ways of acquiring these parameters are demonstrated. The last objective is to identify, stress, and compare soil-structure-interaction issues so that necessary improvements can be done and topics in need of further research can be identified.

The literature review aims to concentrate on the problems occurring at these kinds of structures, on the different approaches to solutions of these problems, on the different design methods, and on the gaps in these design methods. The literature review will be done from a geotechnical point of view. More specifically, for integral abutment bridges, the movement of the bridge abutment and the corresponding soil response such as the likely soil behaviour and the amount and distribution of lateral earth pressures behind abutments will be investigated. For culvert structures, the focus will be on the pressure generated around long-span culverts, on choosing correct soil parameters, and on historical development comparisons of the design methods for these types of structures.

The influence of soil parameters on integral bridge design and the lateral response of soil behind integral bridge abutments are aimed to be demonstrated by means of widely accepted methods, such as the national highway codes of different countries. The results are then compared with the current state of the art in Sweden.

The objective of the above-mentioned studies is to gain more experience and insight about soil-structure-interaction issues of integral bridges and culverts, address the unknowns, answer some questions, and find ways to improve the current design methods.

1.3 Structure of the Thesis

Chapter 2 is the literature review and gives the state of the art on integral bridges and culverts. The main focus is on soil-structure-interaction issues.

Section 2.1 gives a literature survey on integral bridges, giving first a brief information about the types of integral bridge abutments (Section 2.1.1). Advantages and problems and limitations are discussed in Sections 2.1.2 and 2.1.3. A brief summary of integral bridge applications around the world is given in Sections 2.1.4 and 2.1.5.

After highlighting some geotechnical aspects of the soil-structure interaction of integral bridges in Section 2.1.6, an overview on the research done in general is given in Section 2.1.7. In Sections 2.1.8 and 2.1.9, general design issues, and, more specifically, the design of abutments are discussed and several design proposals for the earth pressure distribution behind abutments are compared by means of a numerical example.

Section 2.2 gives a literature survey on culverts. Section 2.2.1 gives general information and identifies the types of culverts. Section 2.2.2 gives an overview on the research including geotechnical issues. Section 2.2.3 summarizes several design methods for different types of culverts.

Section 2.3 is a summary of the current methods of analysis and design of soil-structure interaction.

Section 2.4 very briefly discusses soil modeling in the analysis of soil-structure-interaction problems.

Chapter 3 focuses on the stiffness characteristics of soil for interaction problems. Especially the elasticity modulus of soil is described in this chapter. Basic descriptions are given in Section 3.1. Section 3.2 gives a brief history of how to formulate the elasticity modulus as well as a presentation of the current methods for calculating the elasticity modulus to be used in the design of culverts and integral bridges. Finally, in Section 3.3, comparisons and a discussion of the methods are done by demonstrating the results of some numerical examples.

Chapter 4 aims to demonstrate the effects of soil stiffness in the design of culverts and integral bridges. Section 4.1 uses a widely accepted design method for culverts and calculates the most sensitive design bending moment to soil parameters. The results are discussed and comparisons with different soil parameters are done. Section 4.2 takes a slab-frame bridge example and structurally analyzes it. The relationship between soil stiffness (in terms of the level of compaction) and the bending moments at the abutment front is shown.

Chapter 5 concludes this thesis. Section 5.1 gives conclusions from the literature review, while Section 5.2 draws conclusions from the results of the comparisons of the methods for calculating the elasticity modulus of soil. Conclusions about the work done on the effects of soil stiffness on integral-bridge and culvert design are given in Section 5.3. Finally, in Section 5.4, further research proposals are given.

Chapter 2

Literature Review

The goal of this chapter is to give a compilation of current accumulated knowledge (state of the art) in different phases and applications of integral bridges and culverts. It also aims at the assessment of uncertainties as well as the identification of the problems in need of further research.

In the second section a literature survey is given on integral bridges that has been diagnosed from a geotechnical point of view. the third section is about the soil-structure-interaction of buried structures, especially culverts. Section four is a summary of current methods of analysis and design of soil-structure interaction. Section five discusses soil modelling since it is considered the most essential part of dealing with the soil-structure interaction problem.

2.1 Soil-Structure-Interaction for Integral Bridges

The term 'integral bridge' is generally used for single or multiple span, continuous, jointless (without deck joints and slide bearings between spans and abutments) bridge structures. The names 'jointless bridges', 'continuous bridges' and 'rigid frame bridges' are also used in the literature. The term continuous usually implies multi-span continuity and the term integral implies deck-abutment integrity.

The backfill soil behind the abutment of such bridges is of a carefully compacted, usually industrially prepared, high quality cohesionless type of soil whose parameters are easily obtained. So whenever backfill soil is mentioned in this thesis it will refer to this kind of soil.

Handling the soil-structure-interaction problems in integral bridges seems to have always been problematic. Integral bridges have complex and uncertain behavior. Secondary forces due to temperature effects, creep and shrinkage are considered to be the main factors that lead to some uncertainties. From the geotechnical point of view, the unknowns lie in the behavior of the abutment and the soil under these effects. The magnitude and distribution of soil pressure on abutment walls and movements induced have to be better understood.

In sections 2.1.1 to 2.1.5 general information such as types, advantages, problems and applications is presented. In section 2.1.6 geotechnical aspects of lateral soil-structure interaction of integral bridges are introduced. Section 2.1.7 gives a summary of research efforts on the topic. Finally section 2.1.8 gives the current state of design in different countries and design proposals from researchers.

2.1.1 Types of Integral Bridge Abutments

The types of abutments according to Springman [79] are:

- full-height sheet pile walls,
- full-height embedded walls,
- full-height concrete walls with spread base,
- full-height concrete walls on piled foundation,
- shallow bank-seat (or perched) abutments on piles, and
- shallow bank-seat (or perched) abutments on spread footings.

The British Design Manual BA 42 [6] divides integral bridge abutments into the following categories (also see Figure 2.1):

- frame abutments
- bank pad abutments
- embedded abutments
- end screen abutments

Taylor [87] suggests that full height frame and embedded wall abutments are suitable for short single span bridges where piled abutments have wider applicability. Spread footings are suitable on reinforced soil or for very stiff foundations.

Integral stub abutments with piles are more flexible and total stresses are less than bridges resting on spread footings (see Thippeswamy et al. [88]).

In practice shallow bank seat piled abutments seem to be preferred to the full height abutments for limiting the passive pressures and amount of backfill.

It should be noted that the terms "bank-seat", "bank-pad", and "stub" are used for the same category of integral bridge abutments throughout the thesis.

In general the integral bridge abutment types (a) frame abutments, (c) embedded/pile abutments and (e) end-screen abutments are more common compared to

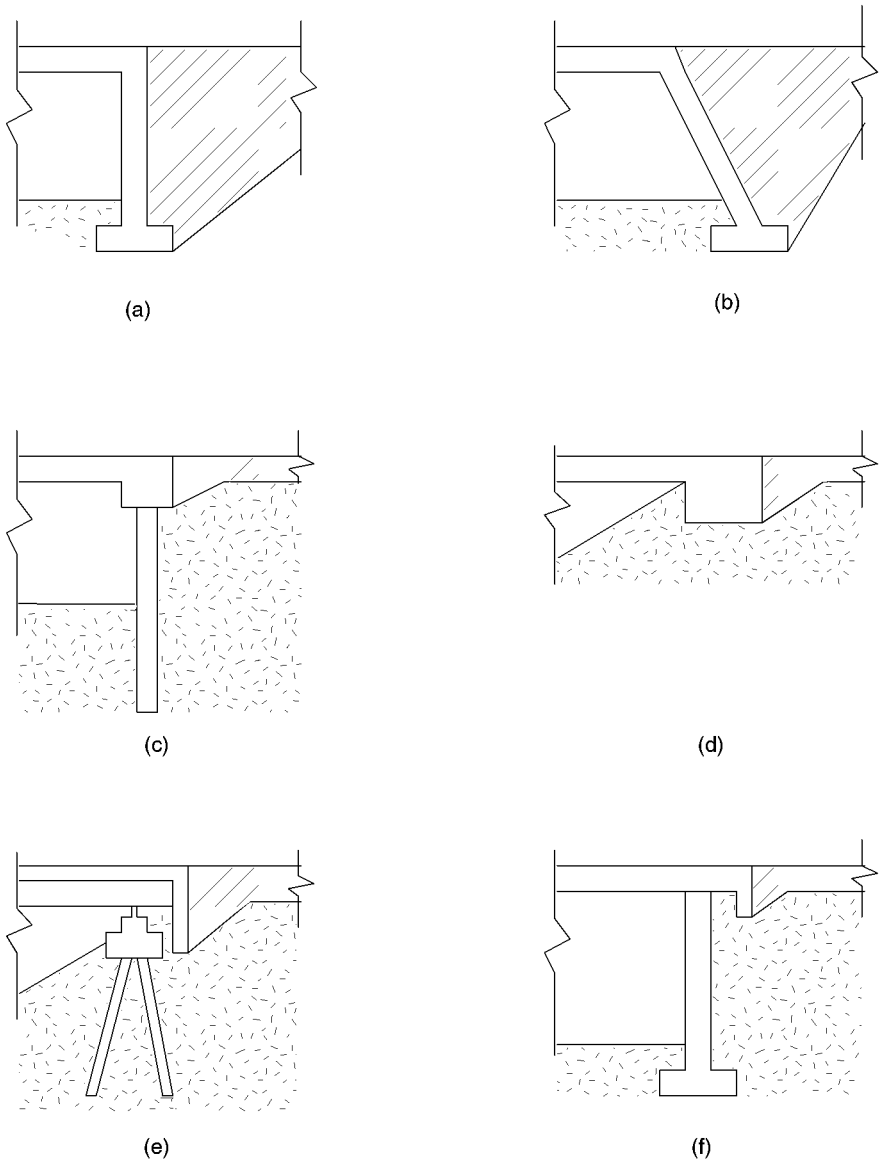

Figure 2.1: BA 42 classification of integral bridge abutments (redrawn from [6]): (a)(b) frame abutments, (c) embedded abutment, (d) bank pad abutment, (e)(f) end screen abutments. Backfill soil is shown as hatched in the figures.

the others. In the scope of this thesis these three types of abutments, mostly the frame type integral bridge abutment, will be focused upon.

Approach slabs are commonly used in integral bridges in order to minimize settlement at the vicinity of the abutments. "Run-on slabs" and "approach panel" are also frequently used terms in literature.

2.1.2 Advantages of Integral Bridges

Integral bridges are getting increasingly popular as a result of efforts to avoid problems occurring at bridges with movement joints and bearings. Since it was realized that the expansion joints had a tendency to lock up (usually because of penetration of water into these joints and the damaging effects of de-icing chemicals, Xanthakos [104]) and could not operate well and the maintaining and repair costs were very high.

The advantages of integral bridges can be summarized as follows:

- They are, most of the time, more economical to build. The initial cost of construction is less than for bridges with joints. Future modifications (e.g., widening) are also more economical [17].
- They have increased durability since they do not have deck joints nor end-bearings. In this way they perform more effectively and remain in service with less maintenance and repair need. The problems and high maintenance costs due to immobilization and corrosion of the movable joints are reduced by the use of continuous structures [17, 19, 79].
- They are capable of sustaining high longitudinal compression without distress [17].
- They can be constructed rapidly [17].
- The riding quality is improved and vehicle noise is reduced (as the joints are eliminated and the road surface is smooth) [79].
- Impact loads are reduced and snowplow damage is less [17].
- They have structural continuity for live load resistance and adequate response to earthquakes (depending on structure type and connection details) [17, 79].
- Integral bridges with stub type piled abutments have a simpler design. Furthermore, the abutment foundations are designed for vertical loads only, they need not be designed to resist horizontal loads since the abutment is supported by the bridge deck towards horizontal loads coming from the earth [17, 19].
- They have a better overall structural performance especially under seismic loads compared to bridges with joints [36].

Hambly [40] concludes that damage can be acceptable to some level and dealing with problems coming from integral bridges can be less expensive and preferred to complex solutions of bridges of other types.

2.1.3 Problems and Limitations Concerning Integral Bridges

- The cyclic movement of the integral bridge abutment due to deck expansion and contraction with seasonal and daily temperature changes can lead to the compaction of the backfill soil, causing a further increase in the passive pressures behind the abutment.
- Using an uncompacted backfill layer behind the abutment to reduce the passive pressures however has the undesirable effect of creating settlement at the backfill [89].
- Settlement at the backfill can also occur under vertical loads and due to bridge shortening, both of which eventually lead to a support loss for the approach slab, and eventually cause cracking or failure of the approach slab [4, 73].
- Separation of the approach slab from the abutment may occur due to the reasons given above [4, 73].
- Traditionally, good compaction is needed to avoid settlement problems in the backfill, and therefore in the carriageway. In the construction of integral abutment bridges, good compaction becomes a drawback since it increases the risk of high passive pressure development behind the abutment [20]
- Drainage problems may occur close to the abutment [73].
- Water can undermine the abutments [4].
- Cracks may develop in wing walls due to rotation and contraction of the superstructure [4, 73].
- Cracking in the abutment around girders is also a problem.
- Transverse cracking of decks on the inside of the abutment diaphragm is another problem which may be encountered [73].
- Sliding of the foundation may result in yielding in the soil, which then may lead to excessive settlements or ground instability [19].
- Abutment piles can be subjected to high bending stresses due to expansion and contraction of the bridge deck [17] and the thermal movements can cause a reduction in the vertical load capacity of the piles [4, 39, 80].
- Skewed integral bridges may rotate with repeated increase and decrease of earth pressures behind the walls [4].

- Regarding passive pressure effects, the length of integral bridges is limited [4, 15, 17].
- Integral abutments should also not be used for extreme skews (>30 degrees) [17].
- Integral abutments are suitable if the lateral movement of each abutment is expected to be less than 51 mm [52].
- Subsoil stability is essential to avoid vertical abutment settlements. They cannot be applied on weak embankments and subsoil [4, 17].

2.1.4 Integral Bridge Applications in Sweden

In Sweden, the integral reinforced concrete slab frame bridge (shown in Figure 2.1(a)) has been very frequent for over 70 years. It has been one of the most common bridge types with 8000 out of 14000 of Swedish Road Administration owned bridges. Bridges with integrated breast walls (shown in Figure 2.1(e and f)) are also commonly used for medium lengths up to 80 m for reinforced concrete and to 60 m for composite bridges (see Sundquist et al. [82]).

A reinforced concrete frame bridge of 150 m length with the abutment walls hinged at the top and bottom, and another one of 110 m hinged at the bottom of the abutment were mentioned by Broms et al. ([12, 13]). Some examples of integral bridges in Sweden are presented by Hambly [40] such as composite bridges in Borlänge with vertical screen walls (breast walls) at the abutments, and a 70 m multi-span concrete integral bridge in Leksand.

A typical integral abutment reinforcement detail can be seen in Figure 2.2.

In Sweden, approach slabs are seldom used. Link slabs are more common. Link slabs are buried under the backfill soil to some level and linked to the end screen (see Figure 2.3).

According to Vägverket [95], in Sweden, the recommended maximum bridge length for steel bridges is 40 m to 60 m depending on average low temperatures. For concrete bridges this limit is 60 m to 90 m.

According to a damage assessment made on 54–80 m long existing bridges with end screens, 90 % of the bridges have been found to have cracks and other damages near the end screen. 52 % of the bridges have cracks in the bridge deck (see Enquist [34]).

2.1.5 Integral Bridge Applications Around the World

The first applications of integral bridges date to Roman times [16]. From then until the mid-20th century they were constructed as arch bridges. After the mid-20th century, however, concrete rigid frame bridges became popular. In parallel to

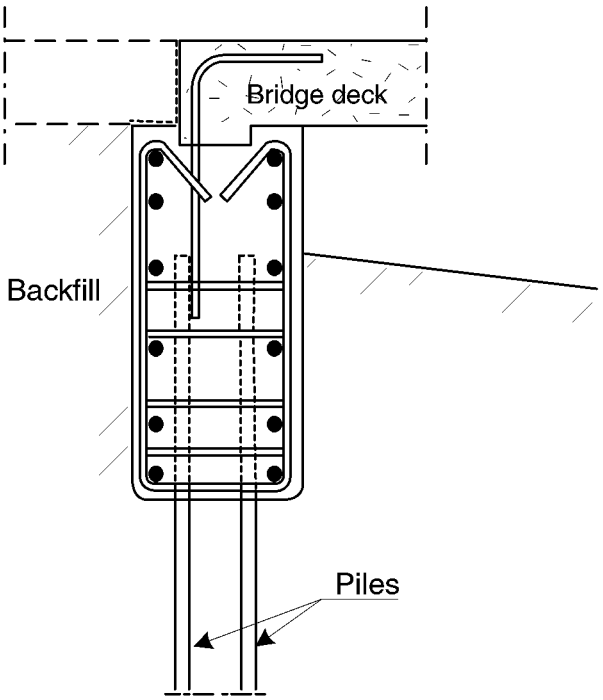

Figure 2.2: A typical integral abutment reinforcement detail

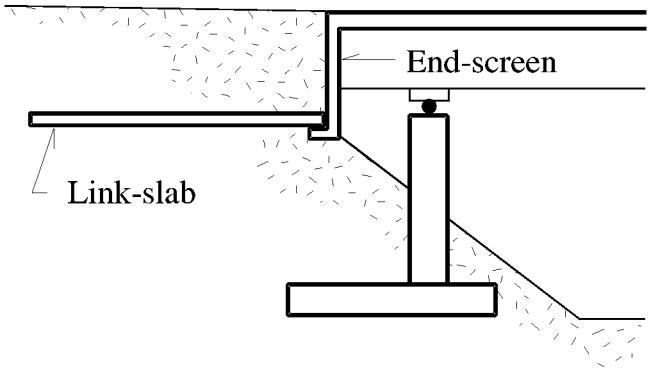

Figure 2.3: A typical link slab application together with an end-screen

rigid frame bridges, multiple span continuous slab, beam or girder bridges were also constructed. Apart from the conventional integral bridge with wall abutments, stub type abutments on a strip of flexible piles started being used.

Integral bridges have been widely used in North America and Europe. According to Card and Carder [19] the first examples of integral bridges were built in North America (For example, the ones built in Ontario, Canada) in the early 1930s and have been widely used from then on. In the last 25 years, applications with longer spans increased due to good performance of their predecessors. Bridges having lengths up to 200 m and 100 m, in concrete and steel respectively, are currently being built (see Card et al. [19] and Xanthakos [104]).

In the USA there are significant variations in the design criteria and limitations among various state highway agencies. Various details of integral bridge abutments in the US can be seen in Burke [15].

Russel and Gerken [73] report that 32 states in the USA use integral bridges with pre-stressed girders.

According to Hambly [40], integral bridges are commonly built on piles and have approach slabs at the abutment/pavement interface. He states that bridges with length up to 220 m and 130 m, in concrete and steel respectively, are built and the maximum allowed movement was 50 mm.

The allowed maximum length of integral bridges is quite variable. According to Russel and Gerken [73], in the USA, the maximum allowable length for composite integral bridges varies between 60 and 150 m, for pre-stressed concrete superstructures the maximum length changes from 60 to 240 m, and for cast-in-place reinforced concrete bridges it changes between 45 and 240 m. As of 1983 the length limitations for non-skewed integral abutment bridges are 45–120 m for steel, 45–240 m for concrete and 60–240 m for pre-stressed concrete bridges (see Wolde-Tinsae et al. [101]).

For many of the states 90 m seems to be the upper limit for the bridge length (see Kukreti et al. [52]).

The upper limit for the skew angle changes between 10 and 30 degrees in the USA (see Russel et al. [73]).

According to Taylor [87], in the UK, bridges are designed for 120 years life time, whereas in the USA this is shorter, namely 50 years. In the USA, full height wall abutments are no longer preferred. Mostly stub abutments on piles are used. Steel H-piles are the simplest and most successful among the types of piles. But reinforced concrete piles are used in the seismic design in California. Run-on slabs are abandoned in the UK, whereas they are still very popular in the USA.

In the UK, integral bridge applications are reported to be limited to 50 m and they perform adequately, Card et al. [19]. Hambly [40] states that integral bridges were widely used in the UK, especially before the 1970s. He gives some examples of single or multi-span, racked back and box type abutments dating from the 1950s to

1960s and stated that the problems met their remedies and they overall performed successfully.

Some major Danish bridge projects favor long, multi-span, continuous superstructures but introduce joints, at least, at the abutments, allowing free horizontal movement of the deck (see Veje [93]). These structures do not fall into the category of bridges that will be mentioned in this report but yet show the tendency in building bridges with fewer joints.

2.1.6 Geotechnical Aspects

The movement of integral bridge abutments, especially due to thermal expansion and contraction of the bridge deck, can create passive and active soil conditions in the backfill. The soil reaction is nonlinear and varies with depth. The earth pressures are dependent on the stiffness of the soil and the amount and nature of the wall displacement, which can be a translation and/or a rotation. This interdependency of the nature and amount of displacements both in the soil and the structure to the stresses created at the process is the soil-structure-interaction problem that has to be dealt with. (Deflections create reactions, and reactions create deflections.) According to Thomson [89], it requires complete knowledge of soil stress characteristics, friction characteristics, and the mode of wall movement.

Solutions usually require iterative analysis where the soil reactions are adjusted according to the amount and mode of deformations behind the abutment where the deformations depend on the relative stiffness of the abutment wall, bridge superstructure and the soil itself.

Passive pressure that develops behind the integral bridge abutment depends on the soil density, soil to wall friction angle, mode of wall displacement, effect of backfill confinement, and repeated loading (see Thomson [89]).

Maximum passive pressures can be calculated using several approaches. The most common ones are the Coulomb and Rankine theories. These theories are preferred because of their simplicity but could somehow be conservative for bridge abutment applications according to Arsoy [4]. According to Duncan et al. [30] however a third theory which is called the log spiral earth pressure theory seems to give more realistic values when compared to passive pressure load test results.

The value of the lateral earth pressure coefficient K increases in the long term. As K increases towards the passive limit with progressive cycles, yielding of soil and hence plastic deformations can occur. In the long run, the soil behind the abutment will tend to reduce in volume and increase in strength.

On the other hand, a progressive increase in displacements will lead to an increase in shear strains and stresses in soil which will eventually cause shear stiffness to reduce leading shear failure (see Springman et al [79]). Unless stated otherwise, the concerned backfilling soil will be of cohesionless type throughout this report.

The backfill may have small cohesion values though. In conventional abutment design, ignoring cohesion would be conservative whereas in an integral bridge situation cyclic movements could be sufficient to eliminate the existing cohesion effects in granular backfill (see Barker et al. [9]). Considering that the passive pressures are usually underestimated behind the integral bridge abutments, this rather conservative approach should compensate for that.

The stress behavior of cohesionless soils due to cyclic strain is highly complex and cannot be properly modelled by elasticity. Several aspects of soils like particle repacking, dilatancy, hysteresis, cyclic mobility and stress paths should also be considered (see Springman et al. [78]).

The increase in soil pressure is explained by the following mechanisms:

- The loose soil particles filling the crack between backfill and the abutment wall (only applicable to cohesionless soils) may lead to increase in the backfill soil pressure [19, 79].
- Compaction due to squeezing of the soil, reorientation and crushing of the particles leading to an equilibrium density compatible with the strain it is subjected to, also increases the pressure [56, 79, 89].
- Yielding in the soil causes plastic deformations and locking-in of the high lateral stresses [19].

Soil behavior under cyclic movements depends on the type and characteristics of soil, frequency and magnitude of loads, and soil displacement (see Card et al. [19]).

Most of the time drained conditions are considered because the loading is slow enough to let the excess pore pressures to dissipate. The limiting case, according to Springman et al. [79], is observed when the minimum void ratio is reached and densification restricts pore pressure dissipation.

The higher the abutment, the more significant the passive resistance behind the abutment. Hence some additional axial and bending moments are induced in integral bridge decks as restraint and stiffness increases. However the stub abutment type with piles can be flexible enough to accommodate these additional forces without serious structural distress (see Xanthakos [104]).

Card and Carder [19] reviewed several case studies by Broms and Ingelson (1971 and 1972), Rogers (1987), Sinyavskaya and Pavlova (1971) and Smoltczyk et al. (1977) and compared their findings by using the shear strain to soil behaviour relationship provided by Ishihara [44] in 1982 (see Figure 2.4). They assumed an abutment rotation about abutment toe and a triangular displacement (see Figure 2.5). They defined the shear strain by the following equation:

$$\gamma = 2\frac{\delta}{H_a} \tag{2.1}$$

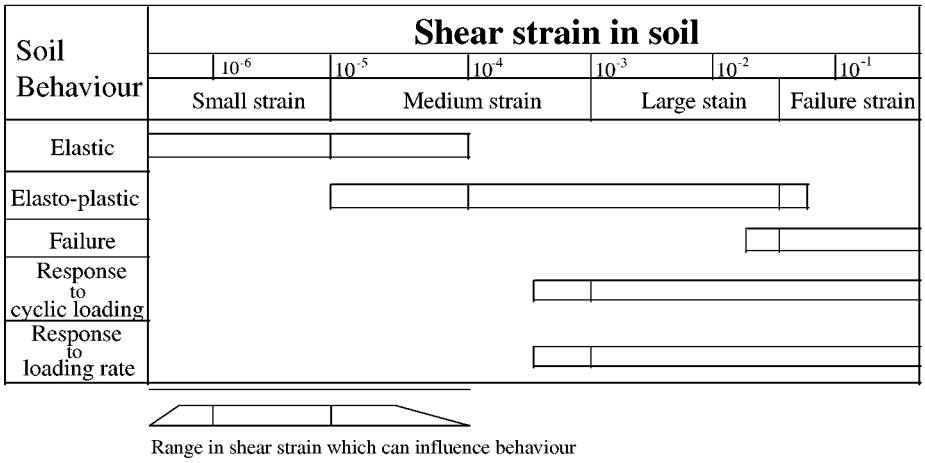

Figure 2.4: Soil behaviour to shear strain relationship (after Ishihara [44])

where:

γ = shear strain in the backfill
δ = horizontal displacement at the top of the wall
H_a = height of abutment

The observed abutment rotations and recorded earth pressures are summarized in Table 2.1. Springman et al. [79] found this strain calculation feasible for integral bridge abutments and useful in the sense that it offers a direct link of strain with bridge displacement and abutment wall height. However, due to cyclic decrease of strain, it was found to be problematic to relate this to the strain in the fill at the levels defined by Ishihara [44].

The rate at which K_p is mobilized is much higher for compacted soils. Rotation of the wall results in the highest value of K_p (see Thomson [89]).

There is certainly an increase in lateral earth pressures by the process of cyclic loading on the abutments due to thermal movements of the bridge superstructure. According to [19]'s comparisons, the long term increase in the earth pressure is unrelated to the magnitude of the shear strain. The magnitude of shear strain appears to influence the rate of increase in the passive earth pressure. Shear strains cause increase in the earth pressure up to a limiting value of K_p. The movements can be big enough to induce shear strains in which soil shows elasto-plastic behavior. Table 2.2 shows recommendations of soil behavior and earth pressure coefficients to be applied depending on the values of shear strains generated by the rotation of the abutment (obtained using Equation 2.1). If the behavior of the soil is in elastic limits the deformations are fully recoverable, therefore no increase in lateral soil pressures should occur. When the soil behaves elasto-plastic, the passive earth pressures will tend to increase and abutments will be subjected to bigger forces due to cyclic movements of the deck. This is explained by the process of consolidation

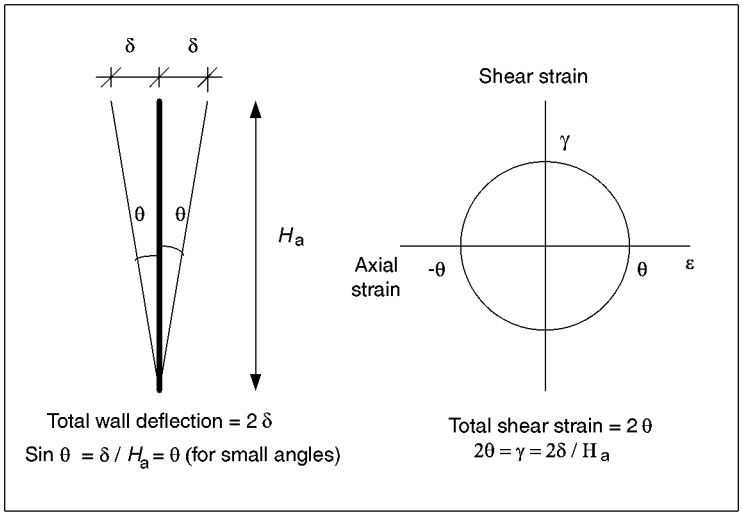

Figure 2.5: Shear strain due to abutment rotation (after Card et al. [19])

and strengthening of soil (cohesive or non cohesive) under drained conditions when subjected to a sufficiently long interval cyclic loading. This increase in stiffness will result in increased lateral pressures behind the bridge abutments.

Card et al. indicate that the thermal movements may also cause instability problems such as sliding of the footing and excessive settlements. The stiffness and strength of cohesive soils may decrease that leads to yielding.

For abutments on spread footings sliding resisting effects are more significant. Large cyclic horizontal movements induce shear stresses beyond the elastic limit of the soil. Due to yielding of the soil, the stiffness and the strength are reduced and residual shear strength parameters are to be introduced.

According to Burke [16], the maximum passive earth pressure used for the design of integral bridges with capped pile stub-type abutments can be idealized as:

$$P_p = \gamma_s \tan^2\left(45 + \frac{\phi}{2}\right) D_s + 2c \tan^2\left(45 + \frac{\phi}{2}\right) \tag{2.2}$$

where:

P_p = maximum passive pressure (N/m^2)
γ_s = unit weight of soil (N/m^3)
ϕ = angle of internal friction (degrees)
D_s = depth below approach slab (m)
c = soil cohesion (Pa)

Table 2.3, given by BA 42, indicates that the passive earth pressure mobilized during thermal movements can be seriously affected by the inclination of the abutment walls

Table 2.1: Summary of abutment rotations and recorded earth pressures (after Card et al. [19])

Reference	Abutment rotation	Induced shear strain	Likely soil behaviour	Measured earth pressures behind abutment	
				Initial value	Long-term value
Broms and Ingleson (1971)	$1.5 \cdot 10^{-3}$	$3 \cdot 10^{-3}$	e-p	K_0	$2 \cdot K_0$ after 1 year, trend still increasing
Broms and Ingleson (1972)	$1.3 \cdot 10^{-3}$	$2.7 \cdot 10^{-3}$	e-p	K_0	$2 \cdot K_0$ after 3 years, trend still increasing
Sinyavskaya and Pavlova (1971)	$2-4 \cdot 10^{-4}$	$4-8 \cdot 10^{-4}$	e-p	K_0	$0.45 \cdot K_p$ after 1 year, increasing to K_p after 10 years
Smoltczyk *et al.* (1972)	$4.5 \cdot 10^{-4}$	$9 \cdot 10^{-4}$	e-p	K_0	$1.5 \cdot K_0$ after 1 year
Smoltczyk *et al.* (1972)	$2.5 \cdot 10^{-4}$	$5 \cdot 10^{-4}$	e-p	K_0	$2.25 \cdot K_0$ after 5 years

Table 2.2: Influence of shear strain on soil behavior and lateral earth pressure coefficient values (after Card and Carder 1993)

Shear strain $2 \cdot \delta / H_a$	Likely soil behavior	Earth pressures to be applied for SLS check
$\leq 10^{-5}$	elastic	K_0
10^{-5} to 10^{-3}	elasto-plastic	K_0 to K_p
$\geq 10^{-3}$	elasto-plastic	K_p

and that the passive earth pressure coefficient (K_p) increases very rapidly with the internal friction angle (ϕ').

According to Thomson [89], complete stress-strain characteristics of the soil should be known in order to be able to predict K_p. Coulomb's equation shows the closest agreement with the measured values.

Compaction plays an important role in the level of lateral pressures on the walls as they have an effect on the initial lateral earth pressure coefficient and define

Table 2.3: Passive earth pressure coefficients (K_p) depending on abutment inclinations and internal friction angles

	Inclination of abutment back face		
ϕ'	vertical	20° forwards	20° backwards
30°	5	3	7
35°	6	4	12
40°	9	5	20
45°	15	6	37

how much more densification is possible. It was found that lateral earth pressure increased due to compaction especially close to the top of the wall (see Broms et al. [12]).

The influence of the wall friction, δ_w, on the earth pressure coefficient should also be considered since it is practically almost unavoidable and has an increasing effect on K_p. According to Springman et al. [79] K_p values can be increased 2 to 4 times when δ_w is increased from 0 to the value of the internal angle of friction ϕ of the soil. However the δ_w/ϕ ratio is not likely to exceed 0.7.

The force needed to displace the wall towards the soil is affected by the wall-to-soil friction angle. As the wall moves the friction angle develops at a nonlinear rate. This determines the lateral earth pressure coefficient (K) as well as the friction angle as the wall displaces (see Thomson [89]).

The coefficient of earth pressure (K) values can be predicted using some charts (see Figure 2.6).

Based on an extensive survey on the passive earth pressures behind integral abutment walls, Ting et al. [90] concluded the following:

- The peak wall force on an abutment that rotates towards the backfill soil is slightly larger than on the wall that laterally translates towards the backfill soil.
- A passive wall force is achieved at a normalized displacement (displacement divided by wall height) level of 5 % for dense sands and 20 % for loose sands.
- The lateral earth pressure on the abutment wall is triangular for wall translation but for wall rotation it is not triangular. Stresses are high close to the ground surface and low near the wall base.
- Integral abutment bridges under thermal loading conditions show a combination of translation and rotation as if the rotation is about a point which is located below the bottom of the wall.

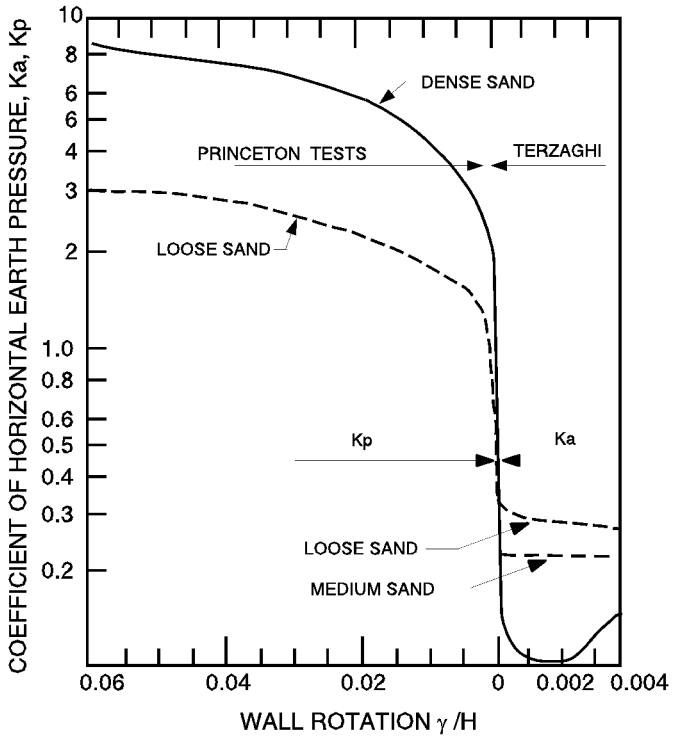

Figure 2.6: Prediction of the coefficient of earth pressures (K) for different wall rotations (redrawn from the US Department of Navy 1986 "Soil Mechanics Foundations and Earth Structures" as reported by Thomson [89])

2.1.7 Overview of the Research on Integral Bridges

Broms and Ingelson [12,13] measured the lateral earth pressure acting on the abutments of several rigid frame bridges of 150 and 110 m length in Sweden. The measurements were done during compaction and after the completion of the bridges. They concluded that the earth pressure was approximately constant immediately after the placement of the fill. The pressure at the center of the abutment was found to be larger than at the top and bottom. The modulus of horizontal subgrade reaction increased with the distance below the ground surface. When the abutment was displaced laterally, the pressure distribution was hydrostatic, and parabolic when it rotated about its lower edge. It was concluded that the earth pressure increases due to self compaction during the cycles of thermal expansion and contractions and the maximum earth pressure can reach up to passive earth pressure level.

Jorgenson [47] took field measurements from a six-span concrete integral bridge. Bridge movements were monitored for approximately one year and the abutment-pile behavior was observed. Jorgenson reports that the movements in two ends of the bridge due to the change in length were not equal to each other. No vertical movements in abutments were recorded. The pile stress calculated from the maximum movement measurement was big enough to initiate a yield stress but not enough to generate plastic a hinge.

Greimann et al. [39] developed a nonlinear finite element procedure for evaluating pile-soil interaction in integral bridge abutments. Piles were represented by beam-column elements and soil was idealized as nonlinear springs. They concluded that thermal expansion introduced some additional vertical loads leading to reduction in the vertical load carrying capacity of the piles.

Girton et al. [38] worked on verification of design procedures for piles in integral abutment bridges. They used experimental data collected for two years from two skewed bridges in Iowa. Data consisted of air and bridge temperature, bridge displacements and pile strains. They recommended coefficients of thermal expansion. They concluded on some design aspects which will be mentioned in Section 2.1.8.

Sandford and Elgaaly [74] made field measurements on a 20 degree, 50.3 m span skewed bridge in Maine to investigate the soil pressures behind the skewed bridge abutments and the skew effects on these pressures. The results were found to be similar to those by Broms and Ingelson [12]. Concerning skew effects, they recorded more than two times greater soil pressures at the obtuse side of the abutment compared to the acute side. The ratio was said to reach 4 at the extremes of the abutment. They observed that the effect of skew diminishes with time giving no sign of being affected by the cyclic stiffening of the soil behind. The average soil pressure at the girder level was found to be 5 times higher than at rest level. Some design recommendations were also made (see Section 2.1.8).

According to Russel [73], the US Federal Highway Administration started a research program (in 1994) to establish a better understanding of the behavior of integral bridges. Their research includes a literature survey, as well as analytical and exper-

imental work on a very wide range of bridge structure types.

Springman and Norrish [78] carried out centrifuge model tests to examine the behavior of full height abutments with spread base and piles. A 10 m beam centrifuge was used for a 1/60 scale model. It has the advantages of observing deformation mechanisms in serviceability limits and failure modes in ultimate limits. They concluded that large shear stain cycles can cause increase in the bending moments of the wall, axial deck loads and severe slumping of the backfill. The failure mechanism was observed to be a clear wedge behind the wall. The bending moments increased by 32 percent after the 75^{th} cycle of 30 mm horizontal displacement.

Fang et al. [35] carried out experiments to investigate the earth pressure against a rigid wall that was moved towards a mass of dry sand with a free horizontal top boundary. The experiments revealed that the passive earth pressure is linear when the wall is horizontally translated (at each stage of the wall motion). For rotations about a point above the top and below the base of the wall, the earth pressure is found to be significantly affected by the mode of the displacement and the location of the point of rotation. For rotation about right at the bottom of the wall, the passive earth pressure was found to be nonlinear and the maximum stresses were measured at about mid-height of the wall.

Thippeswamy et al. [88] analyzed five jointless bridges in service by means of 2-D frame models using one dimensional beam theory. They conclude that the earth pressure, even in the passive case, produces negligible stresses at all locations of varying bridge systems (stub-type abutments with or without piles).

Centrifuge tests conducted by Springman et al. [79] show that horizontal stresses created by cyclic expansions and contractions of the deck remain approximately constant to depths of up to 6 m. The pressure distribution acting on abutment is similar in form to the classical compaction stress distribution and typically have magnitudes between 25 and 50 kPa. This observation suggests that the use of a constant soil stiffness value with depth (for a given strain) is reasonably realistic and that the upper bound mean effective stress (p') in operation during deck expansion lies between about 50 and 100 kPa. According to test results K_p increases from the first cycle on but the change is not dramatically pronounced after the 20^{th} cycle.

Carder and Card [20] inquired the methods of avoiding the development of high lateral pressures on the abutments due to cyclic movements of the abutments. As a result, the usage of low stiffness and a stress absorbing compressible elastic layer between backfill and the abutment wall was said to be able to cope with this kind of problem. It was also indicated that the usage of a compressible layer could be more economical if a new integral bridge is going to be constructed. The materials considered to be suitable for this purpose were

- polystyrene products,
- polyethylene foam,
- geocomposite materials, and

- rubbers.

The function of these materials was explained as

- to expand without allowing a void into which water and debris can enter,
- to act as a stress absorbing layer and to prevent movements from the abutment to the backfill, hence to prevent passive earth pressure development in the backfill, and
- to reduce wall friction between the abutment and the backfill.

According to the result of this study, where two different compressible layer thicknesses were studied (0.3 and 1.0 m), the materials showed a nonlinear elastic behavior up to some acceptable degree (strain range 0.8 % up to 5.3 %). The importance of engineering the thickness and of the development of the performance specification of these compressible layer candidates was emphasized.

Ting et al. [90] studied a 3D and 2D FE model of a 45.7 m long integral abutment bridge system with piles. Nonlinear soil behavior is handled using nonlinear springs having stiffness values varying with depth. A 44.4°C thermal loading level was selected where the soil compaction levels were varied. Ting et al. [90] and later Faraji et al. [36] concluded the following:

- The level of compaction behind the wall is vitally important. When it varies from loose to dense the axial forces and moments can double.
- The soil pressure behind the abutment wall is slightly nonlinear for a displacement of about 0.01 m and it is expected to be more pronounced as the displacement gets bigger.
- Full passive soil resistance is almost achieved near the ground surface, and at greater depths the pressure was about half of the passive value.
- The compaction level adjacent to the piles below the abutment does not affect the wall displacements and moments to a significant degree.

Lehane et al. [56], considering the effects of deck thermal expansion on frame type bridges, developed a simple elastic model where an equivalent abutment height with a single translational spring is used to simulate the soil structure interaction. The backfill was modelled as a linear elastic continuum with a stiffness E_s. Calculations using a frame analysis program and finite elements were compared and the results were found to comply well. They state that additional stresses due to thermal movements are not particularly sensitive to the value of soil stiffness, therefore using a linear modulus E_s will be sufficient for design. The formulation of E_s was done by best fit correlation of the data of shear stiffness from recent research. Assuming

$$\nu = 0.25$$

and

$$E_s = 2G(1+\nu)$$

the following formula for Young's Modulus was obtained:

$$E_s = 150 \cdot F(e) \cdot \left(\frac{p'}{p_a}\right)^{0.5} \cdot \left(\frac{0.01}{\gamma}\right)^{0.4} \tag{2.3}$$

where:

E_s	=	secant modulus (MPa)
$F(e)$	=	$(2.17-e)^2/(1+e)$ normalizing function for shear stiffness
e	=	void ratio
p'	=	mean effective stress (MPa)
p_a	=	atmospheric pressure (MPa)
γ	=	average shear strain level (%)

The average strain is likely to be in the range $\delta/2H_a$ to $2\delta/3H_a$ where δ is half the thermal expansion of the deck and H_a is the height of the retained fill (see Lehane et al. [56]).

Thomson [89] carried out full-scale tests on integral bridge abutments on spread footings and piles, while the abutment was passively displaced into the backfill. Earth pressures and deflections were measured. It was found that the use of uncompacted sand cushion behind the abutment helped to reduce lateral earth pressures but have a tendency to compact after one cycle of abutment movement. Equations were developed for predicting lateral earth pressures (while K_0 after compaction and K_p values are predicted at the beginning). Current design charts were modified.

As a conclusion of a literature survey and experimental study, Thomson [89] reports the following:

- For wall rotation about the top, the distribution of lateral soil pressures on the wall is parabolic with the maximum value at the bottom. The K_p value is the lowest.
- For wall translation, the distribution of lateral earth pressure is linear having the maximum value at the bottom. The magnitude and the distribution in this mode of movement are closest to the theory.
- For wall rotation about the bottom, the distribution of lateral earth pressure is also parabolic with maximum values towards the upper half of the wall height (from 25 % to 50 % of the abutment height).
- The exact location of the resultant force on the abutment depends on the wing-wall geometry. As the angle between the wing-wall and the abutment changes from parallel position to perpendicular, the resultant force moves up.

Carder et al. [21] state that the secant and tangent moduli for well graded aggregate tend to be fairly constant at about 100 MPa until the compressive strain exceeds 0.1 %. Then the modulus sharply increases to a value 2.25 and 10 times higher, respectively, for the secant and tangent moduli.

England et al. [33] investigated integral bridges having lengths of 60 m, 120 m and 160 m with stiff abutment walls of 7 m with pinned bases. 1 in 12 scale model tests were conducted as well as computer analyses. The following conclusions were obtained:

- Stress changes in the backfill escalate quickly to reach the hydrostatic stress state (K=1) and settle at peak ratios.
- On the other hand settlements continue to change for further cycles (110 mm adjacent to the wall in 120 years for a 60 m bridge).
- The code BA 42 assumes conservative design loading for integral bridge abutments. However for a suitable choice of K^* the approach given by BA 42 (see Section 2.1.9) is sufficient in the calculation of stress escalation.
- A new equation for K^* however was proposed (see section 2.1.9).

As a result of controlled cyclic loading to granular soils and laboratory triaxial tests Carder et al. [21] conclude that granular soils are likely to perform adequately under the strain limits that are likely to be developed beneath the spread base foundations. In clay soils however, it may result in yielding and reduction in bearing capacity.

Barker et al. [8] made field measurements on two full height integral bridge abutments of about 40 m span. Wall and deck loads, moments, changes in the deck length as well as movement of the abutments were measured. One year after the construction, which was in the summer, the lateral stresses on the abutment of one of the bridges were measured slightly above the K_0 pressure distribution. Stress escalation behind the abutment was reported to take place after many cycles.

Lawver et al. [55] investigated an integral bridge of 66 m and three spans during construction and through several years of service. The bridge was monitored under construction as well as seasonal, environmental and live-loads. All the bridge components have been found to have performed within design limits. It was found that the abutments were translating laterally as a reaction to expansion and contraction of the deck. The effect of temperature changes on the bridge was calculated to be as large as the live-load effects.

Barker et al. [9] evaluated the behavior of a 50 m integral bridge during construction and over the first three years of service. Movements and stress measurements on the abutment as well as strain and temperature measurements of the deck and the abutments were taken. It was observed that the pressures behind the abutment, after backfilling is completed, were following an "at rest earth pressure (K_0)" trend. During expansion times pressures rose a bit above K_0 level and higher earth pressures developed towards the top of the abutment. At the end of this study it was concluded

that in the long run, creep and shrinkage effects become negligible compared to those of thermal expansion and contraction of the deck. This seasonal cyclic action may lead to an increase in the lateral stresses behind the abutment but further monitoring is needed to evaluate the extent and significance of these stresses.

Xu et al. [105] performed a numerical analysis of an embedded integral bridge abutment that is 12 m high, in order to investigate the maximum earth pressure and the distribution of earth pressure. The cyclic horizontal movement ($\pm$10 mm at the top) of the abutment was simulated and it was observed that the resulting bending moments reached a limit value after 20 cycles. The lateral earth pressure (in the middle part) behind the abutment increases by about 20% during these cycles. Although the distribution of the earth pressure is similar to the ones proposed in the design code BA 42, it is still far less in value.

2.1.8 General Design Considerations for Integral Bridges

The analysis method for the integral type of structures was first developed by Cross in 1930 (see Xanthakos [104]). The design of bridge abutments will be focused on in this section.

Usually, classical earth pressure theories (Rankine and Coulomb) are used to deal with the pressure exerted on an abutment by the retaining soil. They are usually designed according to at rest conditions (using K_0). However the worst case for design seems to be the lateral earth pressure which is likely to reach the passive limits.

In the design, the material properties should be realistic. The abutments should be flexible enough to absorb the movement of the deck and stiff enough to resist the other longitudinal forces (like braking forces) (see Card et al. [19]). The abutment stiffness is recommended to be 10 times bigger than the bridge deck stiffness. For bridges having a bridge span/abutment height ratio greater than 3.5 the passive earth pressure value (K_p) should be used in design. Some other design considerations reported by Card et al. [19] are

- limiting the length of bridges to control the amount of passive pressures,
- using porous or granular fill material (with a typical angle of friction of 35 degrees),
- using approach slabs to prevent backfill compaction by traffic,
- using compressible material between the wall and the backfill (eg. expanded polystyrene),
- using lightweight concrete which has 70 percent less weight than equivalent gravel concrete,
- using moderate skews to reduce the length subjected to passive pressure,

- reducing abutment penetration into embankments,
- shortening wing walls, and
- using turn-back wing walls.

In Sweden, the design methods used for integral slab frame bridges are based on experience and simple elastic frame models (see Sundquist et al. [82]).

Burke [16] however recommends bridge design engineers to concentrate on constructing durable bridges rather than making a detailed study of the secondary effects due to shrinkage, creep, passive soil pressure, etc., on integral bridges. He indicates that these effects are negligible if the design is simplified to certain limits. This can be achieved by standardizing bridge details and limiting the bridge geometry and settlements. He indicates that the secondary effects can be neglected if the bridge length is less than 91 m, spans are less than 24 m, the skew angle is less than 30 degrees and the curvature is less than 5 degrees.

The recommended amount of movement of the bridge abutment from the position at time of restraint during construction is $\pm$ 20mm. The piers should be sufficiently flexible to accommodate thermal movements (see BA 42) [6].

It is advised to construct the deck during the hot season (see Springman et al. [79]).

According to Girton et al. [38] bridge temperature changes should be assumed higher than the measured values. A simplified longitudinal expansion or a longitudinal frame model can be used to predict lateral displacements. They recommend the designer to use full passive soil pressure in designing the abutment.

According to Dicleli [26]:

- The conventional design approaches in North America and Europe do not consider the beneficial effects of continuity at the joints and earth pressure forces applied at the abutments in reducing the maximum span moment.
- They also do not take into account the unbalanced longitudinal forces in pier design.
- The effects of temperature change and the axial load applied to the bridge deck are neglected.
- It is advised to use full passive earth pressure for the design of the deck-abutment joints.

2.1.9 Earth Pressure Distribution in the Design of Integral Bridges

Design for Earth Pressure in Sweden

According to Swedish design standards, an additional horizontal earth pressure as a reaction to horizontal movement of the bridge should be taken into account. There are two cases that are given in Bro 2002 [1].

The first one is the reaction pressure ΔP on piles, pillars and frame walls. ΔP, which can be calculated from Equation 2.4, should be used in addition to the existing at rest soil pressure (see Figure 2.7):

$$\Delta P = C \cdot \gamma_s \cdot \frac{H_a}{2} \cdot \beta_r \tag{2.4}$$

where:

ΔP = horizontal soil reaction pressure (kN/m^2)
C = 300 or 600 depending on the forces being advantageous or not
β_r = δ / H_a
δ = horizontal deflection of the abutment (m)
γ_s = soil unit weight (kN/m^3)
H_a = height of the abutment (m)

Equation 2.4 is valid until the depth of $H_a/2$. From that depth on the reaction pressure approaches to 0 at the bottom of the wall. Restraint effects of temperature change are accepted as disadvantageous where C should be taken as 600. When the movement is due to breaking forces, the existence of a mid-span leg will take part in resisting the lateral force that will make the case advantageous. Then C can be taken as 300.

The second case concerns integral bridge abutments with end-screens. The total lateral force acting on the end-screen is calculated from the following equation:

$$\begin{aligned} P &= P_0 && \text{if } \delta = 0 \\ P &= P_0 + C_1 \cdot \delta \cdot \tfrac{200}{H_e} \cdot P_1 && \text{if } 0 < \delta < H_e/200 \\ P &= P_0 + C_1 \cdot P_1 && \text{if } \delta \geq H_e/200 \end{aligned} \tag{2.5}$$

where:

C_1 = 1 or 0.5 depending on the forces being advantageous or not
P_0 = at rest earth pressure
δ = horizontal deflection of the end-screen
P_p = passive earth pressure
P_1 = $P_p - P_0$
H_e = height of the end-screen

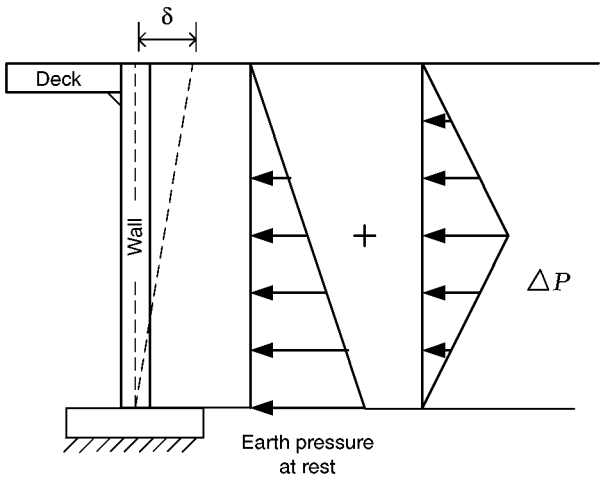

Figure 2.7: Design earth pressures on slab frame bridges (according to the Swedish Bridge Code Bro 2002)

Table 2.4: Lateral earth pressure coefficients of different material (from Bro 2002)

Material	K_0	K_a	K_p
Crushed stone	0.34	0.17	5.83
Subbase material	0.36	0.22	4.60
Clinker	0.43	0.27	3.70
Plastic cell	0.40	0	-

The earth pressure coefficients according to the Swedish Bridge Code Bro 2002 [1] are taken from Table 2.4.

Applications in the UK

According to The Highways Agency Design Manual for Roads and Bridges (BA 42) [6], the pressure distribution behind full height frames and embedded abutments should be taken as in Figures 2.8 and 2.9.

K^* can be calculated from the following formula, which is derived from static tests and can underestimate the stresses in a cyclic situation:

$$K^* = \left(\frac{\delta}{0.05H_a}\right)^{0.4} \cdot K_p \tag{2.6}$$

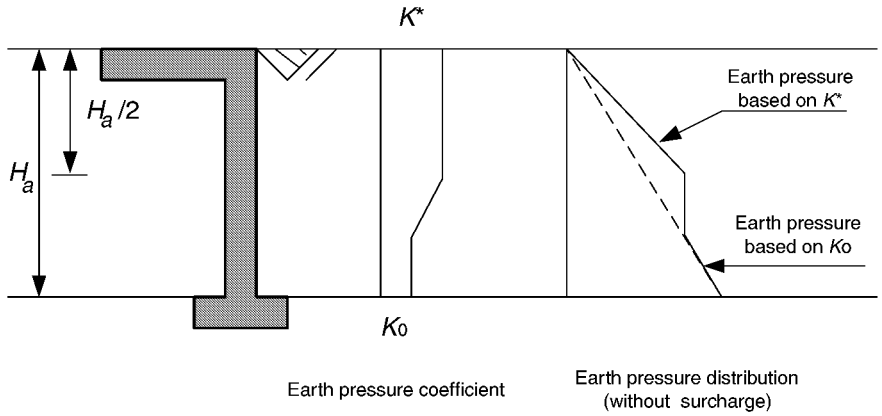

Figure 2.8: Design earth pressure distribution for frame abutment (according to BA 42/96)

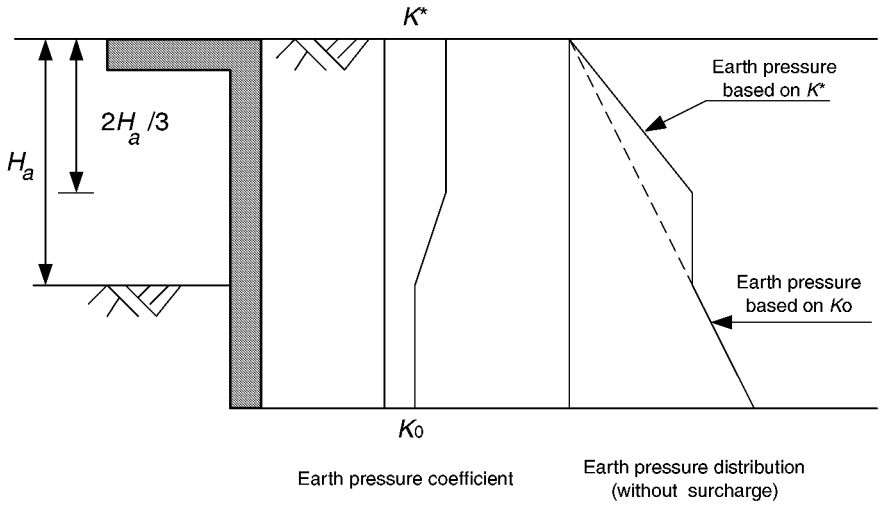

Figure 2.9: Design earth pressure distributions for full height embedded wall abutments (from BA 42/96)

where:

K^* = uniform earth pressure coefficient
δ = top displacement of the abutment
H_a = height of the abutment
K_p = passive earth pressure coefficient

According to BA 42 the earth pressure coefficients should be calculated using material factors of 1.0 and 0.5 for disadvantageous forces and advantageous forces respectively.

Applications in the USA and Canada

Most bridges in the USA are designed according to the American Association of State Highway and Transportation Officials (AASHTO).

Taly [86] reports that AASHTO calculates horizontal soil pressures on the bridge abutments according to the Rankine active soil pressure. The pressure is limited to 4.8 kN/m^2 per meter height of the abutment. K_a is assumed to be equal to 0.3.

It was reported by Kunin [53] that in the USA and Canada, uniform triangular and Rankine load distributions are used for the design according to soil pressure on integral bridge abutments. But some of the agencies do not consider soil pressure at all.

According to Thomson [89] there are two popular design methods for calculating earth pressures namely NAVFACDM 7.2 (The US Department of the Navy 1986) and the Canadian Foundation Manual (Canadian Geotechnical Society 1992). The curves of the latter show a better agreement with the measured K values.

Some Alternative Proposals

Sandford and Elgaaly [74] bring up some considerations special to skewed bridges. They recommend the usage of the pressure envelope proposed by Broms et al. [12] and the Maine Department of Transportation with a slight adjustment, as shown in Figure 2.10.

England et al. [33] concluded that the code BA 42 provides conservative design loading for integral bridge abutments. However for a suitable choice of K^* the approach given by BA 42 is found to be sufficient in the calculation of stress escalation. A new value for K^*, however, was proposed:

$$K^*_{alt} = K_0 + \left(\frac{\delta}{0.03H_a}\right)^{0.6} \cdot K_p \tag{2.7}$$

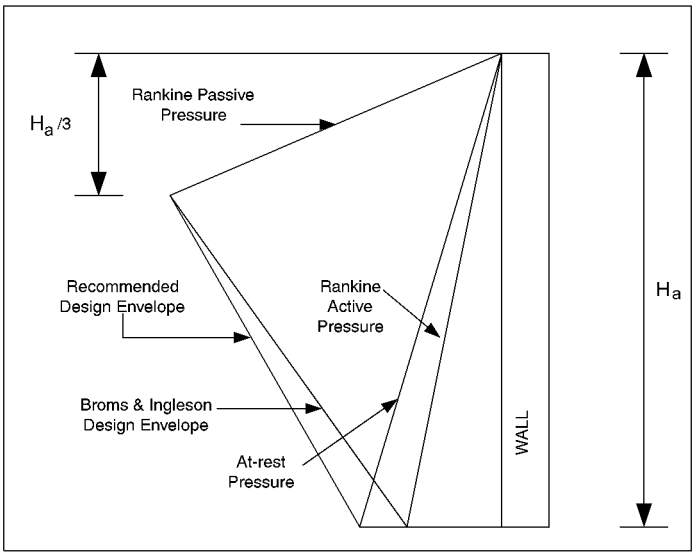

Figure 2.10: Design earth pressure distributions behind abutments (from Sandford [74])

where:

K^*_{alt} = uniform earth pressure coefficient
(K_o) = earth pressure coefficient at rest
δ = top displacement of the abutment
H_a = height of the abutment
(K_p) = passive earth pressure coefficient

Dicleli [26] , however, reports a different approach to estimating the lateral earth pressure coefficient K that could be used in design.

$$K = K_0 + \psi \cdot \delta \leq K_p \tag{2.8}$$

where:

K = uniform earth pressure coefficient
(K_o) = earth pressure coefficient at rest
ψ = slope of the earth pressure variation
δ = top displacement of the abutment towards backfill
(K_p) = passive earth pressure coefficient

The value of ψ depends on the backfill soil type. According to Dicleli [26], typical values can be obtained from elsewhere.[1]

[1]Barker, R. M., Duncan, J. M., Rojiani, K. B., Ooi, P. S. K. and Kim, S. G., Manuals for

Table 2.5: Lateral earth pressure coefficients to be used in the design of integral bridges (recommendations by Springman et al. [79])

				Stiff walls	
Design criterion	Rotation	δ	Flexible Walls	Spread base	Embedded
Serviceability state	$\theta < 0.23°$	0.024	$K < 1$	$K < 2$	$K < 2$
Ultimate state	$\theta > 0.5°$	0.052	$1 < K < 2$	$K \sim 4$	$K \sim 4$
After 100 cycles	$\theta \sim 1°$	0.1	$2 < K < 4$	$K \sim 4$	$K \sim 8$

A triangular earth pressure distribution was assumed. the final displacement of the deck δ is calculated from the difference of the deck elongation due to temperature increase and the deck contraction due to backfill pressure.

Springman et al. [79] recommend some values for the lateral earth pressure coefficients (K) to be used in the design as a result of centrifuge tests and finite element analyses of two different types of integral bridge abutments under cyclic movement. Their recommended K values are given by Table 2.5.

A linear value of K is proposed over the top half of the retained height of the wall. The lateral earth pressure is assumed to remain constant over the bottom half of the spread base abutment.

Thomson [89] proposes that for a deflection mode of simultaneous rotation and translation, the earth pressure distribution increases from the top to a depth of approximately 38% of the abutment height and from that point on it remains constant.

Fang et al.'s [35] model test results for wall rotation show a similar earth pressure distribution nonlinearity with the point of application of a passive thrust of $0.55 \cdot H_a$. Xu et al.'s [105] results also confirm nonlinearity.

Comparisons

Comparison of Earth Pressure Distributions In this section earth pressure distributions on abutment walls due to a cyclic movement of the abutments are going to be compared. the Swedish Bridge Design Code Bro 2002 recommendation for earth pressure will be compared with the British Highways Agency Design Manual and also with some other design proposals from researchers. A numerical example will be carried out to achieve this. The design procedures are discussed in previous sections and described by the help of Figures 2.7 to 2.10.

the Design of Bridge Foundations, NCHRP Report 343, Transportation Research Board, National Research Council, Washington, D.C., 1991.

Table 2.6: Parameters used in the numerical example

Material properties	values
ϕ (° C)	38.3
γ_s (kN/m^3)	19.0
K_0	0.38
K_a	0.3
K_p	4.2
Wall height, H_a (m)	6.0

The soil parameters and the wall geometry used in the numerical example are given in Table 2.6. The C value in Equation 2.4 is taken considering the disadvantageous conditions (i.e., C is taken as 600).

The calculations were carried out for several wall displacement values. These displacements were chosen such that they represent every shear strain level that corresponds to each of the soil behaviors in Table 2.2. The shear strain level is calculated according to Equation 2.1, here repeated for the reader's convenience:

$$\gamma = 2\frac{\delta}{H_a}$$

The displacement amounts of 2 mm, 10 mm and 40 mm fall into the $\leq 10^{-5}$, 10^{-5} to 10^{-3} and $\geq 10^{-3}$ shear strain ranges respectively. They can then be classified as elastic, elasto-plastic and elasto-plastic behavior in Table 2.2.

Comparison of Earth Pressure Coefficients The lateral earth pressure coefficients were calculated for wall displacements of 6 mm, 12 mm, 30 mm, 60 mm which correspond to more or less 30 m, 59 m, 147 m and 294 m bridge lengths (if the coefficient of thermal expansion is taken as 12 E-6 1/°C and change in temperature is taken as 34°C). Table 2.7 displays several K values either recommended or measured by tests from different sources.

Conclusions of Comparisons

The earth pressure distributions according to different design codes and different displacement levels are plotted in Figure B.1. For small displacements the Bro 2002 and BA 42 values agree with each other. But for larger displacements such as bigger than 10 mm the difference is much more pronounced. It can be concluded also looking at Table 2.7 that the Swedish design code Bro 2002 becomes more conservative in estimating lateral wall pressures as the amount of wall deflection increases.

The wall pressure estimation from AASHTO depends on active pressures which is quite unrealistic considering the fact that the wall movements towards the soil create

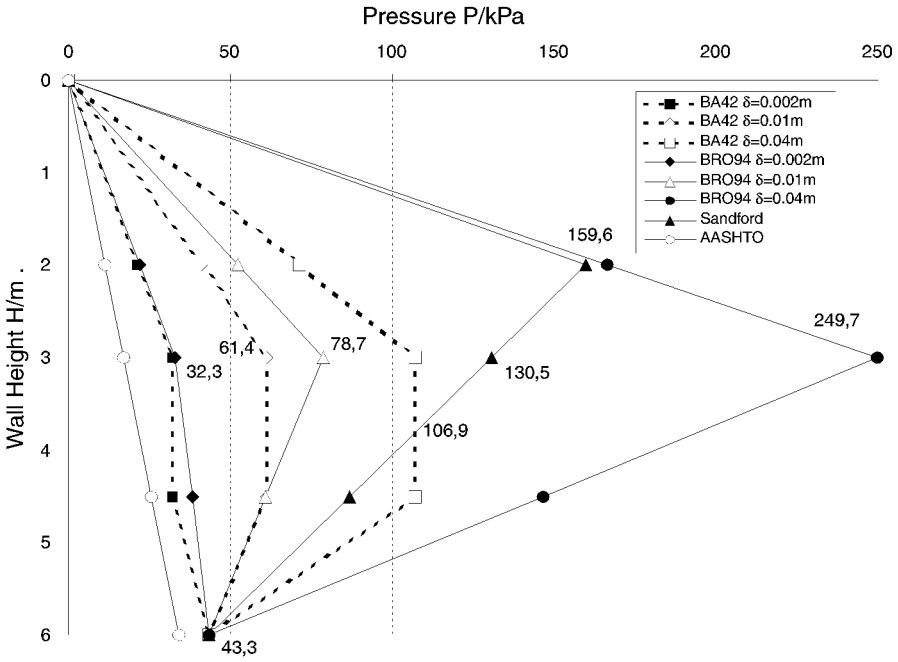

Figure 2.11: Comparison of design earth pressure distributions behind abutments from different sources

References		Deflection of the top of the abutment wall							
		6 mm		12 mm		30 mm		60 mm	
		1st cycle	100th cycle	1st cycle	100th cycle	1st cycle	100th cycle	1st cycle	100th cycle
BRO 2002		0.98		1.58		3.37		6.37	
BA 42		0.88		1.16		1.67		2.21	
Springman et al. 1996	dense sand	0.6-0.7	0.6-1.0	0.7-1.1	0.9-1.2	1.0-1.6	1.6-2.4	1.8-3.0	3.1-3.75
	loose sand	0.4-0.5	0.8-1.0	0.9-1.2	1.0-1.7	1.2-2.1	1.6-2.5	1.8-3.0	2.5-4.2
Hambly & Burland 1979 (presented by Springman'96)	dense sand	1.2		2.0		3.1		4.0	
	loose sand	0.7		1.1		1.6		1.8	
Terzaghi 1954 (presented by Springman'96)	dense sand	-		2.1		3.0		4.0	
	loose sand	-		1.2		1.5		1.8	
England et al. 2000	scaled model test	1.4		1.75		2.95		-	
	numerical prediction	1.1		1.2		1.65		-	

Table 2.7: Experimental K values obtained for different wall deflections (rotation about the base)

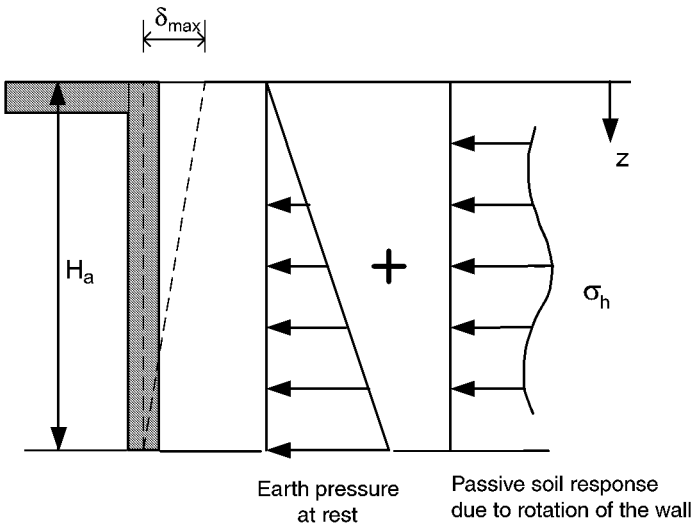

Figure 2.12: A presentation of the wall rotation about its base and the soil pressure distribution behind the integral bridge abutments

a pressure increase on the wall. It can be concluded that the AASHTO design for bridge abutments highly underestimates the pressures.

The K values from the English code BA 42 are lower then the values of two experimental studies (Springman and England). Although the values without considering a cyclic movement are close to each other with the increase in pressure after iterations BA 42 is said to be underestimating the K values in the long term.

The numerical analysis results by England et al. [33] give quite lower values for K than the test results.

The recommended values by Terzaghi, Hambly and Burland agree with each other.

A Proposal for the Passive Earth Pressure Response

Having briefly compared different methods for estimating the potential lateral earth pressure distribution behind integral bridge abutment walls, due to wall movements, a simple elastic approach to estimating the deformation, combined with the hyperbolic elastic modulus distribution in the soil, is used. The main objective of this approach is to form a starting point for developing a numerical model for future stress investigations. The second objective is to find a very simple way of verifying the nature and quantity of the passive earth response behind the abutments.

The soil is thus assumed to be simply elastic, having different layers with different stiffness values. The estimation of the elasticity modulus of the soil is done by means of an approach where many soil parameters are involved, namely the proposed E_t

formula in the TRITA-BKN report [72]. The formula is given in Section 3.2.5.

The author is aware that no general conclusions can be drawn from this naive approach without supporting them with numerical analysis and field measurements. The details of the calculations are given in Appendix B.

2.2 Soil-Structure-Interaction for Culverts

In general, bridges with span length 6 m (20 ft) and under are classified as culverts (see Taly [86]). According to Swedish norms all spans that are greater than 2 m can be classified as bridges. Culverts are generally used over small and intermittent waterways under fills. Today larger spans are used as the knowledge about culverts increased. The simplicity of installations and economical advantages increased the popularity of flexible metal buried structures. This section will mainly focus on the state of the art and design of such structures.

Some of the basic theories and design methods concerning soil-structure interaction of buried structures were initiated starting from the beginning of twentieth century. The subject started to gain more importance with the increasing need to build bigger underground structures subjected to loading that are greater than the previous. It is impossible to keep track of all the technical advances but some of the earliest work of significance will be mentioned in this report.

In the design of rigid buried structures, it is assumed that the structure is mainly affected by the vertical pressures caused by the soil cover and traffic. Since the horizontal deformations are negligibly small the horizontal soil reaction pressure is very small or non-existent. On the other hand, flexible buried structures are subjected to horizontal supporting pressures that result from horizontal displacement into the soil. Hence in the case of flexible structures, it is the interaction between the structure and the surrounding soil that constitutes the structural system.

Flexibility is an advantage for buried structures (see Janson [46]). The strain and stress in the pipe wall reduce with the thickness of the wall. A thin wall is not necessarily a disadvantage as long as the deflections are kept in reasonable limits and the surrounding soil is carefully placed and the soil properties are correctly identified.

2.2.1 Types of Culverts

White et al. [100] classify culverts according to the materials in the following way:

- Corrugated steel culverts:
  - factory made pipes
  - structural plate pipes (span range 1.5 to 8 m)

  - box culverts (span range 8 to 11 m, [62], in use since 1975)
  - long span structures (span range 6 to 12 m)

- Precast concrete pipes: can be circular arch and elliptical in shape and the span is up to 4.5 m for circular and up to 12 m for arch shaped ones.
- Cast-in-place concrete culverts: can be rectangular and arch shaped. The most popular one is the concrete box culvert.

Occasionally aluminum, masonry, timber, cast iron, stainless steel and plastic is also used in making culverts.

There is a variety in culvert shapes (see Figure 2.13). The shape usually depends on structural and hydraulic requirements. A circular shape (see Figure 2.13A) is hydraulically and structurally efficient. Arch (B), pipe arch (E) and elliptical (C) shapes are frequently used in case of limited distance from a channel invert to the pavement. These are not as structurally efficient as the circular ones. Arch culverts allow a less restricted waterway. Box shape culverts are easy to adopt to site conditions but they are less efficient than the other types.

2.2.2 Overview on the Research on Buried Structures

The first achievements of the classical design concept special to buried structures started in the early twentieth century by recognition of the dependency of the loading on the structure on the interaction with the surrounding medium. This new theory was only applicable to buried rigid structures. However the flexible conduit design based on empirical equations and some design charts followed this achievement. But the first well established soil-structure interaction concept came from Spangler[2] when he introduced his Iowa Formula in which soil properties were also included. With this approach, the importance of soil parameters was realized. Spangler calculated the horizontal deflection of the buried flexible pipe by the following formula:

$$\Delta x = D_1 \cdot \frac{K_B \cdot W_c \cdot r^3}{E_p \cdot I_p + 0.061 \cdot E' r^3} \tag{2.9}$$

[2]Spangler, M. G., 1941, The structural design of flexible pipe culverts, Iowa Eng. Exp. Station Bulletin 153, Iowa State Collage, Ames, Iowa

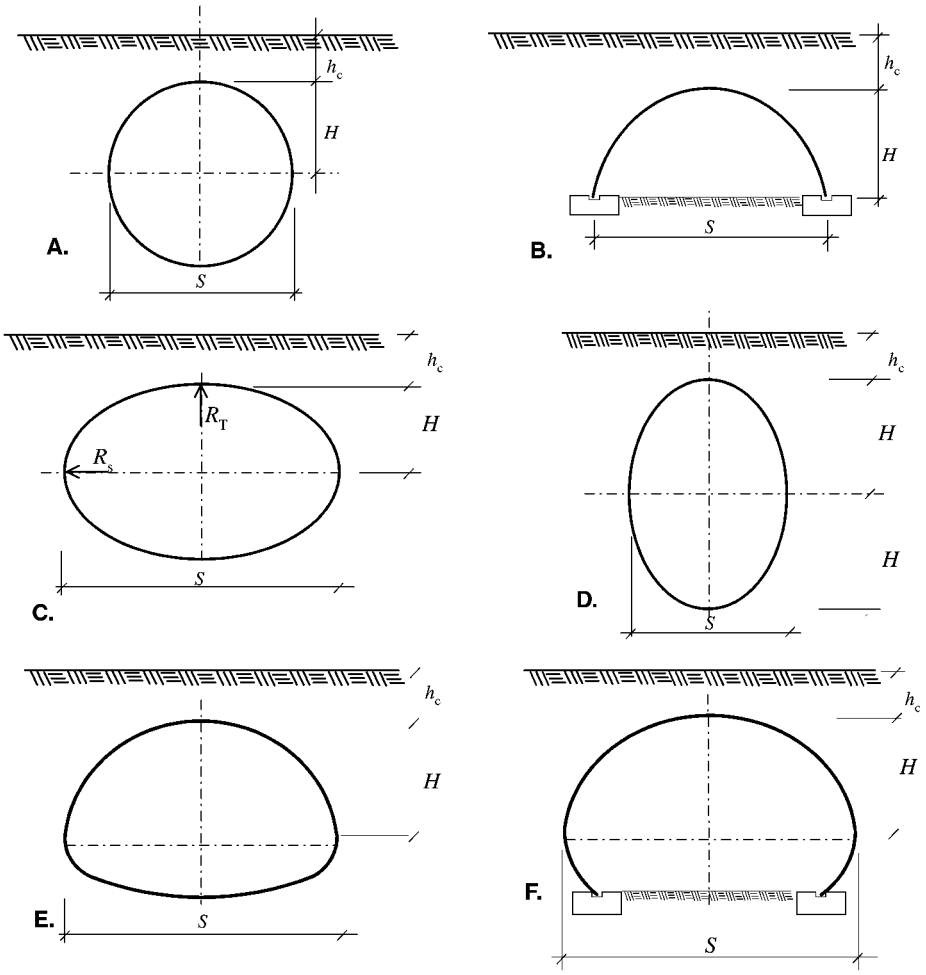

Figure 2.13: Some types of culvert profiles (after Pettersson et al. [72]). H = rise, h_c = cover height, R_T = radius of the crown and S = span

where:

Δx	=	horizontal deflection of the pipe
D_1	=	deflection lag factor
K_B	=	bedding constant
W_c	=	vertical load of soil per unit length of the pipe
r	=	mean radius of the pipe
E_p	=	modulus of elasticity of the pipe material
I_p	=	moment of inertia per unit length of cross section of the pipe
$E' = e_p \cdot r$	=	modulus of soil reaction
e_p	=	modulus of passive resistance, that is the ratio of horizontal pressure to corresponding deflection

The soil pressure distribution according to Spangler (as reported in [46]) is such that there is a horizontal soil reaction pressure of parabolic shape with a maximum value of $(\Delta x/2) \cdot (E_s/s)$. Molin [64] later suggested that a uniformly distributed soil pressure of $K_0 \cdot W_c$ should be added to the lateral pressure defined by Spangler. the Swedish calculation method for buried pipes adopts the soil distribution suggested by Molin [64].

According to Janson [46], most of the studies of flexible pipes buried in the ground are based on the classical Spangler expression.

This was followed by the model studies of Watkins [96], Watkins and Nielson [97], Howard [42], Howard and Salender [43], as well as Burns and Richard [18].

In 1960 came the introduction of the ring compression theory for the design which states that the ring deflection of the structure is negligible and the failure comes with crushing of the pipe walls. White and Layer [99] in 1960 suggested that once flexible pipes are buried at a sufficient depth, the problem can be analyzed as a thin ring in compression. They assumed a uniform pressure P as:

$$P = \gamma_s \cdot h_c + q \tag{2.10}$$

where:

P	=	uniform ring compression pressure (kN/m^2)
h_c	=	depth of cover
γ_s	=	unit weight of soil
q	=	equivalent live load

The ring compression load or circumferential thrust per meter length of the pipe (T) is given by:

$$T = P \cdot \frac{D_p}{2} \tag{2.11}$$

where T is in kN/m and D_p is the diameter of the pipe.

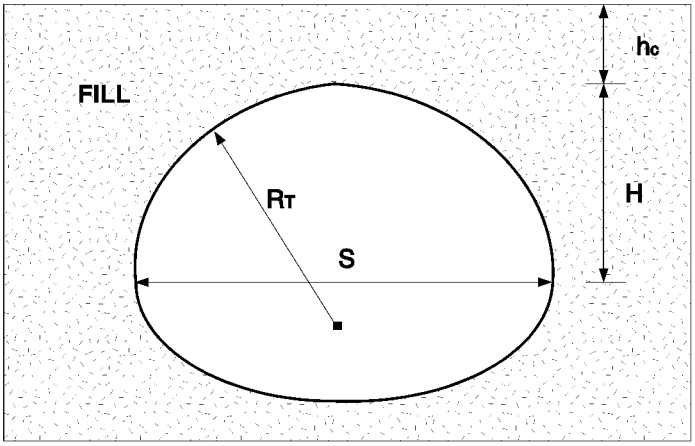

Figure 2.14: Value names used for buried pipe culverts. H is the rise, h_c is the cover height, $R_T$is the radius of the crown, and S is the span of the culvert

Table 2.8: Equations for the maximum thrust (T) according to different sources (after Vaslestad [92])

	Maximum thrust T (kN/m)
Ring compression theory '60	$\gamma_s \cdot h_c \cdot S/2$
AISI '84, AASHTO '83	$\gamma_s \cdot h_c \cdot R_T$
Ontario Highway Bridge Design Code OHBC '83	$\mu_1 \cdot \gamma_s \cdot h_c \cdot R_T$
SCI Duncan '83	$K_{p1} \cdot \gamma_s \cdot S^2 + K_{p2} \cdot \gamma_s \cdot S \cdot h_c$
Leonard's Method	$\gamma_s \cdot S(0.2H + 0.5h_c)$
S = diameter of the culvert / span H = rise / distance between top and level of the largest span R_T = radius of the crown $K_{p1} = 0.2H/S$	h_c = depth of overburden γ_s = unit weight of soil μ_1 = arching factor $K_{p2} = (0.9 - 0.5)H/S$

The maximum thrust on buried pipe culverts according to different sources is summarized in Table 2.8. Figure 2.14 shows the value names for buried pipe culverts that will be used throughout this thesis.

If the design is made by ring compression theory, no deflection criterion is included. Burns and Richard [18] developed a linear elastic solution for the deflection and pressure of pipes. They assumed the soil to be homogeneous, elastic and isotropic.

Some later model tests (by Meyerhof et al. [63]), however, introduced buckling of the culvert wall as another failure mechanism. They developed theoretical buckling criteria and used these for the design of larger flexible culverts. Luscher [59] in 1966 developed an equation for the critical pressure P, causing buckling. Both Meyerhof and Baikie as well as Luscher agree that the buckling strength of a buried circular conduit is proportional to the square root of the deformation modulus of the soil, and is inversely proportional to the square root of the radius. Chelapati and Allgood [2] also used the energy method and proposed a formula for the critical buckling stress by making modifications such that the influence of the surface boundary and soil parameters were included. They also pointed out the importance of the arching effect. Baikie et al. [7] in 1982 reviewed the different methods used to estimate the buckling loads and found that similar expressions have been developed by a number of investigators. The present differences are due to the manner in which the modulus of the deformation of soil is evaluated. After comparing several theoretical models for buckling prediction, Moore [65] concluded that linear "multiwave" buckling solutions based on the elastic continuum representation is the most suitable for the structural analysis and design of buried flexible tubes.

E', which is the basic influential soil factor in the Iowa deflection formula, is not a true soil modulus. It is a parameter which depends on the deflection and the actual pressure developed around the pipe. This makes it an empirical modulus that can only be obtained by field measurements.

According to Hartley and Duncan [41], Krizek et al. (1971) found out that E' substantially controls the pipe deflection, because the stiffness of the pipe has little effect. they also stated that E' varies with the soil type and degree of compaction.

Many researchers (by 1972 at least) had solved buried structure problems by experimental studies. Nielson [68] categorized these studies into model studies and field or full-scale tests.

Field Tests Nielson [68] samples some of the field and full-scale tests such as

- determining the pressure on the culvert and the corresponding displacement,
- determining the maximum load that a culvert can carry,
- determining how large a culvert can be installed without failure,
- employment of different backfill designs including the imperfect ditch method and variations,
- reconstruction of a full size culvert and instrumentation of the culvert such that pressure and deformation measurements could be taken (the results were compared with the Marston-Spangler theory),

- full-scale tests for determination of failure,
- large span culvert tests,
- plastic pipe tests, and
- tests for obtaining possible design procedures.

Model Tests Model tests are usually used for determining the key parameters and demonstrating their influence. They are good for representing complex problems which cannot be evaluated by analytical solutions but have limitations in the quantitative prediction of the full-scale performance in the field because of the difficulties in modelling field conditions.

A model system is formed by establishing *similitude requirements* which are derived from all the variables that influence the system. This procedure consists of introducing dimensionless pi-terms which are derived by using primary independent variables, and comparing the results with the full-scale case which is supposed to have the same pi-terms. The model must be designed so that the individual pi-terms for the model are the same as for the prototype structure. In this way, the results, regardless of the size, will also be the same. Examples which demonstrate this can be obtained from Nielson [68].

According to Nielson [68], model studies have been carried out under many different subjects such as

- deflections under high fills,
- wall buckling,
- dynamic loading,
- effect of soil density and moisture on culvert deflection,
- effects of backfill density on stresses in the pipe,
- imperfect ditch method of construction,
- multiple pipe installations,
- pressure distribution on pipe,
- determination of soil properties, and
- many more special problems.

Nielson [67] concluded that the modulus of soil reaction can be approximated by

$$E' = k \cdot M_s$$

where M_s is the constrained modulus and k is a factor depending on pipe-soil stiffness and Poisson's ratio. k varies between 0.7 and 1.5.

Allgood and Takahashi [2] studied culverts in embankments proposing a design method which deals with arching and maximum induced moments as well as many possible failure mechanisms. They stated that it is more desirable to use the constrained modulus, M_s, instead of E' in the determination of arching.

The historical background of buried structures until 1968 was briefly covered by Linger [57]. Taking culvert design as the main point of interest, Linger implemented the topic in classical concepts and phenomenological concepts.

In 1974, Parmelee et al. [70] made some efforts in the analytical and experimental evaluation of the modulus of soil reaction E'.

Hartley and Duncan [41] stated that E' is a function of the depth and tends to increase with the depth. It was also established that for the loading conditions adjacent to a buried flexible pipeline, $E' \cong M_s$.

Duncan [27, 28] carried out a finite element analysis where nonlinear relationships for the backfill soil were used. The result of this study is used to obtain design coefficients for ring compression and bending moments. Finally the soil-culvert-interaction method (SCI) was introduced. This design method will be detailed later in Section 2.2.3.

Duncan [28] states that ring compression and flexure are the two major modes in the metal culvert soil interaction. Under shallow cover, during backfilling or under live loads, the flexural stiffness and moment carrying capacity are required to prevent the culvert from collapsing. Under deep cover, however, culverts are able to resist imposed backfilling and highway traffic loads entirely through ring compression, provided that the backfill quality is good. The structure is said to be under deep cover if the cover depth, h_c, is bigger than one fourth of the culvert span, S. In other words, when $h_c \geq 0.25 \cdot S$ only ring compression needs to be considered, and when $h_c < 0.25 \cdot S$ the moments in the structure should also be evaluated to check that the structure has sufficient moment capacity to endure the imposed loads.

Duncan et al. [32] extended the work on culverts by working on corrugated metal box culvert structures. They obtained design bending moments for different spans, cover depths and loads by means of the finite element method. Results were then compared by field loading tests. According to the finite element analysis the bending moments in box culverts with spans up to 8 m under a variety of cover depths and live loads were formulated (see section 2.2.3). It was concluded that only the bending moments need to be considered at the design and that the culvert rise does not have a considerable effect on moments due to live load.

Seed et al. [75] made field measurements on long span flexible metal culverts during backfill operations and compared them with the results of conventional finite element analysis and finite element analysis with compaction effects (both using the hyperbolic analysis proposed by Duncan). They conclude that the compaction induced soil pressures have an undeniable effect on the deformations and final state

of stress of the culvert structure.

Sharma et al. [76] performed a finite element analysis of a rib-reinforced, long span steel arch culvert. Simulations of the construction phases were also done. Three types of soil (good, average and poor) were used at the analysis. The comparison of displacements, thrust, and bending moments at element nodes, revealed that the calculated factors of safety were larger than the design values. The computed deformation was found to be less than the observed deformation. They concluded that slight deformations do not significantly affect the stability of the culvert.

According to the report by Payne [71] of the ICE panel discussions on aspects of soil structure interaction, the following conclusions were obtained:

- Undertaking a simple analysis as reliance upon a sophisticated analysis in isolation is fraught with difficulties.
- Any analysis is only as good as its input data.
- Site investigation data can be erroneous and should be thoroughly studied.
- Sophisticated analysis is excellent at showing trends rather than an absolute value.
- A structure cannot be analyzed before it has been designed.

The problems and limitations in applying ground structure interaction according to the same report are

- nonlinear stress strain behavior of soil,
- time dependent drainage and creep behavior,
- natural variability,
- inadequate ground investigation,
- 2D idealization of 3D problems,
- controlling construction sequence, and
- idealization of structure.

McCavour et al. [62] performed measurements on two 12-m span corrugated steel box culverts with a minimum cover of 300 mm. The measurements were then compared with the results from a finite element model analysis. The tangent Young's modulus, which was proposed by Duncan, was used. They concluded that the response of the culvert to the applied static load is strongly influenced by the compactness of the soil. Displacements were reduced by a factor of 3 as the densification increased.

Moore and Taleb [66] analysed the live-load response of a 9.5 m span and 3.7 m rise metal arch culvert. As a result of the comparisons of 2D analysis with the measured data, it was concluded that 3D-modelling, hence analysis avoiding equivalent line load is important. The linear elastic finite element approach was found to underestimate live-load thrusts. The reason for this was predicted to be overestimating the stiffness of the soil lying over the culvert (by means of neglecting the shear failure in the soil).

Taleb and Moore [85], with the belief that the behaviour of shallow buried structures can be significantly influenced by the process of backfilling, also investigated the response of the same culvert to earth loading and compared their results with field measurements that were reported by Webb et al. [98]. Their FEM model aimed at compensating for the limitations (such as the effect of soil compaction on culvert response) of the previous FEM models of the same kind of structures. This was achieved by loading and unloading each layer of the backfill with an artificial surcharge. The elastic-plastic soil model with a linear variation of the elastic modulus with depth was adopted for improving the predictions. Pre-test calculations were compared with the field measurements in order to improve the analysis model. A new procedure was developed in the light of these comparisons. The analysis revealed the following results:

- The bending moments and deformations during backfilling were successfully predicted.
- The shear strength of the soil is fully mobilized.
- The compaction model has little effect on stress predictions.
- The type of the backfill had an effect on deformations and bending moments but not on the final soil stresses and thrust.

Webb et al. [98] report that most of the crown rise during backfilling resulted from the placement and the spreading rather than the compaction of the backfill. The live load effects were found different from the current design. The actual pressure distributions generate large moments that could be the controlling factor for shallow cover culverts.

Manko et al. [60] carried out static load tests done on two box culvert road bridges that are made of corrugated steel plates. The bridges, which have span lengths of approximately 12.3 and rises of 3.85 m and 4.75 m, were constructed over the Bystrzyca Dusznicka River in Poland. Their findings showed that the measured displacements were up to 30 % less than calculated. The permanent deflection during construction was not more than 25 % of elastic deflection. Static tests also witnessed permanent deflection which was believed to be partly the deformation of load carrying structures and partly the sagging of the continuous footings and some readout errors. According to them, the calculated values were conservative because the calculation methods assumed smaller steel stiffness and less interaction between soil and the steel structure. It was also noted that the road pavement had an effect

of distributing loads on to larger surfaces than in calculations. Normal stresses were also found significantly less than theoretical values.

Similar work with the addition of dynamic tests has been carried out again by Manko et al. [61] on a steel box culvert over Gimån in Sweden. Dynamic coefficients from these tests were found to be smaller than standards.

Bayoğlu Flener [10] analysed the performance of a long span corrugated steel culvert railway bridge under construction and in service. Dynamic tests were carried out measuring strains and deformations. Temperature readings were taken along with the measurements during the process of compaction of the backfill material. Comparisons of moments during compaction showed that there was a good agreement between the test results and theoretical values. There was however a considerable discrepancy in axial forces during compaction. This was believed to be due to the vast temperature differences between readings that could not be compensated. The theoretical calculation of the rise of the crown during compaction was found to be conservative when it comes to arch structures. The theoretical calculation of the crown moment due to live load seemed to be conservative too, while the theoretical axial force reasonably agreed with the measured axial force.

2.2.3 Design of Culverts

In this section only the design elements regarding soil-structure interaction will be presented. In other words soil pressure will be our main concern.

Design of reinforced concrete box culverts

Tadros et al. [83] made a survey of the United States highway departments and presented a current state of the art of reinforced concrete box culvert design in the USA. At the time of the survey the AASHTO specifications recommended the usage of a vertical pressure of 19.2 kN/m^2 and a horizontal soil pressure of 4.8 kN/m^2 equivalent hydrostatic pressure for the design of RC box culverts. The used design values for horizontal soil pressure showed quite a variety among the States. Starting from 4.8 it increases up to 6.4, 9.6 and 14.4 kN/m^2 in some of the States. According to Tadros et al. [83] four groups of researchers conducted projects which have included field tests. Considering field observations and the survey done, the following results were obtained:

- A big amount of soil friction, which applies a downward drag that causes an increase in the bottom pressures, was observed.
- For most of the pipe and arch structures, the vertical pressures changed negligibly as horizontal pressures increased with time.
- Horizontal and vertical loads were not symmetrical about the culvert vertical centerline.

- Both horizontal and vertical loads were higher than the AASHTO design loads. This implies that AASHTO underestimates the soil pressure on RC box culverts.
- Improvements that would result in safer and more economical culvert structures can be done.

Tadros et al. [84] verified the tendency of pressures being higher than the AASHTO values by means of an extensive computer analysis using the CANDE software. They also proposed formulas for estimating soil pressures on the culvert. For silty sand for example the horizontal pressure would be calculated using an earth pressure coefficient of 0.567, which resulted in a considerably larger soil pressure distribution compared to AASHTO.

Design of steel culverts

Duncan has proposed a design method for metal culverts, called the "soil culvert interaction method" (SCI) as mentioned in Section 2.2.2 (see also Duncan et al. [27, 28]).

According to this method, the maximum ring compression force, T, is calculated from:

$$T = K_{p1} \cdot \gamma_s \cdot S^2 + K_{p2} \cdot \gamma_s \cdot h_c \cdot S + K_{p3} \cdot LL \tag{2.12}$$

where:

T	=	ring compression force (kN/m)
K_{p1}	=	ring compression coefficient from backfill = 0.2 H/S
K_{p2}	=	ring compression coefficient for cover = 0.9-0.5 H/S
K_{p3}	=	ring compression coefficient for live load (dimensionless)
γ_s	=	unit weight of the backfill soil (kN/m^3)
S	=	span (m)
h_c	=	cover depth (m)
S	=	span (m)
LL	=	live load (kN/m)

This method also takes moments into account. The maximum bending moment value that was used in this design method was related to the relative stiffness of the backfill and the culvert by means of a dimensionless flexibility number. The flexibility number (N_f) which is given by Equation 2.13 provides the value of the moment coefficient that is used to calculate the maximum moment at the quarter point. In this way, the interaction between the culvert and the surrounding soil was included in the design by using stiffness values of both materials.

$$N_f = E_s \cdot \frac{S^3}{E_{st} \cdot I_{st}} \tag{2.13}$$

where:

N_f = flexibility number of the culvert (dimensionless)
E_s = secant modulus of the soil at quarter point level (MPa)
E_{st} = elasticity modulus of the culvert (MPa)
I_{st} = moment of inertia of the culvert (m^4/m)
S = span of the culvert (m)

The values for the elasticity modulus of the culvert (E_{st}), the moment of inertia of the culvert (I_{st}), and the span of the culvert (S) are readily available while the modulus of soil (E_s) is much more complicated to obtain since the stress strain behavior of soils is non-linear and stress dependent. The E_s values were evaluated by studying a large number of soils and approximate relationships between E_s and backfill depth were proposed. Curves for the soil types GW, GP, SW, and SP were plotted.

The maximum bending moment for cover-depth = 0 is:

$$M_1 = K_{M1} \cdot R_B \cdot \gamma_s \cdot S^3 \tag{2.14}$$

where:

M_1 = maximum bending moment at $h_c = 0$ (kNm/m)
K_{M1} = moment coefficient (dimensionless)
R_B = moment reduction factor (dimensionless)
S = span of the culvert (m)
γ_s = unit weight of the soil (kN/m^3)

The total bending moment (at the quarter point) due to backfill and live load is:

$$M = M_1 - R_B \cdot K_{M2} \cdot \gamma_s \cdot S^2 \cdot h_c + R_L \cdot \ K_{M3} \cdot S \cdot LL \tag{2.15}$$

where:

M = total bending moment due to backfill and live load (kNm/m)
K_{M2} = moment coefficient (dimensionless)
R_L = moment reduction factor (dimensionless)
K_{M3} = moment coefficient (dimensionless)
γ_s = unit weight of the soil (kN/m^3)

Safety checks are done against wall compression failure and development of plastic hinge.

The SCI design also helps in the determination of the minimum depths of cover and the maximum fill heights.

Design of corrugated steel box culverts

These structures differ from conventional metal culverts by their large crown radius, straight sides and big span/rise ratio. The traditional design methods can be applied to structures that carry most of the load by arching action but not to metal box culverts. Duncan et al. [32] concentrated their efforts on defining a special design method for these box structures.

According to their method, the total moment due to backfill and cover loads is calculated as:

$$M_T = K_1 \cdot \gamma_s \cdot S^3 + K_2 \cdot \gamma_s \cdot (h_c - h_{cmin}) \cdot S^2 \tag{2.16}$$

where:

M_T	=	sum of the haunch and crown moments (kNm/m)
K_1	=	constant
K_2	=	constant
γ_s	=	unit weight of backfill
S	=	span (m)
h_c	=	cover depth (m)
h_{cmin}	=	minimum cover depth (m)

The bending moment due to live load is:

$$\Delta M = K_3 \cdot LL \cdot S \tag{2.17}$$

where:

ΔM	=	moment due to live load (kNm/m)
K_3	=	coefficient depending on the h_c/S ratio (dimensionless)
S	=	span (m)
LL	=	live load (kN/m)

2.3 Analysis of Soil-Structure Interaction

The analysis of soil structure interaction can be carried out using hand calculations, published results, simple modelling, model tests and numerical models. Examples are: earth pressure theory, limit analysis, characteristics, limit equilibrium, theory of elasticity, finite elements, finite differences or boundary elements.

Soil structure interaction problems are usually handled by iterative methods. These iterations usually involve an assumption of the stiffness (soil stiffness) of the system. Then an initial value for the deflection can be chosen and forces can be calculated accordingly. The system can then be analyzed by using these forces, which give new deflections. New deflections can lead to adjusting the forces to be used in the

analysis again to get new deflection values. The iterations can then be continued to converge to one deflection value.

Numerical methods made it possible to apply the rules of mechanics to even very complicated problems of soil-structure interaction. It needs a very detailed subsoil investigation and reliable input data, especially if all the stresses and strains of the subsoil are needed for the final engineering decisions as in the case of dams and tunnels etc. The finite element method is believed to be the numerical method which is capable of making the most realistic predictions of deformations and failure mechanisms.

2.3.1 Earth Pressure Theory

Earth pressure calculations aim at demonstrating the geometry and loading where equilibrium of a soil structure is held where the pattern of stresses through the soil would nowhere cause failure in the soil.

2.3.2 Limited Analysis

Limited analysis solutions are derived from bounds theorems of plasticity. (This can be followed from Chen [22].)

2.3.3 Characteristics

Characteristics are lines throughout a region of plastic soil along which the governing partial differential equation may be converted into total differentials and solved more readily. See Sokolovski [77].

2.3.4 Limit Equilibrium

Potential failure mechanisms are examined and it is shown that the forces tending to cause failure are held in equilibrium by the available shear strength in the soil. Several trial mechanisms should be examined.

2.3.5 Elasticity Theory

The theory of elasticity solutions assume that the soil is a linear elastic continuum (not necessarily homogeneous or isotropic). Various solutions for stresses and deformations caused by applied loads can then be derived from the theories of elasticity.

2.3.6 The Finite Element Method (FEM)

Finite element analysis involves the division of the soil into discrete elements in which simplified material properties and deformation behavior are specified. Individual element stiffnesses are derived and assembled to yield a global system of equations which together with the boundary conditions can be solved to yield displacements, strains and hence stresses throughout the region.

FEM is well suited for problems in which the constitution of the material is complex, FEM is very flexible and can be applied to more generalized soil models than those acceptable when using the other methods (BEM, isotropic elastic half-space or the Winkler model). However when the material is linear elastic, it is unnecessary to put finite elements in the interior, since, when the boundary conditions are known, the stress and displacement fields in the interior can be found through fundamental solutions.

The two major approaches in finite elements are the discrete and composite representations. In the discrete representation all the elements of the system are modelled distinctly. In the composite representation different material properties are assigned to different regions.

2.3.7 The Boundary Element Method (BEM)

Boundary element analysis transforms the governing differential equations into integral ones which are then solved numerically on the boundary region. The number of physical dimensions to be considered is reduced by one, resulting in a smaller system of fuller equations and a more efficient solution.

It is a numerical technique which is closely related with FEM. Only boundary functions need to be approximated and solved. In BEM, both the stress end displacement vectors on the boundary are both primary unknowns and, consequently, of equal accuracy. The stress end displacement in interior points are calculated exactly from the given boundary values. BEM gives the possibility of analyzing with infinite or semi-infinite domains, such as the soil in soil-structure interaction. Only the boundary must be considered by the user.

BEM is best suited to cases with homogeneous bodies. Anisotropy, nonlinear elasticity, visco-elasticity, plasticity can be included by use of internal cells but the method loses its advantage over FEM.

2.3.8 Combined FEM and BEM

The coupling of finite elements and boundary elements is a fruitful technique when considering large or infinite domains with a linear behaviour in the main part and a non-linear behavior in a small part. Advantages are: less time for preparing the data, reduced computer costs and more accurate results.

2.4 Soil Modelling

One of the key points in soil structure interaction is to evaluate the behaviour of soil under external loads. For this, complete stress strain characteristics of the soil should be known. But it is extremely difficult to take into account all the material properties of the soil medium considering that there are many different factors affecting these characteristics, like the size and shape and properties of every single soil particle, as well as moisture content and stress history. So an idealisation of the soil for the response of the soil medium but not for the response of the individual soil elements is necessary. Soil modelling should be as realistic as possible. Field testing and sampling play a very important role in obtaining accurate soil properties.

Since designers are more interested in the stresses and strains in the soil around the structures to be designed, but not in the whole medium, the tendency was to model the soil by surface deflection due to external forces (namely forces coming from the structure).

The simplest one of the linear elastic models is the *Winkler soil model* where soil is idealized with springs with spring constant k which is known as the modulus of subgrade reaction. The pressure p at the soil surface is

$$p = k \cdot d$$

where d is the deformation at the foundation surface. The deflection at one level of wall is not presumed to affect the value of the reaction force at another level.

The other extreme of the elastic soil approach takes into account the influence of the loading on the displacement at any point in the medium. The solution of the elastic half space soil for point loads on the surface is done thorough formation of stiffness and flexibility matrices for the soil.

Non-linear elastic soil models are considered to be more realistic. The method is to modify the material parameters from the theory of linear elasticity in an incremental manner to follow anon-linear material behavior. The material parameters are often taken to be functions of the current stress state.

According to Springman et al. [78] the most suitable soil model would be a hyperbolic, hysteretic, and constitutive model.

The hyperbolic model, which is briefly mentioned in sections 3.2.1 and 3.2.2, has been used by may researchers and reported to have provided reasonable results at low stress conditions (relative to the failure stresses). This model does not take plasticity into account despite making use of ϕ and c parameters of the soil (see Bull [14]).

Another popular model is the elastic-perfectly-plastic model. Either the Drucker-Prager or the Mohr-Coulomb yield criterion can be used (see Bull [14]).

With plasticity models, the stress history and stress paths in a body can be considered. This model makes use of yield surfaces for describing the state at different

regions within the body. The material is said to be plastic in regions where the state of stress corresponds to points on the predefined yield surface, and elastic in other regions.

The enlarged understanding of the nonlinear stress-strain behaviour of the ground reveals that it is improper to represent the soil response with a single stiffness value. A proper analysis should take into account the whole soil-structure system.

A three-dimensional analysis of the whole system brings up a huge amount of computations. This difficulty made researchers reduce the problem into simpler yet precise for the case problems by using soil models. Kolar and Nemec [48] worked on an *efficient subsoil model* which would put a bridge between the simple (Winklerian) and full-scale approach. They aimed at a model which is simple enough for straightforward cases and also suitable for more complex analysis. Their 2D model was described by a set of constants namely the foundation compression modulus, the foundation shear moduli and the foundation friction moduli. A more sophisticated model included some further unknown factors like the settlements under the soil surface.

Chapter 3

Stiffness Characteristics for Soil-Structure Interaction

The modulus of elasticity (E) of soil is a very important parameter that affects the response of the soil structure system. The correct determination of the stress strain behavior of the soil surrounding buried structures is essential. This chapter will discuss various ways of obtaining the elasticity modulus. Some recently proposed methods for evaluating E will also be demonstrated. Some numerical comparisons will be conducted to demonstrate the relevance of these different methods.

Section 3.1 gives some basic definitions for soil properties that will be used throughout this chapter. In section 3.2 some methods for determination of the elasticity modulus are briefly described. Some recommended E values are also provided in this section. In section 3.3 some of the methods, which would particularly apply to the design of culverts, and some more general methods are studied in more detail. With the help of numerical examples, Duncan's proposal, two proposals from Pettersson et al. [72], the Lehane et al. [56] formulation, which was proposed for the usage of numerical analysis of integral bridge abutments, and another general formulation proposed by Lade et al. [54] are compared.

The reader should note that the term E will be used for general comments and will most of the time refer to E_s for which most of the equations are given.

3.1 Definitions

Modulus of elasticity or stiffness or Young's modulus (E): For any material, E is the ratio of stress to strain. It is expressed in units of stress and is constant for elastic materials and variable for soils.

Secant modulus (E_s): Elasticity modulus that is determined for inelastic materials from the stress-strain curve. It is the slope of the line that connects the origin to a stress point on the curve (usually half of the maximum stress level).

Table 3.1: Particle size classification of soils

Particle size ranges according to Craig (1987), Das (1985), Geoteknik (1984)											
Clay	Silt			Sand			Gravel			Cobbles	Boulders
	Fine	Medium	Coarse	Fine	Medium	Coarse	Fine	Medium	Coarse		
	0,001	0,006	0,02	0,06	0,2	0,6	2	6	20	60	200
Particle size (mm)											

Tangent modulus (E_t): Instantaneous slope of the stress-strain curve.

Initial tangent modulus (E_i): Initial slope of the stress-strain curve.

Bulk modulus (B): Ratio between the hydrostatic pressure and the corresponding volume change (in case of isotropic compression).

Constrained modulus (M_s): is obtained from consolidation tests where lateral strains are not permitted. M_s is suitable for determining the settlement of a uniformly loaded large area but not appropriate for use in a two or three-dimensional problem.

Shear modulus (G): is equal to the shear stress divided by the shear strain. Also called "modulus of rigidity".

Poisson's ratio (ν): is the ratio of strain in perpendicular directions to the strain in the direction of the load.

Soil compaction: is a way of increasing the stability and the load bearing capacity of soils. Soils can be compacted to a specified standard by means of rollers, vibrators and rammers. The compaction characteristics of a soil can be obtained from standard compaction tests. For a particular compactive effort there is a particular value of water content where the maximum dry density level is reached. The degree of compaction (RP) of a soil is measured in terms of dry density. The required standard of compaction in the field can be specified in terms of a percentage of the maximum dry density obtained in one of the standard laboratory tests (for instance, the Standard Proctor Test).

Particle size classification of soils: The most generally used particle size ranges in classification of soils are shown in Table 3.1.

Soils can also be classified according to their particle size distributions. These distributions are curves plotted on a semi-logarithmic scale and are given after conducting a sieve analysis where the percentage by weight is calculated within different particle size ranges. The particle size corresponding to any specified value on the "percentage smaller" scale can be read from these curves. d_{10} is the particle size where 10 %, by weight, of the particles are smaller. It is called the effective size. d_{60} is the size where 60 %, by weight, of the particles are smaller. The uniformity coefficient (C_u) is d_{60}/d_{10}. The coefficient of curvature (C_c) is $d_{30}^2/(d_{60} \cdot d_{10})$. They can be used to classify soils in the Unified Soil Classification System (see Bowles [11]). Table 3.2

Table 3.2: Classification according to the Unified Soil Classification System

Gravel		Sand	
$C_u < 4$ $1 < C_c < 3$	$C_u > 4$ otherwise	$C_u < 6$ $1 < C_c < 3$	$C_u > 6$ otherwise
Well graded GW	Uniform Poorly Graded GP	Well graded SW	Uniform Poorly Graded SP

demonstrates the classification for gravel (G) and sand (S), where W stands for "well graded" and P for "poorly graded".

3.2 Methods for the Determination of the Elasticity Modulus

3.2.1 History

It is difficult to obtain the correct value of E since it increases with the depth of soil, i.e., the effective overburden pressure.

The elasticity modulus determined from triaxial tests in relation to the confining pressure was given by Das [24] as:

$$E \propto {\sigma_0}^{0.5} \tag{3.1}$$

where:

σ_0 = confining pressure

Since the stresses in soil in the field are not isotropic before loading, E is proportional to the square root of the mean principle stress:

$$E \propto \sqrt{\sigma_v \left(\frac{1 + 2K_0}{3}\right)} \tag{3.2}$$

where:

σ_v = effective overburden pressure before loading
K_0 = in-situ lateral earth pressure coefficient

Konder et al. [49], [50] suggested that the stress-strain curves could be approximated by a hyperbole (see Figure 3.1). The hyperbole is expressed by:

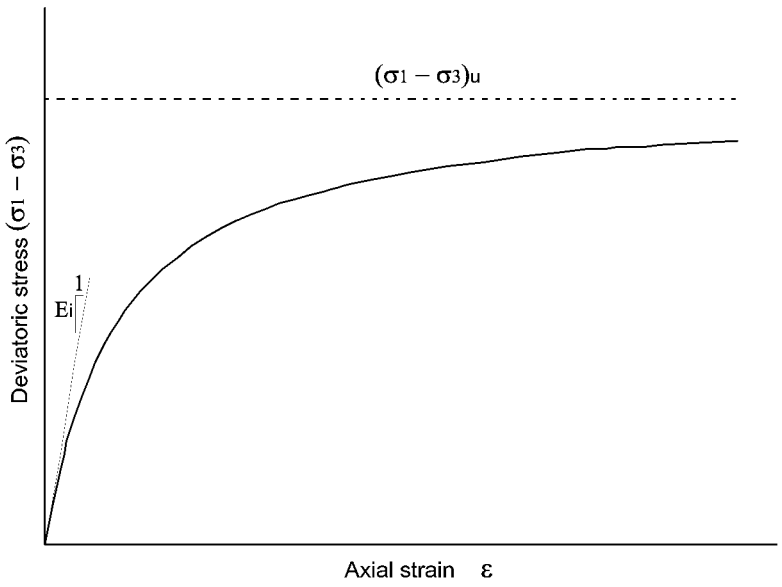

Figure 3.1: Hyperbolic representation of stress-strain relationship (from [103])

$$(\sigma_1 - \sigma_3) = \frac{\varepsilon}{\frac{1}{E_i} + \frac{\varepsilon}{(\sigma_1 - \sigma_3)_u}} \tag{3.3}$$

where:

σ_1	=	normal pressure
σ_3	=	confining pressure
ε	=	normal strain
$(\sigma_1 - \sigma_3)_u$	=	ultimate deviatoric stress
E_i	=	initial tangent modulus

For most soils E_i and $(\sigma_1 - \sigma_3)_u$ depend on the level of confining pressure σ_3. They tend to increase with the confining pressure.

One empirical expression for the initial tangent modulus, which has been found very convenient by researchers and was reported by Janbu [45], is:

$$E_i = m \cdot p_a \cdot \left(\frac{\sigma_3}{p_a}\right)^n \tag{3.4}$$

where:

m	=	experimentally obtained modulus number
n	=	experimentally obtained stress exponent
p_a	=	atmospheric pressure
σ_3	=	confining stress in triaxial test

Table 3.3: Some typical values for modulus of elasticity from different sources

Soil Properties and Conditions		**Recommended E values (MPa)**				
		Das '85 & '99	Bowles '88	Hartley et al.'87	Duncan '78	Lehane et al. '99
Sand	coarse	32.4 - 45.2		(modulus of		
	fine	23.5 - 36.6		soil reaction)		
	loose	10.35 - 24.15	10 - 25			
	dense	34.5 - 55.2	50 - 81			
Sandy silt		10.0 - 13.8	5 - 20			
Sand and Gravel [25]	loose	69 - 172	50 - 150			
	dense		100 - 200			
GW GP SW SP	0 - 15			5 - 17	2.5 - 12.5	
depth of cover (m)	5 - 10			7 - 23		
	10 - 15			7.25 - 25		
	15 - 20			7.5 - 26		
Sand and Gravel	γ=0.01% p'=100					200 - 500
Shear strain (γ) and	γ=0.01% p'=50					150 - 450
Mean effective stress (p')	γ=0.1% p'=100					80 - 200
	γ=0.1% p'=50					50 - 150

The parameters m and n are dimensionless and their values are the same for any system of units. For sands and silty sands the value of n varies between 0.35 and 0.55. The modulus number m was found to vary from 50 to 550 for the same type of material (see Janbu [45]).

This simple equation is widely used since it represents the elastic behavior observed in the triaxial isotropic compression and the material constants can be easily determined from conventional triaxial tests. However, Lade et al. [54] reports that this model violates the principle of conservation of energy.

Krizek et al. [51] suggested that the E of a compacted soil might be a unique function of overburden pressure and dry density.

Due to the difficulty in obtaining undisturbed samples from cohesionless soils many researchers attempted to correlate E with results from field explorations such as the cone penetration test (CPT) and the standard penetration test (SPT) results. The E formulations from such field tests by various researchers are summarized by Das [24] (pp. 359–361) and Tomlinson et al. [91] (pp. 67–69).

Some typical values for E of frictionless materials are summarized in Table 3.3.

3.2.2 Hyperbolic Stress-Strain Model by Duncan et al.

An hyperbolic stress-strain relationship was developed by Duncan et al. [29]. They expressed the non-linear stress-strain relationship by means of an incremental analysis where each increment is considered linear and is governed by Hook's law.

The hyperbolic stress-strain equation (Equation 3.3) was taken as the basis to this approach.

The failure deviator stress $(\sigma_1 - \sigma_3)_f$ is related to the confining pressure σ_3 by the use of the stress difference at failure and the Mohr-Coulomb strength equation:

$$(\sigma_1 - \sigma_3)_f = \frac{2c\cos\phi + 2\sigma_3 \sin\phi}{1 - \sin\phi} \tag{3.5}$$

The failure deviator stress $(\sigma_1 - \sigma_3)_f$ observed from triaxial tests can be compared with the ultimate deviator stress $(\sigma_1 - \sigma_3)_u$. The relation between the two is called the failure ratio:

$$R_f = \frac{(\sigma_1 - \sigma_3)_f}{(\sigma_1 - \sigma_3)_u} \tag{3.6}$$

where:

R_f = failure ratio
$(\sigma_1 - \sigma_3)_f$ = failure deviator stress
$(\sigma_1 - \sigma_3)_u$ = ultimate deviator stress

The tangent modulus (E_t), which is the instantaneous slope of the stress-strain curve, is then obtained by differentiating Equation 3.3 with respect to the strain (see also Wong et al. [102]):

$$E_t = \frac{\partial(\sigma_1 - \sigma_3)}{\partial\varepsilon} \tag{3.7}$$

which results in the following once Equation 3.6 is inserted:

$$E_t = \frac{\frac{1}{E_i}}{[\frac{1}{E_i} + \frac{R_f \cdot \varepsilon}{(\sigma_1 - \sigma_3)_f}]^2} \tag{3.8}$$

In order to achieve a more general and useful expression for E_t Equation 3.8 is made independent of the strain by rewriting Equation 3.3 in terms of strain ε and substituting this back into the Equation 3.8:

$$E_t = \left[1 - R_f \cdot \frac{(\sigma_1 - \sigma_3)}{(\sigma_1 - \sigma_3)_f}\right]^2 \cdot E_i \tag{3.9}$$

Once the previously determined Equations 3.4 and 3.5 are also substituted, the formula for E_t takes its final shape:

$$E_t = \left[1 - \frac{R_f \cdot (1 - \sin(\phi)) \cdot (\sigma_1 - \sigma_3)}{2 \cdot c \cdot \cos(\phi) + 2 \cdot \sigma_3 \cdot \sin(\phi)}\right]^2 m \cdot p_a \cdot \left(\frac{\sigma_3}{p_a}\right)^n \tag{3.10}$$

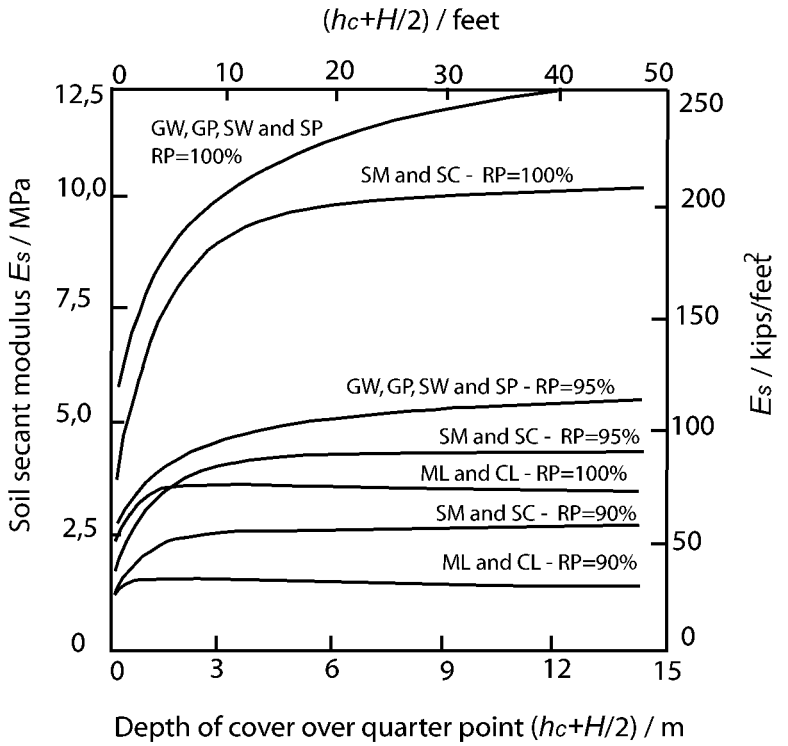

Figure 3.2: Approximate secant modulus for various types of backfill soil (to be used in the SCI method), redrawn from Duncan [27]

where n and m are Duncan's version of the modulus number and stress exponent. The value of R_f varies from 0.5 to 0.9.

3.2.3 Secant Modulus for the SCI Method by Duncan et al.

Duncan has proposed curves for the secant modulus E_s of the backfill soil. They are used for the design of metal culverts. This design method is the soil-culvert interaction method (SCI), which was previously explained in Section 2.2.3.

The E_s values were evaluated by studying tests done on over 100 different soils. The E_s values that represent the behavior of soil under the stress conditions that exist around flexible metal culverts were picked. The results of a large number of finite element analyses also showed that E_s at the depth of the quarter point of the culvert $(H/2 + h_c)$ is approximately the average value for the backfill soil. So the curves were formed giving E_s values at the depth of the quarter point. From these curves E_s can be obtained for different compaction levels and soil grading (see Figure 3.2).

Note that the E_s values that can be obtained from these curves are case specific and

can only be used for calculating the N_f value in the SCI method.

3.2.4 Secant Modulus by Pettersson et al. (Method 1)

Pettersson et al. [72] evaluated a formula from Duncan's E_s curves (see section 3.2.3). The formula below is a mathematical approximation that aims to represent the Duncan's curves and to make calculations of E_s easier and more precise. Note that the elastic modulus is calculated at a depth of $h_c + H/2$.

$$E_s = 1.17^{(RP-95)} \left[0.82 \ln\left(h_c + \frac{H}{2}\right) + 3.65\right] \tag{3.11}$$

where:

E_s	=	secant modulus (MPa)
RP	=	degree of compaction (%) (standard proctor)
h_c	=	depth of cover over the crown (m)
H	=	rise (the vertical distance from springline to crown) (m)

The comparison of Equation 3.11 with the Duncan curves is given in Section 3.3.1.

3.2.5 Tangent Modulus by Pettersson et al. (Method 2)

Pettersson et al.'s Method 2 makes use of Duncan et al.'s formula (Equation 3.10) to calculate E_t in a more sophisticated way. In this case more soil parameters (such as ϕ, C_u, d_{50}, e, γ_s) are involved in calculating the elastic modulus of soil as compared to the E_s in Method 1. The difference between the tangent modulus and secant modulus should also be taken into account while comparing the two methods.

The following steps calculate E_t:

1. Void ratio:

$$e = \frac{G_s \cdot \rho_w}{\rho_d} - 1 \tag{3.12}$$

where:

G_s	=	specific gravity of soil (G_s=2.6)
ρ_d	=	dry density of soil (t/m^3)
e	=	void ratio
ρ_w	=	density of water (1 t/m^3)

2. Modulus number from Andreasson [3]:

$$m = 282 \cdot C_u^{-0.77} \cdot e^{-2.83} \tag{3.13}$$

where:

m = modulus number
C_u = uniformity coefficient
e = void ratio

3. Stress exponent from Andreasson [3]:

$$\beta = 0.29 \cdot \log\left(\frac{d_{50}}{0.01}\right) - 0.065 \cdot \log(C_u) \tag{3.14}$$

where:

d_{50} = particle size such that 50 % by weight of the particles are smaller (in mm)

4. Friction angle according to the Geotechnical Handbook [5]:

$$\phi = 26^\circ + 10 \cdot \frac{(RP - 75)}{25} + 0.4 \cdot C_u + 1.6 \cdot \log(d_{50}) \tag{3.15}$$

5. Relative density:

$$I_D = \frac{(RP - 75)}{25} \tag{3.16}$$

6. Poisson's ratio from Andreasson [3]:

$$\nu = \frac{1 - \sin(\phi)}{2 - \sin(\phi)} \tag{3.17}$$

7. Relation between the constrained modulus and the elastic modulus (see Chen [23], page 155):

$$E = K_\nu \cdot M_s \tag{3.18}$$

where:

M_s = constrained modulus of elasticity
K_ν = $(1 - \nu - 2 \cdot \nu^2)/(1 - \nu)$

8. Tangent modulus of elasticity:

Considering the above relationship, the tangent modulus of elasticity is derived from Equation 3.10. After several simplifications (see Pettersson et al. [72]) the formula can be expressed as:

$$E_t = 0.42 \cdot m \cdot K_\nu \cdot 100\text{kPa} \cdot \left(\frac{(1 - \sin\phi) \cdot \gamma_\text{s} \cdot \text{S}_\text{ar} \cdot (\text{h}_\text{c} + \text{H}/2)}{100\text{kPa}}\right)^{1-\beta} \tag{3.19}$$

Table 3.4: Recommended hyperbolic parameters by Duncan et al. [31]

	RP	γ_s kN/m^3	ϕ (deg)	m	$(1-\beta)$ or n	R_f
	105	23.5	42	600	0.4	0.7
GW, GP, SW and SP	100	22.8	39	450	0.4	0.7
Soils	95	22.0	36	300	0.4	0.7
	90	21.2	33	200	0.4	0.7

Note that the elastic modulus is calculated at a depth of $h_c + H/2$. Despite that the depth of the quarter point seems to determine the depth that the modulus is calculated at, this formula is much more general. Unlike Duncan's E_s curves, it is not aiming at some specific elasticity modulus value.

Table 3.4 gives the standard hyperbolic parameters for coarse aggregate soil groups (after Duncan et al. [31]).

3.2.6 Secant Modulus According to Lehane et al. (Method 3)

Lehane et al. [56] verify the tendency of E being proportional to the square root of stress at shear strain levels (γ) smaller than 0.1 %. They use the symbol p' for the mean effective stress. They report that E is directly proportional to p' at shear strains that are larger than 0.1 %. They also report that at a given density and stress level the stiffness reduces by a factor of 2 – 4 for each log cycle increase in shear strain above the linear elastic limit (0.001 % – 0.01 %).

Lehane et al. focus on the variation of the shear stiffness (modulus) G measured at shear strain levels of 0.001 % and 0.01 %.[1] E is then expressed in terms of G using the following relation (see Gere [37]):

$$E = 2 \cdot G \cdot (1 + \nu) \tag{3.20}$$

and Poisson's ratio is assumed to be equal to 0.3. Under the above conditions the following formula, which initially appears as Equation 2.3 in Chapter 2 of this thesis, but repeated here for convenience, for the secant modulus was proposed:

$$E_s = 150 \cdot F(e) \cdot \left(\frac{p'}{p_a}\right)^{0.5} \cdot \left(\frac{0.01}{\gamma}\right)^{0.4} \tag{3.21}$$

[1]The shear strain distribution imposed in the backfill is not constant. It varies from a maximum value at the abutment (of about the abutment displacement divided by the height above the point of rotation) to zero well away from the abutment. So there is no unique value of shear strain.

where:

E_s	=	secant modulus (MPa)
$F(e)$	=	$(2.17 - e)^2/(1 + e)$ normalizing function for shear stiffness
p'	=	mean effective stress (MPa)
γ	=	average shear strain level (%)
p_a	=	atmospheric pressure (0.1 MPa)

The mean effective stress (p') is the mean value of effective stresses acting in the three principal stress directions.

$$p' = \frac{(\sigma_v + 2 \cdot \sigma_3)}{3} \tag{3.22}$$

The upper bound of p' lies between 50 and 100 kPa. By means of inserting Equation 3.12 into Equation 3.21, the secant modulus expression can then be transformed into a new one such that it depends on the dry density rather than the void ratio. The plot in Figure 3.3 can be obtained with this new relation, using upper bound p' values of 50 and 100 kPa. The dashed curves for lower stress values (approximately for 1.5 m cover depth) were also found necessary and added by the author of this thesis.

3.2.7 Elasticity Modulus According to Lade et al. (Method 4)

Some researchers, including Panos et al. [69] and Liu et al. [58], agree that the elastic behavior of soils at any general state of stress can be adequately expressed by Young modulus suggested by Lade et al. [54]. The modulus, which is based on the principles of energy conservation,[2] is given as a function of the first stress invariant I_1, the second deviatoric stress J_2 and two dimensionless material constants N and λ:

$$E = N \cdot p_a \left[\left(\frac{I_1}{p_a} \right)^2 + R \cdot \frac{J_2}{(p_a)^2} \right]^{\lambda} \tag{3.23}$$

$$R = 6 \cdot \frac{1 + \nu}{1 - 2\nu} \tag{3.24}$$

$$J_2 = \frac{1}{6} \cdot [(\sigma_1 - \sigma_2)^2 + (\sigma_2 - \sigma_3)^2 + (\sigma_3 - \sigma_1)^2] \tag{3.25}$$

$$I_1 = \sigma_1 + \sigma_2 + \sigma_3 \tag{3.26}$$

[2]The principle of conservation of energy states that mechanical energy is neither generated nor dissipated in a closed loop stress or strain path.

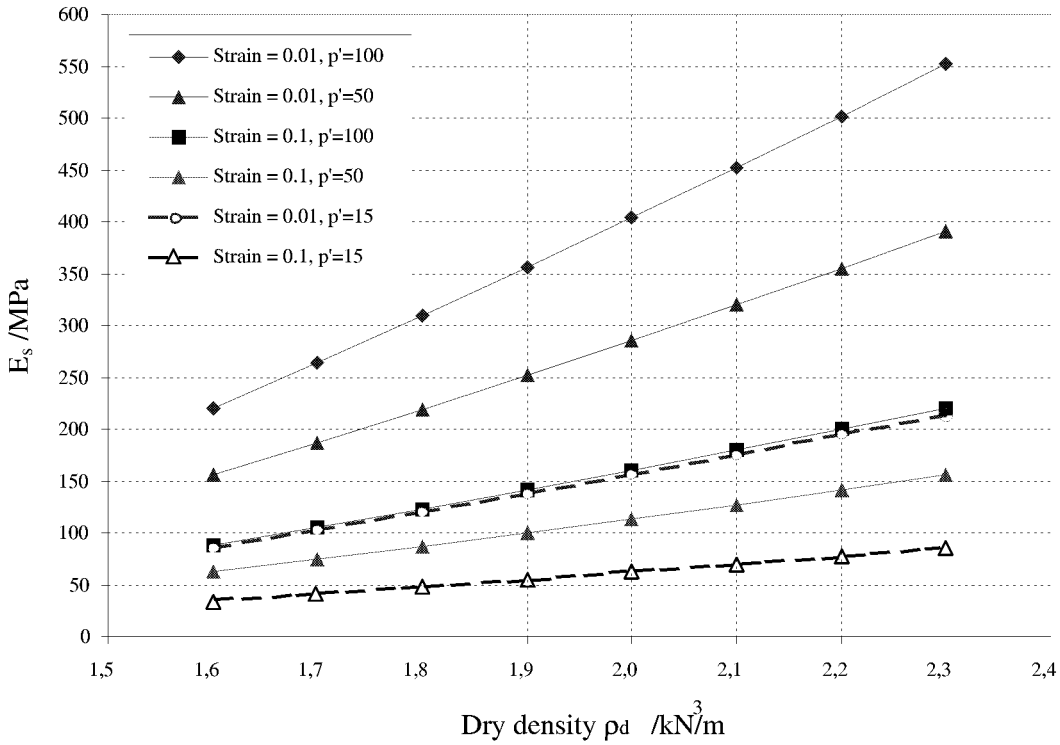

Figure 3.3: Secant modulus versus dry density of backfill soil, after Lehane et al. [56]

Table 3.5: Value range of the parameters used in Equation 3.23 (after Lade et al. [54])

N	λ	m (Equation 3.27)	n (Equation 3.28)
$440 - 1270$	$0.22 - 0.33$	$710 - 2310$	$0.44 - 0.66$

Table 3.6: Soil parameters chosen for comparison of the methods for calculating elasticity modulus

RP	90/95/100	ϕ	35.6/37.6/39.6
C_u	5.0	γ_{opt}	19.5 kN/m^3
d_{50}	1.0	β	0.53
$\gamma_s = RP \cdot \gamma_{opt}/100$	17.5/18.5/19.5 kN/m^3	m	646/1065/1829
e	0.48/0.40/033	H	2 m

In these formulations σ_1, σ_2 and σ_3 are the major principal stresses.

The parameters N and λ were determined using the stress paths from triaxial compression and three-dimensional cubic triaxial tests. The calculation of the elastic modulus was performed using stress paths lengths. Tests on different types of sands were performed to determine the parameter values. Table 3.5 summarizes the range of parameter values for different sands.

Equating Young's modulus from Equations 3.4 and 3.23 Lade et al. derived the following expressions for the modulus number m and the exponent n:

$$m = 3^{(2\lambda)}N \tag{3.27}$$

$$n = 2\lambda \tag{3.28}$$

3.3 Comparisons and Discussion of Methods

The above mentioned methods will be compared in the following sections. The effect of soil properties on the determination of the elasticity modulus is going to be emphasized. It is also important to agree on realistic soil parameters to be able to estimate stiffness in a realistic way. The soil parameters listed in Table 3.6 are used in the calculations. If additional parameters are going to be used, they will be announced in the relevant section.

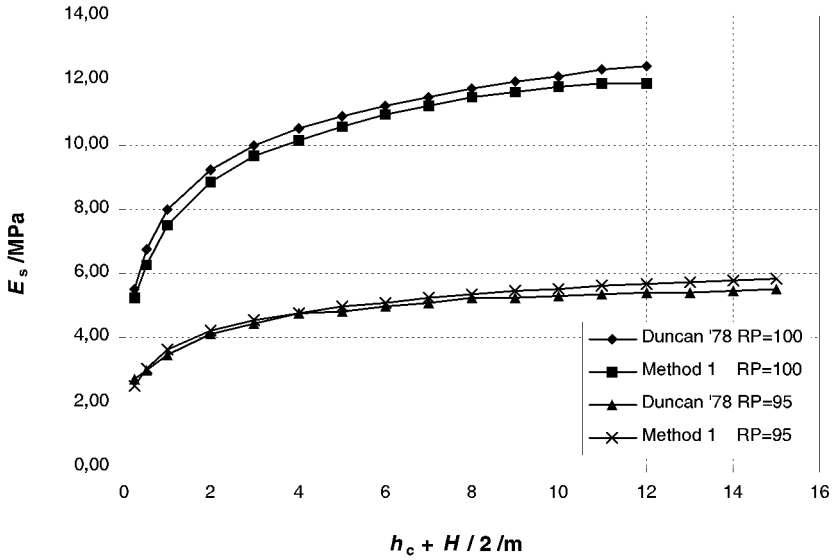

Figure 3.4: Comparison of Duncan's E_s curves with the formulation in Pettersson et al.'s Method 1. Only the curves for GW, GP, SW, and SP type of soils were compared

3.3.1 Comparison of Duncan's E_s Curves with Pettersson et al.'s Method 1

The E_s values were measured from Duncan's curves (see Figure 3.2) by means of fine-meshing and compared with the values obtained from Equation 3.10. In Figure 3.4 the agreement can clearly be seen. So the curves from Equation 3.10 can be said to be a good representation of Duncan's secant modulus curves.

3.3.2 Comparison of Methods 1 and 2 of Pettersson et al.

As explained before, the formula in Method 1 is a specific formula to predict the secant modulus of elasticity at the quarter point in a soil-culvert structure. Method 2 calculates the tangent modulus of elasticity in general. According to the author of this thesis it is possible to compare the two methods as long as the relationship between the secant modulus and the tangent modulus is considered.

$$E_t = 0.65 \cdot E_s \tag{3.29}$$

This relationship was derived using the theoretical equations in Section 3.2.2. The details of the calculations can be seen in Appendix A.

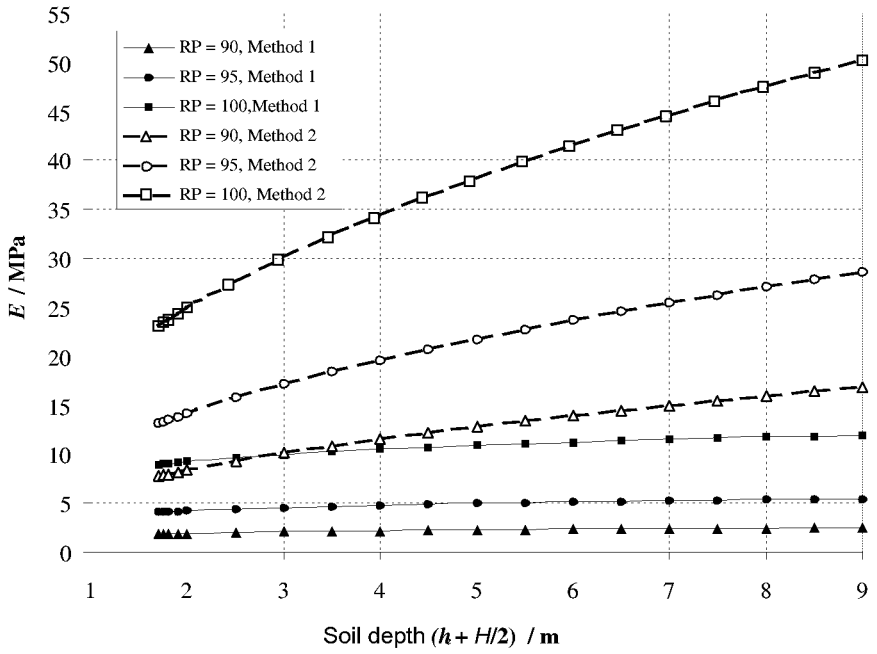

Figure 3.5: Elasticity modulus versus depth of soil cover. Comparison of Methods 1 and 2 of Pettersson et al. (Note that Method 1 calculates the secant modulus and Method 2 calculates the tangent modulus.)

Figure 3.5 shows the E_t and E_s values that were calculated according to Equation 3.11 (Method 1) and Equation 3.19 (Method 2) using the same soil properties and different degrees of compaction values (see Table 3.6).

As can be observed from Figure 3.5, Method 1 reveals considerably smaller E_s values compared to Method 2's E_t values. Considering that the secant modulus is larger than the tangent modulus, the difference is even more pronounced. The difference between the moduli calculated by these two methods is more enhanced as the cover depth increases. It can be concluded that Duncan's E_s values (that are to be used in the SCI method) are much more conservative compared to the E_t values calculated by hyperbolic equations.

The first method is more conservative compared to the second one since it assumes soil to be less stiff. This can lead to over-design of the structure.

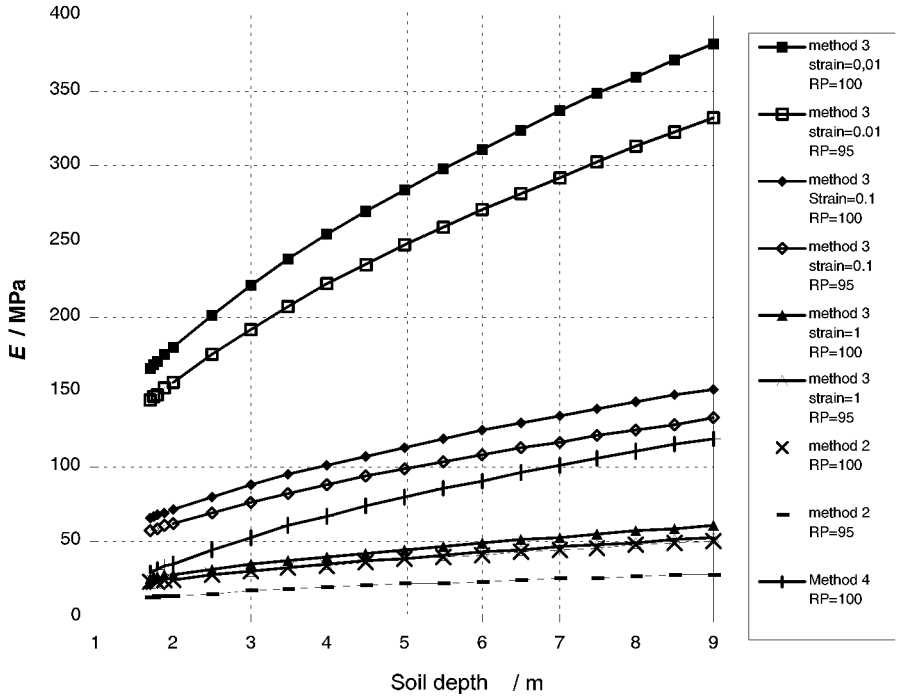

Figure 3.6: Elasticity modulus versus depth of soil. Comparison of Method 2 of Pettersson et al., Lehane et al.'s Method (Method 3) and Lade et al.'s Method (Method 4)

3.3.3 Comparison of Pettersson et al.'s Method 2, Lehane et al.'s Method, and Lade et al.'s Method

The values of the elasticity modulus from the second, third and fourth methods are compared. The soil parameters in the calculations were taken as in Table 3.6. It should again be noted that in these comparisons, the general term for the elasticity modulus is used. The difference between the tangent modulus and the secant modulus should be taken into account while comparing.

Figure 3.6 shows that there is a significant difference between the values of the modulus calculated by the different methods. Lehane et al.'s method, namely Method 3, gives secant modulus values varying largely with change in shear strain levels. The lowest shear strain level in the calculations is 0.01 %. It represents a medium level strain according to the classification given by Ishihara [44] and it is also the upper bound of the elastic limit, which is between 0.001 % and 0.01 %. Above this shear strain level, the soil material starts to behave as elasto-plastic. The highest strain level that is used in the calculations is 1 %, which represents a very large shear

strain level and is the upper limit strain that Lehane's E_s formula is valid for.

Figure 3.6 also shows that a 10 fold (one log cycle) increase in shear strains leads to more than a 2 fold decrease in the secant modulus values.

Method 2 of Pettersson et al. and Lehane et al.'s method (Method 3) tend to agree if E_s in Method 3 is calculated at very high shear strain levels. As Lehane et al.'s method forces us to know the shear strain levels at the point where E is to be calculated, the comparison between the two methods becomes difficult. (It should be taken into account that Method 2 assumes that the lateral soil pressures are at-rest soil pressures, in other words, that there is no movement or strain yet). In general however we can conclude that Method 2 is more conservative compared to Method 3.

A more common strain level would be 0.1 % (for a 50 m long, 6 m high bridge that is exposed to a 40° C temperature change).

Lade et al.'s method (Method 4) seems to be more sensitive to soil depth. For low soil depths (as low as 2 m), the E values from Method 4 are close to Method 3 with high shear strains (1 %). By increasing the soil depth, they seem to get closer to the E values calculated by Method 3 at 0.1 % strains.

Chapter 4

The Effect of Soil Stiffness on the Design of Culverts and Integral Bridges

In this chapter, the author intends to demonstrate the extent of significance of knowledge of soil stiffness in design of structures like culverts and integral bridges. Maximum bending moments are usually the most critical design criteria for structures. The sensitivity of these design criteria to soil stiffness is going to be investigated. In other words the change in the bending moments with the change in soil stiffness will be calculated. For culverts, a well established design method (Duncan's SCI Method) has been selected. For integral bridges, a slab-frame bridge is taken as an example and is analysed by the Swedish method (see [81]).

Section 4.1 uses the SCI design method for culverts and calculates the most sensitive design bending moment to soil parameters. Results are discussed and comparisons with different soil parameters are done. Section 4.2 takes a slab-frame bridge as an example and analyzes it. The relationship between soil stiffness (in terms of degree of compaction) and bending moments at the abutment front are shown.

4.1 Maximum Bending Moment for Culverts

It has been indicated in Section 3.2.1 that the stiffness of the backfill is an important factor that is used in the design of culverts. According to the soil-culvert-interaction (SCI) method (see [27,28]) E_s is included in the process of calculating the maximum bending moment by means of a dimensionless flexibility number N_f (previously mentioned in Section 2.2.3).

4.1.1 The SCI Method

This method is valid for arches and closed shape culvert structures with shallow cover depth ($h_c \leq 0.25S$). Moment equations may be used to calculate the bending moments due to backfill soil and live loads.

The SCI method calculates the moments that occur at the quarter point, which corresponds to the half height of the rise of the culvert. The E_s values for backfill soil are also calculated for the quarter point according to Figure 3.2. Duncan [27,28] reports that the elasticity modulus value in the vicinity of the quarter point of the culvert is approximately equal to the average value for the backfill.

The equations that are used in this method were given in Section 2.2.3 and the values for all the coefficients for moment calculations can be taken from the figures provided by Duncan [27].

4.1.2 Geometry and Material Parameters

The soil unit weight varies with the relative compaction (RP). The range of RP is taken as 85 % to 100 %. The corresponding unit weights (γ_s) of the soil are calculated by the following relation (see [72]):

$$\rho = \rho_{opt} \frac{RP}{100} \tag{4.1}$$

where the optimum density ρ_{opt} (according to Standard Proctor) is taken as 2.1 t/m^3. The resulting γ_s values highly agree with the literature (see McCavour et al. [62]).

The corrugated steel parameters, though, were kept constant throughout the calculations. An intermediate value for I_{st} was used (for approximately 6 mm thick steel).

A few variations of culvert geometry were tried to emphasize the rise/span ratios. All parameters are summarized in Table 4.1.

4.1.3 Calculations

The steps of calculating moments according to the SCI method are summarised below:

1. The secant modulus of elasticity of the soil is obtained from the curves for E_s, which depends on the depth of cover at the quarter point and the relative compaction RP (see Figure 3.2).
2. The flexibility number of the culvert is calculated according to Equation 2.13.

Table 4.1: Geometry and material parameters used for moment calculations of steel culverts (using the SCI method)

Parameter	Unit	Culvert 1	Culvert 2	Culvert 3
E_{st}	kPa	2x10^8	2x10^8	2x10^8
I_{st}	m^4/m	2.75x10^{-6}	2.75x10^{-6}	2.75x10^{-6}
H	m	3	3	6
S	m	8	12	12
H/S	-	0.38	0.25	0.5
ρ_{opt}	t/m^3	2.1	2.1	2.1
RP	%	85-100	85-100	85-100
γ_s	kN/m^3	18-21	18-21	18-21
LL	kN/m	104	104	104
h_c	m	0.3-2.0	0.3-2.0	0.3-2.0

3. The maximum bending moment for a cover-depth of 0, M_1, is calculated according to Equation 2.14.

4. For calculating the coefficients, N_f should be calculated using the E_s value corresponding to the zero depth of cover.

5. If the final depth of cover is greater than or equal to one quarter of the span ($h_c \geq 0.25S$), the bending need not be investigated.

6. If the final depth of cover is less than one quarter of the span ($h_c < 0.25S$), the bending moment due to backfill is calculated as follows:

$$M_{soil} = M_1 - R_B \cdot K_{M2} \cdot \gamma \cdot S^2 \cdot h_c \tag{4.2}$$

7. The bending moment due to live load is calculated from the following:

$$M_{LL} = R_L \cdot \ K_{M3} \cdot S \cdot LL \tag{4.3}$$

8. The total moment (which was previously expressed in Equation 2.15) would then be:

$$M = M_{soil} + M_{LL} \tag{4.4}$$

9. For calculating the coefficients, N_f should be calculated using the E_s value, which corresponds to the final depth of cover.

4.1.4 Results and Comparisons

A summary of the results of the calculations of moments by the SCI method can be observed from Figures 4.1 to 4.4.

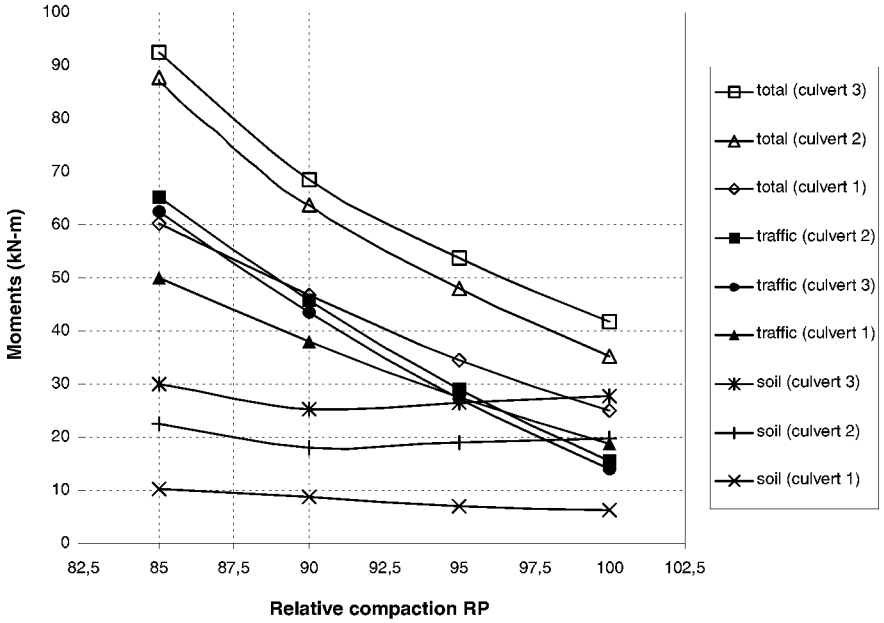

Figure 4.1: SCI design bending moments versus relative compaction for a depth of cover of 0.5 m for 3 different culverts. (Unit weights are calculated by Equation 4.1 with an optimum unit weight of 21 kN/m^3.)

Table 4.2: Comparison of the results of the moment calculations according to the SCI method

	Culvert	% Decrease in Moments			Notes
		M_{soil}	$M_{live\ load}$	M_{total}	
As γ_s changes from 18 to 21 kN/m^3	1	38,2	62,7	58,6	hc=0,5m
	2	11,7*	76,3	59,8	
	3	7,1*	77,7	54,9	
As h_c changes from 0,3 to 2,0 m	1	85,6	77,2	78,5	independent of γ_s
	2	54,7	77,8	70,7	
	3	55,1	77,0	68,5	
* Moments do not constantly decrease as the unit weight increases					

Table 4.2 displays the change of bending moment with changing unit weight and depth of cover.

According to Figure 4.1, culverts 1, 2 and 3 show more or less the same behaviour. Live load (traffic) moments are much more sensitive to backfill properties. They decrease by an average of 72 % as degree of compaction increases from 85 % to 100 %. The total moments decrease by an average of 58 %. Soil moments decrease by 38 % for culvert 1. In the case of culverts 2 and 3 the moments due to soil load slightly decrease and increase. It is not possible to give a percentage comparison since they do not follow a consistent trend. Since the change in moments due to soil load with changing soil compactness is small compared to live load moments, it can also be argued that the bending moments generated by soil loads are independent of soil stiffness. As the soil gets stiffer, the unit weight of soil increases as well as the friction angle. The coefficient of lateral pressure, K, will then probably decrease to the level where the same lateral stresses will be achieved. It can be concluded that in this design method the traffic moments can be seriously affected by the compactness level of the soil. The effect is more pronounced as the soil gets looser. This shows the necessity of obtaining realistic soil parameters.

In all culvert types the decrease in live load (traffic) moments is much more pronounced when the cover depth is small. The moments due to soil backfill and cover, though, decrease in a linear fashion as the cover depth increases (see Figures 4.2 to 4.4).

The moments calculated according to the SCI method with different cover depths

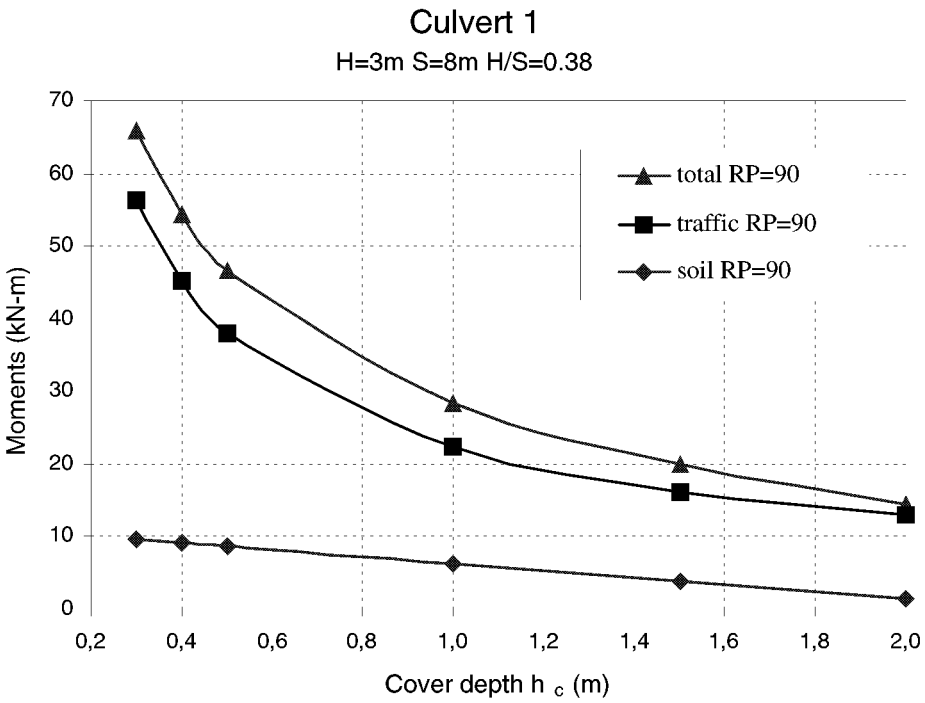

Figure 4.2: SCI design bending moments versus depth of cover for culvert 1

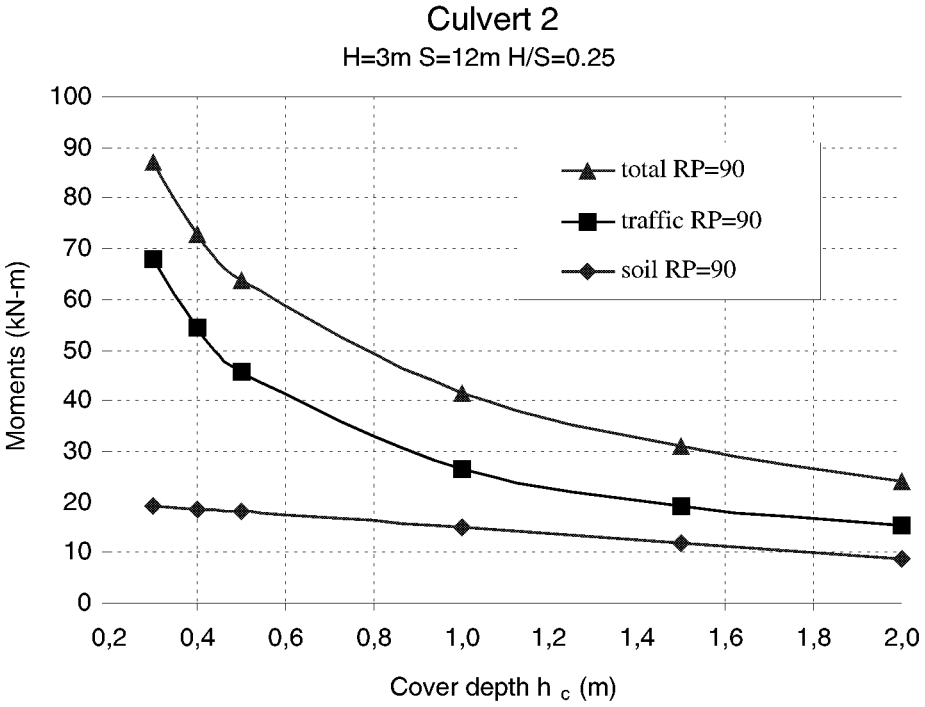

Figure 4.3: SCI design bending moments versus depth of cover for culvert 2

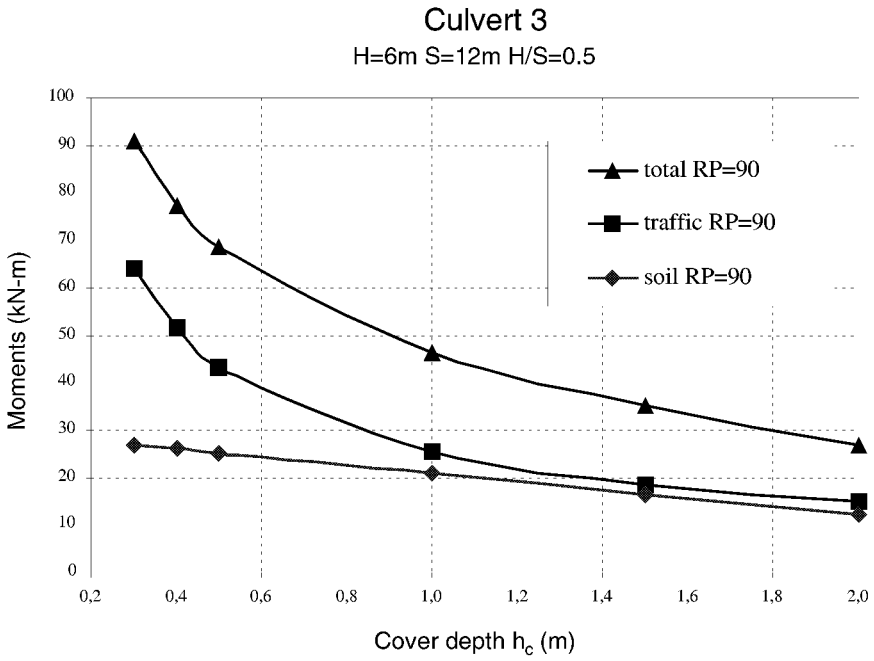

Figure 4.4: SCI design bending moments versus depth of cover for culvert 3

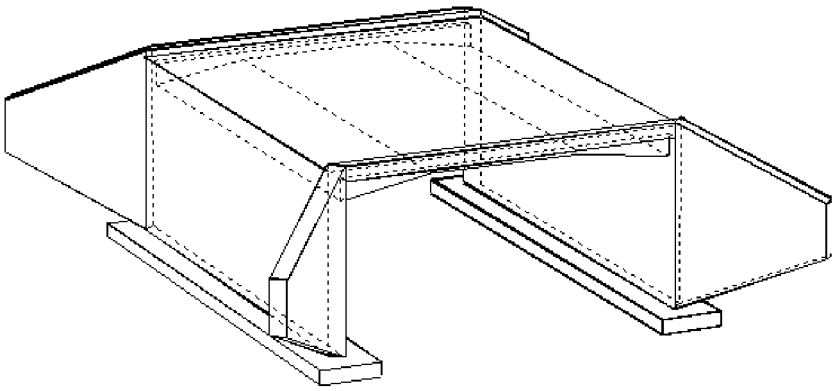

Figure 4.5: A typical slab-frame bridge

on 3 different culvert geometries reveal that the total moment decrease is between 68 % and 78 % with increasing depth of cover (see Table 4.2). The live load moment decreases by about the same amount. This can be explained as the positive effect of soil confinement. The amount of change in moments with cover depth is independent of the soil unit weight, i.e., the same percentage difference is observed for all soil unit weight levels (for example from 18 kN/m^3 to 19 kN/m^3 then to 20 kN/m^3 etc.).

4.2 Maximum Bending Moment for Slab-Frame Bridges

The slab-frame bridge is quite a common type of integral bridge in Sweden (see Figure 4.5).

In this section the bending moments on a slab-frame bridge will be calculated. Several load types and combinations will be considered. But the main focus will be on the moments due to soil loads in reaction to a lateral movement of the bridge deck. The relation between the soil stiffness and maximum moments will be investigated. The significance of the changes in the maximum moments with changing soil parameters will be highlighted.

4.2.1 Geometry and Parameters

The dimensions and parameters used in this problem are summarized in Table 4.3.

Different soil parameters were used to be able to observe the changes in the design moment values, which will eventually affect the final design dimensions of the integral bridge. The ones that appear in Table 4.3 are the most typical values with which the first calculations were carried out. Two important soil parameters that are involved

Table 4.3: Material parameters, geometry and loading conditions used for the slab-frame bridge problem

type	description	symbol	unit	quantity
soil	unit weight	γ_s	kN/m^3	19
	lateral earth pressure coefficient	K		0,38
	settlement modulus	E_k	kPa	40000
	foundations bending stiffness/length	$\gamma_r = 1/(k\theta_k/L_f)$	rad/(kNm/m)	5,08E-05
concrete	unit weight	γ_c	kN/m^3	24
	elasticity modulus	E_c	kPa	22200000
	elasticity modulus for soil calculation	E_c	kPa	32000000
	coefficient of thermal expansion	T_c	1/ deg	0,000012
geometry	slab thickness	t	m	0,5
	wall height	H_a	m	4,85
	bridge length	L	m	6,5
	thickness of soil cover above the bridge	h_c	m	0,35
	footing width	W	m	2
	footing length	L_f	m	8
loads	own weight	q_o	kN/m^2	12
and	pavement	q_p	kN/m^2	2,1
other	trapezoidal soil load	q_{min}	kN/m^2	2,5
conditions		q_{max}	kN/m^2	37,5
	uniformly distributed traffic load	p_t	kN/m^2	4
	temperature change	rise	deg	15
		drop	deg	28
	unequal temperature	rise	deg	10
		drop	deg	5
	horizontal displacement	δ	m	0,01

Table 4.4: Settlement modulus values used in calculations for slab-frame bridges

Relative stiffness	High	Medium	Low	Very low
E_k (kPa)	40000	25000	15000	4000

in the calculations are the unit weight of backfill soil (γ_s) and the deformation property of the underlying foundation soil (E_k).

The deformation property of the soil comes in the form of a factor called the "settlement modulus", as described and tabulated in [94]. Once this modulus is decided, it is possible to evaluate the rotational stiffness of the foundation according to the following equation (see Vägverket [94]).

$$k_{\theta_k} = \frac{E_k \cdot W^2 \cdot L_f}{\beta_f} \tag{4.5}$$

where:

k_{θ_k} = characteristic bending deformation modulus (kNm/rad)
E_k = settlement modulus (kPa)
W = width of the foundation (m)
L_f = length of the foundation (m)
β_f = factor depending on W/L_f ratio

Eventually, the value γ_r, which designates the rotational deformation property of the foundation per unit length, is used in the static calculations. It is in rad/(kNm/m):

$$\gamma_r = \frac{1}{k_{\theta_k}/L_f} \tag{4.6}$$

The unit weight of the soil has to be carefully chosen, taking into account the typical soil properties of the cohesionless soil backfill used for this kind of structures. The range for γ_s is taken from 17 kN/m^3 to 21 kN/m^3. The range of k_{θ_k} is determined by different E_k values that are chosen from [94]. See Table 4.4 for the representative E_k values for each range of stiffness.

4.2.2 Calculations

Static System

Loads are taken according to Bro 2002 norms. A static analysis is done according to the method in Sundquist [81]. The system is divided into two systems. One of them is a loaded system with a lateral support at one end of the slab that hinders the lateral movement of the slab part of the bridge (see Figure 4.6(ii)). The second system consists of an unloaded frame that is under deformation effects of the lateral movement δ of the top of the abutment wall (see Figure 4.6(iii)).

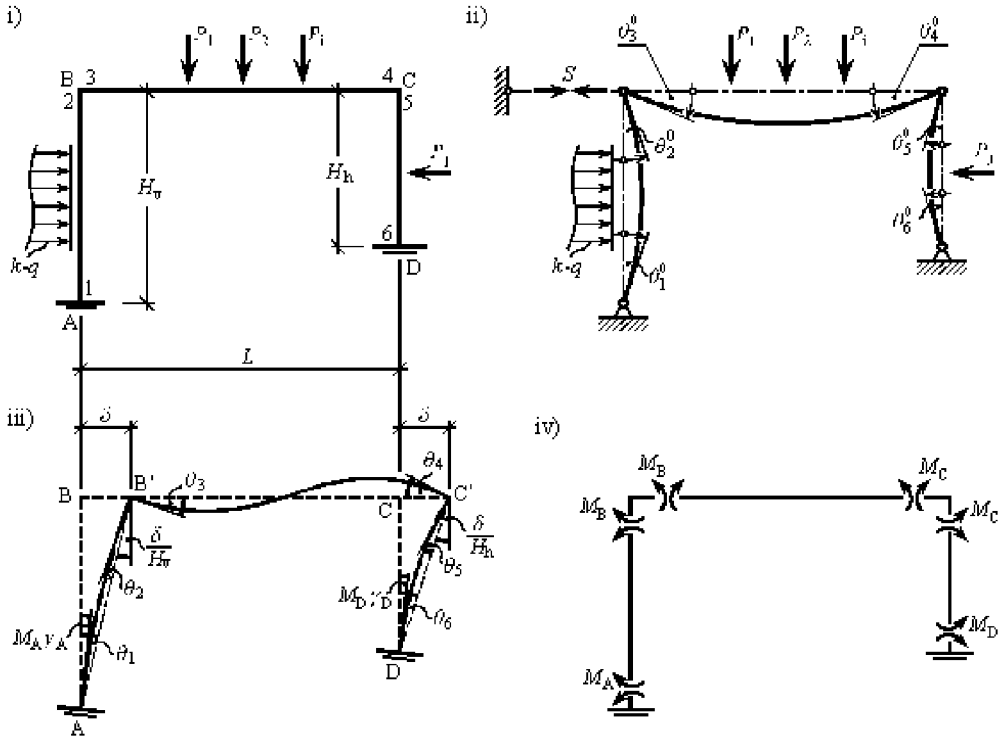

Figure 4.6: Angle changes and value names for the moments and forces in the frame for the analysis of a slab-frame bridge: (i) representation of the loads, (ii) deformations under loading with no lateral freedom of the joints, (iii) deformations due to the lateral movement and foundation rotations, and (iv) section moments

Stability equations are obtained by means of combining these two systems with respect to the angle continuation at the joints. The equation system is determined after addition of the horizontal equilibrium. The equilibrium equations can be simultaneously solved for moments at each joint and the lateral displacement by forming a matrix system that consists of a coefficient matrix and a column vector. Details can be obtained from [81].

Loads

The considered loads are

- uniformly distributed traffic loads,
- trapezoidal earth pressure,
- constrained loads (such as shrinkage, support movement, temperature change and unequal temperature),
- point traffic loads,
- fatigue loads,
- triangularly distributed backfill soil reaction, and
- horizontal brake force, H_b.

Moments due to the braking load and triangularly distributed backfill soil reaction

Figure 4.7 shows the schematic load distribution for this calculation.

Steps for the calculation:

1. Deformation due to the brake force (δ_{H_b}):

   This deformation is not the final deformation of the frame since there exists a reaction from the backfill soil that is created by this deformation. That reaction pressure is assumed to be triangularly distributed with a maximum value of ΔP (see Figure 2.7).

2. Final deformation of the frame (δ_{frame}):

   The problem is that ΔP is not known. An approximate equation (see Equation 2.4) for ΔP as given in the Swedish bridge norms is going to be used. If this equation is reorganized for the deformation the following is obtained:

$$\delta_{frame} = \frac{2 \cdot \Delta P}{C \cdot \gamma_s} \tag{4.7}$$

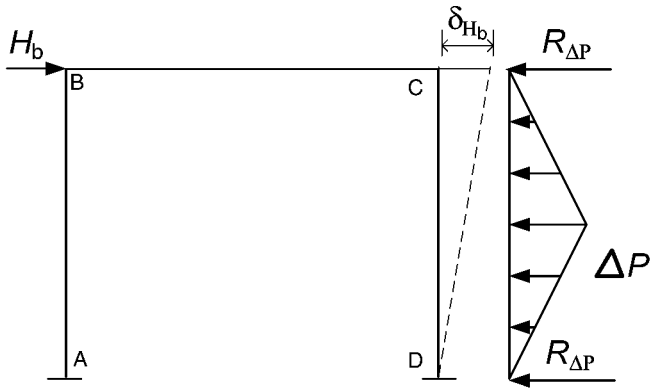

Figure 4.7: Braking load and corresponding soil reaction forces for the analysis of a slab-frame bridge according to braking

3. Deformation due to triangular soil reaction pressure $\Delta P = 100$ and the support reaction force R_{100} (δ_{100}):

   Since ΔP is unknown, an arbitrary value (such as 100) is given to it. The deformation (δ'_{100}) from the set of stability equations, which were obtained previously, is calculated. The corresponding support reaction R_{100} due to this triangular soil load would then be $R_{100} = 100 \cdot H_a/2/2$. The deformation due to R_{100} ($\delta_{R_{100}}$) can be calculated the same way as δ_{H_b}.

   δ_{100} will then be the sum of the deformation calculated with the triangular load and the deformation generated by the support reaction R_{100}:

$$\delta_{100} = \delta'_{100} + \delta_{R_{100}} \tag{4.8}$$

4. Deformation due to triangular soil reaction pressure ($\delta_{\Delta P}$):

   By simply proportioning with δ_{100} the following equation can be written:

$$\delta_{\Delta P} = \delta_{100} \cdot \frac{\Delta P}{100} \tag{4.9}$$

5. Setting up the equation for calculating ΔP:

   δ_{frame} can be equated with the difference of the deformation due to the brake force and the deformation due to the triangular reaction pressure:

$$\delta_{frame} = \delta_{H_b} - \delta_{\Delta P} \tag{4.10}$$

   ΔP can now be calculated by equating Equation 4.7 to Equation 4.10 and inserting Equation 4.9.

6. Equation for the bending moments:

$$M_{SFB} = M_{H_b} - M_{R_{\Delta P}} - M_{\Delta P} \tag{4.11}$$

Table 4.5: Summary of the calculations and moments at the abutment front for medium and high stiffness levels

	Ek=40 000 (high stiffness)			Ek=25 000 (medium stiffness)		
	γ_s=17	γ_s=19	γ_s=21	γ_s=17	γ_s=19	γ_s=21
δ_{H} (m)	0,0019	0,0019	0,0019	0,0021	0,0021	0,0021
$\delta_{100\ from\ table}$	0,0015	0,0015	0,0015	0,0017	0,001702	0,001702
R_A (kN/m^2)	121,3	121,3	121,3	121,3	121,3	121,3
δ_{RA}	0,01	0,009	0,01	0,010	0,010	0,010
δ_{100}	0,01	0,011	0,01	0,012	0,012	0,012
C	300	300	300	300	300	300
γ_s	17	19	21	19	19	21
Δp_{max_real} (kN/m^2)	3,82	4,16	4,49	4,04	4,39	4,73
Real R_A	4,63	5,04	5,44	4,89	5,33	5,73
MOMENTS						
M_{3H}	51,3	51,3	51,3	54,2	54,2	54,2
M_{4H}	-51,3	-51,3	-51,3	-54,2	-54,2	-54,2
$M_{3\Delta pmax}$	-0,6	-0,7	-0,7	-0,8	-0,9	-1,0
$M_{4\Delta pmax}$	-1,6	-1,8	-1,9	-1,6	-1,7	-1,8
M_{3RA}	9,5	10,4	11,2	10,6	11,5	12,4
M_{4RA}	-9,5	-10,4	-11,2	-10,6	-11,5	-12,4
M_3	42,5	41,7	40,9	44,4	43,6	42,7
M_4	-40,2	-39,2	-38,3	-42,0	-40,9	-39,9

4.2.3 Results and Comparisons

All moments are calculated at the abutment front. Of all the results of the calculations, only the moments due to the triangular soil reaction resulting from the brake forces will be displayed in detail in this section (see Tables 4.5 and 4.6).

The extent to which moments are affected by the change in soil parameters can be observed from Figure 4.8. It should be considered that the settlement modulus and the unit weight of soil are not independent. As the soil gets denser the stiffness increases. Hence, calculations for data pairs such as E_k=4000 kPa and γ_s=21 kN/m^3 do not make sense. To overcome this problem E_k and γ_s were taken into the calculation in realistic pairs only once in the moment calculations.

As expected, moments are reduced as the backfill soil gets stiffer. There is an approximately 18.6 % decrease in the moments as the soil stiffness (expressed as the settlement modulus) changes from very low stiffness (E_k=4000 kPa) to high stiffness (E_k=40000 kPa).

Table 4.6: Summary of the calculations and moments at the abutment front for low and very low stiffness levels

	E_k=15 000 (low stiffness)			E_k=4 000 (very low stiffness)			
	γ_s=17	γ_s=19	γ_s=21	γ_s=16	γ_s=17	γ_s=19	γ_s=21
δ_H (m)	0,0022	0,0022	0,0022	0,0023	0,0023	0,0023	0,0023
$\delta_{100\ from\ table}$	0,0019	0,0019	0,0019	0,0021	0,0021	0,0021	0,0021
R_A (kN/m^2)	121,3	121,3	121,3	121,3	121,3	121,3	121,3
δ_{RA}	0,011	0,011	0,011	0,011	0,011	0,011	0,011
δ_{100}	0,012	0,012	0,012	0,013	0,013	0,013	0,013
C	300	300	300	300	300	300	300
γ_s	17	19	21	16	17	19	21
Δp_{max_real} (kN/m^2)	4,20	4,57	4,92	4,22	4,42	4,79	5,15
Real R_A	5,10	5,54	5,96	5,11	5,35	5,81	6,24
MOMENTS							
M_{3H}	56,5	56,5	56,5	59,41	59,4	59,4	59,4
M_{4H}	-56,5	-56,5	-56,5	-59,41	-59,4	-59,4	-59,4
$M_{3\Delta pmax}$	-1,0	-1,1	-1,2	-1,21	-1,3	-1,4	-1,5
$M_{4\Delta pmax}$	-1,5	-1,6	-1,8	-1,35	-1,4	-1,5	-1,7
M_{3RA}	11,5	12,5	13,5	12,15	12,7	13,8	14,8
M_{4RA}	-11,5	-12,5	-13,5	-12,15	-12,7	-13,8	-14,8
M_3	46,0	45,1	44,2	48,5	48,0	47,0	46,1
M_4	-43,4	-42,3	-41,2	-45,9	-45,3	-44,1	-42,9

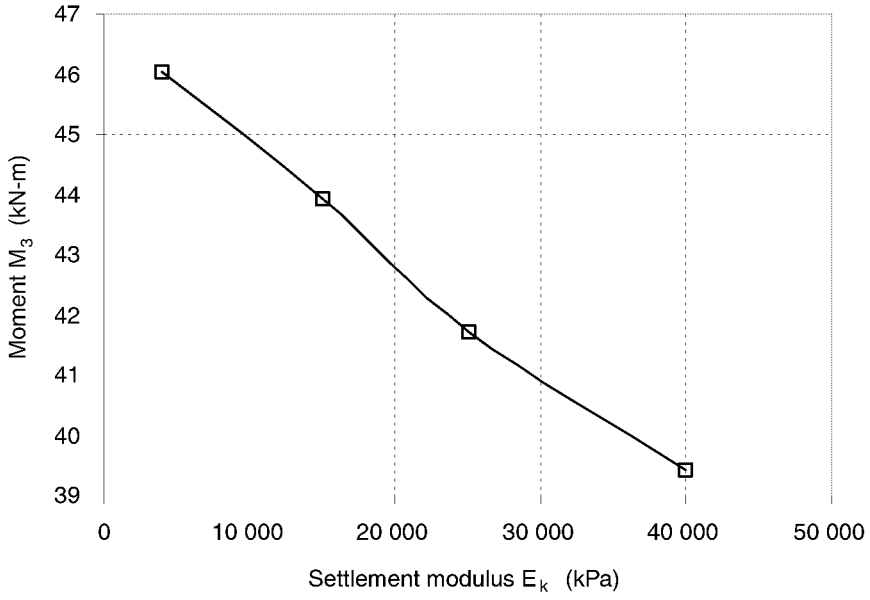

Figure 4.8: Change in moments with change in soil stiffness, which is expressed as the settlement modulus E_k

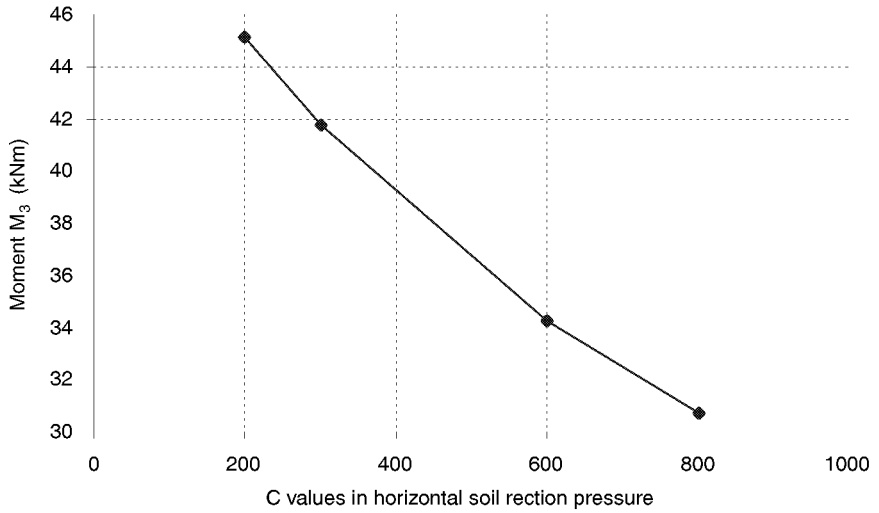

Figure 4.9: Change in moments with change in the parameter C in the ΔP formula

In these example calculations, the effect of change of the parameter C in the ΔP formula on moments was also investigated. Moments were calculated for E_k=25000 kPa and γ_s=19 kN/m^3. C was changed between 200 and 800. The resulting M_3 values are plotted in Figure 4.9. The amount of decrease is approximately 25 %. C is believed to somehow represent the soil stiffness and is certainly an influential factor in the moment calculations. There are only two values (300 and 600) that can be used for C in the design of integral bridges. Here for exercise the range is extended to minimum 200 and maximum 800.

Chapter 5

Conclusions

5.1 Conclusions from the Literature Review

As a result of our survey, the following conclusions were obtained:

- The earth pressure coefficient of the backfill soil for integral bridges and culverts, and hence the intensity of earth pressure, is a function of the displacement or rotation of the abutment wall.
- There is a lack of knowledge on soil-structure interaction due to cyclic loading of bridge abutments:
  - The experimental and analytical work was limited to bridge sizes up to 160 m. The research could be extended towards longer bridges.
  - It is largely accepted that the lateral pressure coefficient K increases with the cyclic movement of the bridge abutment towards the soil, but its extent has still not been established.
  - There seems to be no way of properly choosing the lateral earth pressure coefficient K for different types of granular material. Most of the researchers have worked on a type of soil that makes the resulting K *experiment-specific*. The research could be extended towards different soil types, where K can be correlated to the soil properties.
  - The behaviour under large wall displacements is not studied enough.
- Due to unknowns in the soil behaviour, the design procedures were kept simple and conservative.
- There is still a need to develop models of varying range sophistication. This can help the engineer to choose the most suitable model at the analysis or design phase.
- There are problems in
  - obtaining a non-linear stress-strain behaviour of soil,

  - evaluating the time-dependent drainage and creep behaviour,
  - obtaining adequate soil parameters, and
  - idealizing the structure.

- The current design methods for integral bridge abutments and culverts can be improved. As an outcome of the comparison of some of the current design codes and the latest research results, the following conclusions can be made for passive resistance (passive earth-pressure ratio):
  - The Swedish design code Bro 2002 becomes more conservative as the deflection increases.
  - The value from the English code BA 42 is lower than the values of the two experimental studies by Springman and England [33, 79].
  - BA 42 is said to be underestimating the K values in the long term.
  - The numerical analysis results give lower values for K than the test values.

5.2 Conclusions about the Stiffness Characteristics of Soil

This thesis defined and gave a history of the methods of determination of the elastic modulus of soil. Then the focus went to the comparison of several different state-of-the-art methods, such as the one used in Duncan et al.'s [27] SCI method, Pettersson et al.'s [72] reformulations, as well as Lehane et al.'s [56] and Lade et al.'s [54] comparable methods for determining the elasticity modulus of soil.

As a result of these comparisons, it can be concluded that Duncan et al.'s E_s values (that are to be used in the SCI method) and Method 1 of Pettersson et al. are much more conservative compared to the E_t value calculated by hyperbolic equations and the E_t value of Method 2 of Pettersson et al. This can lead to over-design of the culvert structure, since it assumes soil to be less stiff.

A comparison of Method 2 of Pettersson et al., which is a more sophisticated version of Duncan et al.'s hyperbolic equation for E_t, with Lehane et al.'s and Lade et al.'s reveals that there are significant differences between these different methods.

5.3 Conclusions about the Effect of Soil Stiffness on the Design of Culverts and Integral Bridges

5.3.1 Soil Stiffness in the Design of Culverts

The results of the calculations done on three different culverts with height-to-span ratios changing between 0.25 and 0.5 suggest that all culverts show approximately

the same behaviour. A change of 15 % in the relative compaction of the backfill causes a 72 % change in live-load moments. This shows that live-load moments are very sensitive to the stiffness of the backfill soil.

Changes in bending moments due to the soil load do not show consistent tendencies. The amount of changes is not considerably big. This could be explained with the observation that an increase in soil stiffness decreases the lateral earth pressure coefficient, and hence leaves lateral pressures on the structures unaffected. This makes considerations of moments due to soil loads uninteresting for soil-structure-interaction purposes.

The soil-structure interaction of culverts shows its importance when it comes to the design of culverts due to live loads.

Calculations with different cover depths showed the sensitivity of again the bending moments due to live loads. The bending moment due to soil load is directly proportional to the cover depth. From 2 m to 0.3 m cover, the total bending moments can increase as much as 3 to 5 times (the figures for the amount of change can be followed from Table 4.2), depending on the culvert geometry. For low covers, the moments are much more sensitive to changes in cover depth. This demonstrates how and when arching effects actually kick in.

The comparisons made in Section 4.1 demonstrate the positive effects of the soil confinement and the importance of obtaining realistic soil parameters in the design of culverts.

5.3.2 Soil Stiffness in the Design of Integral Bridges

The results of the moment calculations made for a typical slab frame bridge reveal that the moments at the abutment front are reduced by 18.6 % as the backfill soil stiffness (expressed as a settlement modulus) changes from very low stiffness (E_k=4000 kPa) to high stiffness (E_k=40000 kPa).

The effect of change of the parameter C in the ΔP formula on the moments is also significant. The amount of decrease is approximately 25 % as C increases from 200 to 800. It is definitely an influential factor in the moment calculations. If we assume that C strictly represents the soil stiffness, then a proper definition as well as a formula to represent it should be made.

5.4 Further Research

As a result of the above conclusions, the author suggests the following further research:

- The remedies, which aim at eliminating or reducing the excess lateral pressures (passive pressures) behind the abutment wall, can be studied.

- The relationship between the soil deformation characteristics and the structure stiffness can be explored to assess the variation of earth pressure with the amount and type of deflection of the structure. This can preliminarily be studied by computer models and analysed with several wall stiffnesses. The results can then be supported by in-situ or laboratory model tests.
- The influence of the soil deformation characteristics (such as E) on the load distribution on the structure can be deeply studied.
- The increase in passive pressures can be formulated such that it permits us to choose a realistic K value as the bridge length, abutment wall height, amount of wall rotation, and soil properties are specified.
- The performance of long-span flexible culverts should be studied and current design methods should be improved such that they allow the engineer to use more realistic soil parameters.
- The design of integral bridges needs also an improvement in the calculation of the lateral earth pressure distribution behind the abutment walls. The C values should be more clearly specified and adjusted, taking the soil stiffness into account.

Bibliography

[1] Bro 2002. *Allmän Teknisk Beskrivning for Broar (the Swedish Bridge Code)*, chapter 2, sections 21.13 and 21.23. 2002.

[2] J. R. Allgood and S. K. Takahashi. Balanced design and finite element analysis of culverts. *Highway Research Record*, 413:45–56, 1972.

[3] L. Andreasson. Kompressibilitet hos friktionsjord (in Swedish). Technical Report 36:1973, Statens Institut för Byggnadsforskning, Stockholm, 1973.

[4] S. Arsoy, R. M. Barker, and J. M. Duncan. Behavior of integral abutment bridges. Final contract report 00-CR3, Federal Highway Administration & Virginia Transportation Research Council, Virginia, USA, 1999.

[5] S. Avén. *Geoteknik Handboken Bygg (Geotechnical Handbook for Construction)*. Liber Förlag, Stockholm, 1984.

[6] BA-42. *The Design of Integral Bridges. Design Manual for Roads and Bridges*, chapter 1.3.12. 1996. The Highways Agency. The Stationary Office, UK.

[7] L. D. Baikie and G. G. Meyerhof. Buckling behaviour of buried flexible structures. *Proc. 4th Int. Conf. Numerical Methods in Geomechanics, Edmonton, Canada*, pages 875–882, 1982.

[8] K. J. Barker and D. R. Carder. Performance of the two integral bridges forming the A62 Manchester road overbridges. Technical Report 436, Transport Research Laboratory, Crowthorne, England, 2000.

[9] K. J. Barker and D. R. Carder. Performance of an integral bridge over the M1-A1 link road at Bramham crossroads. Technical Report 521, Transport Research Laboratory, Crowthorne, England, 2001.

[10] E. Bayoğlu Flener. Field testing of a long-span arch steel culvert railway bridge over Skivarpsån, Sweden. TRITA-BKN Rapport 72, Department of Civil and Architectural Engineering, Division of Structural Design and Bridges, Royal Institute of Technology, KTH, Stockholm, Sweden, 2003.

[11] J. E. Bowles. *Foundation Analysis and Design*. McGraw-Hill, New York, 1988.

[12] B. B. Broms and I. Ingelson. Earth pressure against the abutment of a rigid frame bridge. *Geotechnique*, 21(1):15–28, 1971.

[13] B. B. Broms and I. Ingelson. Lateral earth pressure an a bridge abutment. *European Conference on Soil Mechanics and Foundation Engineering*, 1:117–123, 1972.

[14] J. W. Bull, editor. *Soil Structure Interaction: Numerical Analysis and Modelling.* E and FN Spon., London, 1994.

[15] M. P. Burke. Integral bridges. *Transportation Research Record*, 1275:53–61, 1990.

[16] M. P. Burke. Design of integral concrete bridges. *Concrete International*, 15(6):37–42, 1993.

[17] M. P. Burke. Integral bridges: Attributes and limitations. *Transportation Research Record*, 1393:1–8, 1993.

[18] R. M. Burns, O. J.and Richard. Attenuation of stresses for buried cylinders. *Proc. Symp. on Soil-structure Interaction, University of Arizona, Tucson*, pages 378–392, 1964.

[19] G. B. Card and D. R. Carder. A literature review of the geotechnical aspects of the design of integral bridge abutments. Project Report 52, Transport Research Laboratory, Crowthorne, England, 1993.

[20] D. R. Carder and G. B. Card. Innovative structural backfills to integral bridge abutments. Technical Report 290, Transport Research Laboratory, Crowthorne, England, 1997.

[21] D. R. Carder and J. P. Hayes. Performance under cyclic loading of the foundations of integral bridges. TRL Report 433, Transport Research Laboratory, Crowthorne, England, 2000.

[22] W. F. Chen. *Limit Analysis and Soil Plasticity.* Elsevier Science Publishers, New York, 1975.

[23] W. F. Chen and A. F. Saleeb. *Constitutive Equations for Engineering Materials: Elasticity and Modelling*, volume 1. John Wiley and Sons, Inc., USA, 1982.

[24] B. M. Das. *Advanced Soil Mechanics.* McGraw-Hill, Singapore, 1985.

[25] B. M. Das. *Principles of Foundation Engineering.* PWS Publishing, fourth edition, 1999.

[26] M. Dicleli. A rational design approach for prestressed-concrete-girder integral bridges. *Engineering Structures*, 22:230–245, 2000.

[27] J. M. Duncan. Soil-culvert interaction method for design of metal culverts. *Transportation Research Record*, 678:53–59, 1978.

[28] J. M. Duncan. Behaviour and design of long-span metal culverts. *ASCE Journal of the Soil Mechanics and Foundation Engineering Div.*, 105(3):399–418, March 1979.

[29] J. M. Duncan and C. Y. Chang. Non-linear analysis of stress and strain in soils. *ASCE Journal of the Soil Mechanics and Foundation Engineering Div.*, 96:1629–1653, 1970.

[30] J. M. Duncan and R. L. Mockwa. Passive earth pressures: Theories and tests. *Journal of Geotechnical and Geoenvironmental Engineering*, 127:248–257, 2001.

[31] J. M. Duncan, Wong K. S., Byrne P., and P. Mabry. Stress, strain and bulk modulus parameters for finite element analysis of stresses and movements in soil masses. Technical Report UCB/GT/80-01, University of California, Berkeley, 1980.

[32] J. M. Duncan, R. B. Seed, and R. H. Drawsky. Design of corrugated metal box culverts. *Transportation Research Record*, 1008:33–41, 1985.

[33] G. L. England, N. C. M. Tsang, and D. I. Bush. *Integral Bridges: A fundamental approach to the time-temperature loading problem.* Thomas Telford Ltd., London, 2000.

[34] A. Enquist. Pm beträffande med Ändskärm - brolängder. Technical report, Vägverket, VB, 1991.

[35] Y. S. Fang, T. J. Chen, and B. F. Wu. Passive earth pressures with various wall movements. *Journal of Geotechnical Engineering, ASCE*, 1270:1307–1323, 1994.

[36] S. Faraji, J. M. Ting, D. S. Crovo, and H. Ernst. Nonlinear analysis of integral bridges: Finite-element model. *Journal of Geotechnical and Geoenvironmental Engineering*, 127:454–461, 2001.

[37] J. M. Gere and S. P. Timoshenko. *Mechanics of Materials.* Stanley Thornes Ltd., United Kingdom, fourth SI edition, 1999.

[38] D. D. Girton, T. R. Hawkinson, and L. F. Greiman. Validation of design recommendations for integral abutment piles. *Journal of Structural Engineering*, 117(7):2117–2134, 1991.

[39] L. F. Greimann, P. S. Yang, and A. M. Wolde-Tinsae. Nonlinear analysis of integral abutment bridges. *Journal of Structural Engineering*, 112(10):2263–2280, October 1986.

[40] E. C. Hambly. Integral bridges. *Proceedings of the Institution of Civil Engineers, Transport*, 123(1):30–38, February 1997.

[41] J. D. Hartley and J. M. Duncan. e' and its variation with depth. *Journal of Transportational Engineering*, 113(5):538–553, 1987.

[42] A. K. Howard. Laboratory load tests on buried flexible pipe. *Journal of the AWWA*, 64:655–662, 1972.

[43] A. K. Howard and Salender C. E. Laboratory load tests on buried reinforced thermosetting, thermoplastic, and steel pipe. *Journal of the AWWA*, 66:540–552, 1974.

[44] K. Ishihara. Evaluation of soil properties for use in earthquake response. *Proc. Int. Symp. on Numerical Models in Geomechanics, Zurich*, pages 237–259, 1982.

[45] N. Janbu. Soil compressibility as determined by oedometer and triaxial tests. *Proc. European Conf. on Soil and Foundation Eng.*, 1:19–25, 1963.

[46] L-E. Janson. *Plastic Pipes for Water Supply and Sewage Disposal.* Borealis, Majornas CopyPrint AB, Stockholm, Sweden, 2003.

[47] J. L. Jorgenson. Behaviour of abutment piles in an integral abutment in response to bridge movements. *Transportation Research Record*, 903:72–79, 1983.

[48] V. Kolar and I. Nemec. *Modelling of Soil-Structure Interaction*, volume 58 of *Developments in geotechnical engineering.* New York, Prague: Elsevier, Academia, 1989.

[49] R. L. Konder. Hyperbolic stress-strain response: cohesive soils. *Journal of Soil Mech. and Foundations Div., ASCE*, 89:115, 1963.

[50] R. L. Konder and J. S. Zelasko. A hyperbolic stress-strain formulation of sands. *Proc. of the 2nd Pan American Conference on Soil Mech. and Foundation Eng., Brazil*, 1:289, 1963.

[51] R. J. Krizek and K. J. Neil. Material properties effecting soil-structure interaction of underground conduits. *Highway Research Record*, 413:13–29, 1972.

[52] A. R. Kukreti and A. A. Soltani. Performance evaluation of integral abutment bridges. *Transportation Research Record*, 1371:17–25, 1992.

[53] J. Kunin and S. Alampalli. Integral abutment bridges: Current practice in United States and Canada. *ASCE Journal of Performance of Constructed Facilities*, 14:104–111, 2000.

[54] P. V. Lade, R. B. Nelson, and H. A. Mang. Modelling the elastic behaviour of granular materials. *International Journal for Numerical and Analytical Methods in Geomechanics*, 11:521–542, 1987.

[55] A. Lawver, C. French, and C. K. Shield. Field performance of integral abutment bridge. *Transportation Research Record*, 1740:108–117, 2000.

[56] B. M. Lehane, D. L. Keogh, and E. J. O'Brian. Simplified elastic model for restraining effects of backfill soil on integral bridges. *Computers and Structures*, 73:303–313, 1999.

[57] D. A. Linger. Historical development of the soil-structure interaction. *Highway Research Record*, 413:5–12, 1972.

[58] C. H. Liu, J. Y. Wong, and H. A. Mang. Large strain finite element analysis of sand. *Computers and Structures*, 74(3):253–265, 2000.

[59] U. Luscher. Buckling of soil-surrounded tubes. *Journal of Soil Mechanic and Foundation Engineering Div., ASCE*, pages 211–228, 1966.

[60] Z. Manko and D. Beben. The study of two road bridge structures made of corrugated steel plates structures super-cor type sc-56b and super-cor type sc-54b under static load. Technical report, The Scientific Research Centre for the Development of Bridge Industry "MOSTAR", Wroclow, Poland, December 2001.

[61] Z. Manko and D. Beben. The study of road bridge structure made of corrugated steel plates structures super-cor type sc-56b under static and dynamic load in Gimån (Sweden). Technical report, The Scientific Research Centre for the Development of Bridge Industry "MOSTAR", Wroclow, Poland, October 2002.

[62] T. C. McCavour, P. M. Byrne, and T. D. Morrison. Long-span reinforced steel box culverts. *Transportation Research Record*, 1624:184–195, 1998.

[63] G. G. Meyerhof and L. D. Baikie. Strength of culvert sheets bearing against compacted sand backfill. *Highway Research Record*, 30:1–19, 1963.

[64] J. Molin. Flexible pipes buried in clay. *Proc. Int. Conference of Underground Plastic Pipe. ASCE, New Orleans, USA*, pages 322–337, 1981.

[65] I. D. Moore. Elastic buckling of buried flexible tubes — a review of theory and experiment. *Journal of Geotechnical Engineering*, 115(3):340–358, March 1989.

[66] I. D. Moore and B. Taleb. Metal culvert response to live loading – performance of three dimentional analysis. *Transportation Research Record*, 1656:37–44, 1999.

[67] F. D. Nielson. Design of circular soil-culvert systems. *Highway Research Record*, 413:67–76, 1972.

[68] F. D. Nielson. Experimental studies in soil structure interaction. *Highway Research Record*, 413:30–44, 1972.

[69] P. Panos and Y. Sun. Ottawa sand: Experimental behaviour and theoretical predictions. *Journal of Geotechnical Engineering*, 118:1906–1923, 1992.

[70] R. A. Parmelee and R. B. Corotis. Analytical and experimental evaluation of modulus of soil reaction. *Transportation Research Record*, 518:29–38, 1974.

[71] I. Payne. Aspects of soil structure interaction. *Ground Engineering*, 28(1):29–34, January-February 1995.

[72] L. Pettersson and H. Sundquist. Design of long span metal culverts. TRITA-BKN Rapport 58, Department of Structural Engineering, Royal Institute of Technology, KTH, Stockholm, Sweden, 2002.

[73] H. G. Russel and J. Lee. Jointless bridges: The knowns and the unknowns. *Concrete International*, 16(4):44–48, April 1994.

[74] T. C. Sandford and M. Elgaaly. Skew effects on backfill pressures at frame bridge abutments. *Transportation Research Record*, 1415:1–11, 1993.

[75] R. B. Seed and C.-Y. Ou. Measurements and analysis of compaction effects on a long-span culvert. *Transportation Research Record*, 1087:37–45, 1986.

[76] S. Sharma and Hardcastle J. H. Evaluation of culvert deformations using the finite element method. *Transportation Research Record*, 1415:32–39, 1993.

[77] V. V. Sokolovski. *Statics of Granular Media.* Pergamon Press, London, 1965.

[78] S. M. Springman and A. R. M. Norrish. Soil-structure interaction: Centrifuge modelling of integral bridge abutments. *Proc. of Henderson Colloquium. Towards joint free bridges*, pages 251–263, 20-21 July 1994.

[79] S. M. Springman, A. R. M. Norrish, and C. W. W. Ng. Cycling loading of sand behind integral bridge abutments. Technical Report 146, UK Highways Agency, 1996.

[80] D. J. Steiger. Jointless bridges provide fuel for controversy. *Roads and Bridges*, 31:48–54, 1993.

[81] H. Sundquist. Exempel på dimensionering av rambroar (in Swedish). TRITA-BKN Rapport 19, Department of Structural Engineering, Royal Institute of Technology, Stockholm, Sweden, 1995.

[82] H. Sundquist and G. Racutanu. Swedish experiences of integral bridges. *IABSE Symp. Structures for the Future – Search for Quality*, pages 50–51, Rio de Janeiro 1999.

[83] M. K. Tadros, C. Belina, and D. W. Meyer. Current practice of reinforced concrete box culvert design. *Transportation Research Record*, 1191:65–72, 1988.

[84] M. K. Tadros, J. B. Benak, and M. K. Gilliland. Soil pressure on box culverts. *ACI Structural journal*, 86:436–450, 1989.

[85] B. Taleb and I. D. Moore. Metal culvert response to earth loading – performance of two dimentional analysis. *Transportation Research Record*, 1656:25–36, 1999.

[86] N. Taly. *Design of Modern Highway Bridges.* McGraw-Hill, 1998.

[87] H. Taylor. Integral bridges: The maintenance-free option. *Concrete*, 32(1):18, January 1998.

[88] H. K. Thippeswamy and H. V. S. GangaRao. Analysis of in-service jointless bridges. *Transportation Research Record*, 1476:162–170, 1995.

[89] T. A. JR. Thomson. *Passive Earth Pressures Behind Integral Bridge Abutments.* PhD thesis, University of Massachusetts Amherst, Massachusetts, USA, 1999.

[90] J. M. Ting and S. Faraji. Streamlined analysis and design of integral abutment bridges. Final research report UMTC-97-13, University of Massachusetts Transportation Center, Massachusetts, USA, 1998.

[91] M. J. Tomlinson and R. Boorman. *Foundation Design and Construction.* Pearson Education Limited, Singapore, 1995.

[92] J. Vaslestad. *Soil Structure Interaction of Buried Culverts.* PhD thesis, Norwegian Institute of Technology, Trondheim, Norway, 1990.

[93] E. M. Veje. Danish integral bridges. *Proc. Henderson Colloquium Towards Joint Free Bridges, Cambridge UK*, page 97, 1993.

[94] Vägverket. *Bestämning av jords hållfasthets- ock deformationsegenskaper, Publ 1993:6.* Borlänge, 1993.

[95] Vägverket. *Broprojektering Handbok.* Borlänge, 1996.

[96] R. K. Watkins. Influence of soil characteristics on the deformation of embedded flexible pipe culverts. *Bulletin 223, Highway Research Board, Washington DC*, 223:14–24, 1959.

[97] R. K. Watkins and F. D. Nielsen. Development and use of the modpares device. *ASCE Journal of the Pipeline Division*, 90:155–178, 1964.

[98] M. C. Webb, E. T. Selig, J. A. Sussmann, and T. J. McGrath. Field tests of a large-span metal culvert. *Transportation Research Record*, 1653:14–24, 1999.

[99] H. L. White and Layer J. P. The corrugated metal conduit as a compression ring. *Proc. of Annual Meeting of Highway Research Board*, 39:389–397, 1960.

[100] K. R. White, J. Minor, and K. N. Derucher. *Bridge Maintenance Inspection and Evaluation.* Marcel Dekker Inc., New York, 1992.

[101] A. M Wolde-Tinsae and L. F. Greimann. General design details for integral abutment bridges. *Civil Engineering Practice*, 3(2):7–20, 1988.

[102] K. S. Wong. *Analysis of retaining walls using hyperbolic model*, chapter 17, pages 605–645. In Bull [14], 1994.

[103] K. S. Wong and J. M. Duncan. Hyperbolic stress-strain parameters for nonlinear finite element analyses of stresses and movements in soil masses. Technical Report TE-74-3, University of California, Berkeley, 1974.

[104] P. P. Xanthakos. *Theory and Design of Bridges.* John Wiley and Sons Inc., New York, 1994.

[105] M. Xu, A. G. Bloodworth, and M. K. L. Marcus. Numerical analysis of embedded abutments of integral bridges. *IABSE Symposium, Structures for High-Speed Railway Transportation, Antwerp*, 87:110–111, 2003.

Appendix A

Evaluation of the Secant Modulus - Tangent Modulus Relationship

A.1 Definitions

The definitions of tangent modulus (E_t) and secant modulus (E_s) are given in Section 3.1. They can be formulated from hyperbolic stress strain curves as follows:

$$(E_t) = \frac{\partial(\sigma_1 - \sigma_3)}{\partial\varepsilon} \tag{A.1}$$

$$(E_s) = \frac{\sigma_1 - \sigma_3}{\varepsilon} \tag{A.2}$$

The hyperbolic equation is:

$$(\sigma_1 - \sigma_3) = \frac{\varepsilon}{\frac{1}{E_i} + \frac{\varepsilon}{(\sigma_1 - \sigma_3)_u}} \tag{A.3}$$

A.2 Derivation of the Relation E_t/E_s

If the strain ε is drawn from Equation A.3 and the equation for the failure ratio (Equation 3.6) is inserted, the following equation for the strain is obtained:

$$\varepsilon = \frac{\sigma_1 - \sigma_3}{E_i \cdot [1 - \frac{R_f \cdot (\sigma_1 - \sigma_3)}{(\sigma_1 - \sigma_3)_f}]} \tag{A.4}$$

The strain ε can be eliminated from the secant modulus equation (Equation A.2) by simply inserting the ε expression given by Equation A.4:

$$E_s = E_i \cdot [1 - \frac{R_f \cdot (\sigma_1 - \sigma_3)}{(\sigma_1 - \sigma_3)_f}] \tag{A.5}$$

E_t/E_s can now be calculated using Equation A.5 and Equation 3.9:

$$E_t/E_s = 1 - \frac{R_f \cdot (\sigma_1 - \sigma_3)}{(\sigma_1 - \sigma_3)_f} \tag{A.6}$$

A.3 Further Simplifications

Further simplifications can be done by inserting Equation 3.5 for the term $(\sigma_1 - \sigma_3)_f$ and assuming that $K_0 = 1 - \sin\phi$ and the soil is cohesionless ($c = 0$):

$$E_t/E_s = 1 - \frac{R_f}{2} \tag{A.7}$$

If the failure ratio R_f is assumed to be 0.7, we get:

$$E_t/E_s = 0.65 \tag{A.8}$$

Appendix B

Passive Earth Pressure Response Proposal – Simple Elastic Approach

B.1 Assumptions

- It is assumed that the abutment wall is rigid and does not deform but only rotates and/or laterally translates.
- It is assumed that the E formula and its distribution also represent the lateral deformation characteristics for that soil.
- Knowing the lateral deflection of the wall at every depth interval, the strain level can be estimated.
- For estimating the lateral strains, one needs to know the width of the backfill soil. At this point, an assumption should be made for the width. It is assumed that the backfill material can go through elastic deformation between the abutment wall and the original ground.
- The original ground is assumed to be much stiffer than the backfill material. In this particular problem, it forms a rigid boundary.
- The shear between the layers is not taken into account.

B.2 Equations Used

The calculations are done using the following elastic relations:

$$\varepsilon_h = \frac{\delta_h}{T_h} \tag{B.1}$$

$$\sigma_h = E_t \cdot \varepsilon_h \tag{B.2}$$

where:

E_t = the tangent modulus of elasticity
ε_h = the horizontal strain
σ_h = the horizontal stress
δ_h = the horizontal displacement of the abutment wall
T_h = the width of the soil layer

The equation for the tangent modulus of elasticity is given next. This depth-dependent modulus formula is also given in Section 3.2.5 as Equation 3.19:

$$E_t = 0.42 \cdot m \cdot K_\nu \cdot 100\text{kPa} \cdot \left(\frac{(1 - \sin\phi) \cdot \gamma_\text{s} \cdot \text{S}_\text{ar} \cdot (\text{h}_\text{c} + \text{H}/2)}{100\text{kPa}} \right)^{1-\beta} \tag{B.3}$$

where:

E_t = the tangent modulus (MPa)
ϕ = the internal friction angle
h_c = the depth of cover over the crown (m)
S_{ar} = the arching coefficient
ρ = the unit weight of soil
β = the stress exponent
K_ν = $(1 - \nu - 2 \cdot \nu^2)/(1 - \nu)$
m = the modulus number

In equation B.3, the value H, which corresponds to the rise of the culvert, is taken as 0, while S_{ar} is taken as 1.

B.3 Calculation Steps

1. Once the wall height H_a and the top deflection δ_{max} of the wall are decided, the horizontal deflection of the wall δ_h (due to the rotation about the bottom) at various depths z can be calculated with the help of the following equation:

$$\delta_h = \delta_{max} - \frac{z \cdot \delta_{max}}{H_a} \tag{B.4}$$

2. The strain levels at various depths can now be calculated using Equation B.1. A width T_h for the soil layer has to be chosen first.

3. The elastic modulus for each layer can be obtained according to Equation B.3.

4. Finally, the lateral stress for each layer can be obtained using Equation B.2:

Table B.1: Parameters used in the numerical example

Material properties	values
ϕ (° C)	38.3
γ_s (kN/m^3)	19.0
K_0	0.38
RP	100
C_u	5.0
d_{50} (mm)	1.0
Horizontal displacement δ_h (m)	0.04
Wall height H_a (m)	6.0
Width of soil layer T_h (m)	3.0, 5.0, 10, 20
m	1378
k_ν	0.79
ν	0.28
β	0.53
S_{ar}	1.0

$$\sigma_h = E_t(z) \cdot \frac{\delta_{max} \cdot (H_a - z)}{H_a \cdot T_h} \tag{B.5}$$

B.4 Numerical Example

The values of the soil properties and the other parameters are the same as the values used in the previous comparisons of earth pressure. Table B.1 summarizes these parameters.

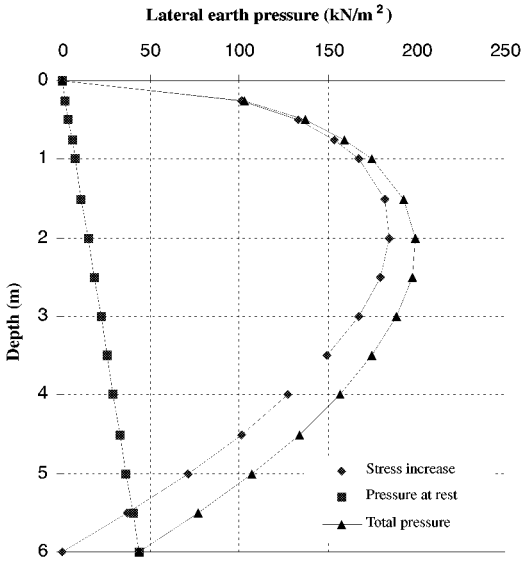

Figure B.1: Calculation of the earth pressure distribution behind the abutment due to wall rotation, for a 3 m wide earth fill

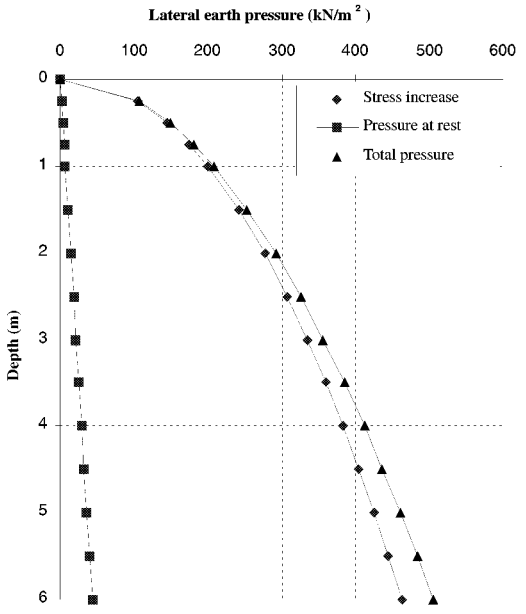

Figure B.2: Calculation of the earth pressure distribution behind the abutment due to wall translation, for a 3 m wide earth fill

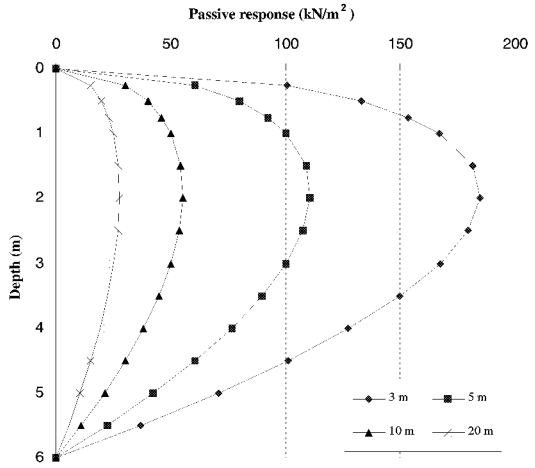

Figure B.3: Lateral earth pressure response to rotation of the wall; each curve is for a different backfill width

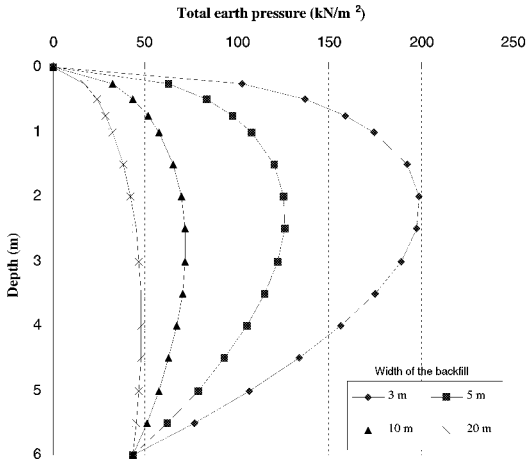

Figure B.4: Total lateral earth pressure distributions due to rotation of the wall

List of Bulletins from the Department of Structural Engineering, The Royal Institute of Technology, Stockholm

TRITA-BKN. Bulletin

Pacoste, C., On the Application of Catastrophe Theory to Stability Analyses of Elastic Structures. Doctoral Thesis, 1993. Bulletin 1.

Stenmark, A-K., Dämpning av 13 m lång stålbalk "Ullevibalken". Utprovning av dämpmassor och fastsättning av motbalk samt experimentell bestämning av modformer och förlustfaktorer. Vibration tests of full-scale steel girder to determine optimum passive control. Licentiatavhandling, 1993. Bulletin 2.

Silfwerbrand, Johan, Renovering av asfaltgolv med cementbundna plastmodifierade avjämningsmassor, 1993. Bulletin 3.

Norlin, B., Two-Layered Composite Beams with Nonlinear Connectors and Geometry Tests and Theory. Doctoral Thesis, 1993. Bulletin 4.

Habtezion, T., On the Behaviour of Equilibrium Near Critical States. Licentiate Thesis, 1993. Bulletin 5.

Krus, J., Hållfasthet hos frostnedbruten betong. Licentiatavhandling, 1993. Bulletin 6.

Wiberg, U., Material Characterization and Defect Detection by Quantitative Ultrasonics. Doctoral Thesis, 1993. Bulletin 7.

Lidström, T., Finite Element Modelling Supported by Object Oriented Methods. Licentiate Thesis, 1993. Bulletin 8.

Hallgren, M., Flexural and Shear Capacity of Reinforced High Strength Concrete Beams without Stirrups. Licentiate Thesis, 1994. Bulletin 9.

Krus, J., Betongbalkars lastkapacitet efter miljöbelastning. 1994. Bulletin 10.

Sandahl, P., Analysis Sensitivity for Wind-related Fatigue in Lattice Structures. Licentiate Thesis, 1994. Bulletin 11.

Sanne, L., Information Transfer Analysis and Modelling of the Structural Steel Construction Process. Licentiate Thesis, 1994. Bulletin 12.

Zhitao, H., Influence of Web Buckling on Fatigue Life of Thin-Walled Columns. Doctoral Thesis, 1994. Bulletin 13.

Kjörling, M., Dynamic response of railway track components. Measurements during train passage and dynamic laboratory loading. Licentiate Thesis, 1995. Bulletin 14.

Yang, L., On Analysis Methods for Reinforced Concrete Structures. Doctoral Thesis, 1995. Bulletin 15.

Petersson, Ö., Svensk metod för dimensionering av betongvägar. Licentiatavhandling, 1996. Bulletin 16.

Lidström, T., Computational Methods for Finite Element Instability Analyses. Doctoral Thesis, 1996. Bulletin 17.

Krus, J., Environment- and Function-induced Degradation of Concrete Structures. Doctoral Thesis, 1996. Bulletin 18.

Editor, Silfwerbrand, J., Structural Loadings in the 21st Century. Sven Sahlin Workshop, June 1996. Proceedings. Bulletin 19.

Ansell, A., Frequency Dependent Matrices for Dynamic Analysis of Frame Type Structures. Licentiate Thesis, 1996. Bulletin 20.

Troive, S., Optimering av åtgärder för ökad livslängd hos infrastrukturkonstruktioner. Licentiatavhandling, 1996. Bulletin 21.

Karoumi, R., Dynamic Response of Cable-Stayed Bridges Subjected to Moving Vehicles. Licentiate Thesis, 1996. Bulletin 22.

Hallgren, M., Punching Shear Capacity of Reinforced High Strength Concrete Slabs. Doctoral Thesis, 1996. Bulletin 23.

Hellgren, M., Strength of Bolt-Channel and Screw-Groove Joints in Aluminium Extrusions. Licentiate Thesis, 1996. Bulletin 24.

Yagi, T., Wind-induced Instabilities of Structures. Doctoral Thesis, 1997. Bulletin 25.

Eriksson, A., and Sandberg, G., (editors), Engineering Structures and Extreme Events proceedings from a symposium, May 1997. Bulletin 26.

Paulsson, J., Effects of Repairs on the Remaining Life of Concrete Bridge Decks. Licentiate Thesis, 1997. Bulletin 27.

Olsson, A., Object-oriented finite element algorithms. Licentiate Thesis, 1997. Bulletin 28.

Yunhua, L., On Shear Locking in Finite Elements. Licentiate Thesis, 1997. Bulletin 29.

Ekman, M., Sprickor i betongkonstruktioner och dess inverkan på beständigheten. Licentiate Thesis, 1997. Bulletin 30.

Karawajczyk, E., Finite Element Approach to the Mechanics of Track-Deck Systems. Licentiate Thesis, 1997. Bulletin 31.

Fransson, H., Rotation Capacity of Reinforced High Strength Concrete Beams. Licentiate Thesis, 1997. Bulletin 32.

Edlund, S., Arbitrary Thin-Walled Cross Sections. Theory and Computer Implementation. Licentiate Thesis, 1997. Bulletin 33.

Forsell, K., Dynamic analyses of static instability phenomena. Licentiate Thesis, 1997. Bulletin 34.

Ikäheimonen, J., Construction Loads on Shores and Stability of Horizontal Formworks. Doctoral Thesis, 1997. Bulletin 35.

Racutanu, G., Konstbyggnaders reella livslängd. Licentiatavhandling, 1997. Bulletin 36.

Appelqvist, I., Sammanbyggnad. Datastrukturer och utveckling av ett IT-stöd för byggprocessen. Licentiatavhandling, 1997. Bulletin 37.

Alavizadeh-Farhang, A., Plain and Steel Fibre Reinforced Concrete Beams Subjected to Combined Mechanical and Thermal Loading. Licentiate Thesis, 1998. Bulletin 38.

Eriksson, A. and Pacoste, C., (editors), Proceedings of the NSCM-11: Nordic Seminar on Computational Mechanics, October 1998. Bulletin 39.

Luo, Y., On some Finite Element Formulations in Structural Mechanics. Doctoral Thesis, 1998. Bulletin 40.

Troive, S., Structural LCC Design of Concrete Bridges. Doctoral Thesis, 1998. Bulletin 41.

Tärno, I., Effects of Contour Ellipticity upon Structural Behaviour of Hyparform Suspended Roofs. Licentiate Thesis, 1998. Bulletin 42.

Hassanzadeh, G., Betongplattor på pelare. Förstärkningsmetoder och dimensioneringsmetoder för plattor med icke vidhäftande spännarmering. Licentiatavhandling, 1998. Bulletin 43.

Karoumi, R., Response of Cable-Stayed and Suspension Bridges to Moving Vehicles. Analysis methods and practical modeling techniques. Doctoral Thesis, 1998. Bulletin 44.

Johnson, R., Progression of the Dynamic Properties of Large Suspension Bridges during Construction A Case Study of the Höga Kusten Bridge. Licentiate Thesis, 1999. Bulletin 45.

Tibert, G., Numerical Analyses of Cable Roof Structures. Licentiate Thesis, 1999. Bulletin 46.

Ahlenius, E., Explosionslaster och infrastrukturkonstruktioner - Risker, värderingar och kostnader. Licentiatavhandling, 1999. Bulletin 47.

Battini, J-M., Plastic instability of plane frames using a co-rotational approach. Licentiate Thesis, 1999. Bulletin 48.

Ay, L., Using Steel Fiber Reinforced High Performance Concrete in the Industrialization of Bridge Structures. Licentiate Thesis, 1999. Bulletin 49.

Paulsson-Tralla, J., Service Life of Repaired Concrete Bridge Decks. Doctoral The-

sis, 1999. Bulletin 50.

Billberg, P., Some rheology aspects on fine mortar part of concrete. Licentiate Thesis, 1999. Bulletin 51.

Ansell, A., Dynamically Loaded Rock Reinforcement. Doctoral Thesis, 1999. Bulletin 52.

Forsell, K., Instability analyses of structures under dynamic loads. Doctoral Thesis, 2000. Bulletin 53.

Edlund, S., Buckling of T-Section Beam-Columns in Aluminium with or without Transverse Welds. Doctoral Thesis, 2000. Bulletin 54.

Löfsjögård, M., Functional Properties of Concrete Roads - General Interrelationships and Studies on Pavement Brightness and Sawcutting Times for Joints. Licentiate Thesis, 2000. Bulletin 55.

Nilsson, U., Load bearing capacity of steel fibree reinforced shotcrete linings. Licentiate Thesis, 2000. Bulletin 56.

Silfwerbrand, J. and Hassanzadeh, G., (editors), International Workshop on Punching Shear Capacity of RC Slabs - Proceedings. Dedicated to Professor Sven Kinnunen. Stockholm June 7-9, 2000. Bulletin 57.

Wiberg, A., Strengthening and repair of structural concrete with advanced, cementitious composites. Licentiate Thesis, 2000. Bulletin 58.

Racutanu, G., The Real Service Life of Swedish Road Bridges - A case study. Doctoral Thesis, 2000. Bulletin 59.

Alavizadeh-Farhang, A., Concrete Structures Subjected to Combined Mechanical and Thermal Loading. Doctoral Thesis, 2000. Bulletin 60.

Wäppling, M., Behaviour of Concrete Block Pavements - Field Tests and Surveys. Licentiate Thesis, 2000. Bulletin 61.

Getachew, A., Trafiklaster på broar. Analys av insamlade och Monte Carlo genererade fordonsdata. Licentiatavhandling, 2000. Bulletin 62.

James, G., Raising Allowable Axle Loads on Railway Bridges using Simulation and Field Data. Licentiate Thesis, 2001. Bulletin 63.

Karawajczyk, E., Finite Elements Simulations of Integral Bridge Behaviour. Doctoral Thesis, 2001. Bulletin 64.

Thöyrä, T., Strength of Slotted Steel Studs. Licentiate Thesis, 2001. Bulletin 65.

Tranvik, P., Dynamic Behaviour under Wind Loading of a 90 m Steel Chimney. Licentiate Thesis, 2001. Bulletin 66.

Ullman, R., Buckling of Aluminium Girders with Corrugated Webs. Licentiate Thesis, 2002. Bulletin 67.

Getachew, A., Traffic Load Effects on Bridges. Statistical Analysis of Collected and Monte Carlo Simulated Vehicle Data. Doctoral Thesis, 2003. Bulletin 68.

Quilligan, M., Bridge Weigh-in-Motion. Development of a 2-D Multi-Vehicle Algorithm. Licentiate Thesis, 2003. Bulletin 69.

James, G., Analysis of Traffic Load Effects on Railway Bridges. Doctoral Thesis 2003. Bulletin 70.

Nilsson, U., Structural behaviour of fibre reinforced sprayed concrete anchored in rock. Doctoral Thesis 2003. Bulletin 71.

Wiberg, A., Strengthening of Concrete Beams Using Cementitious Carbon Fibre Composites. Doctoral Thesis 2003. Bulletin 72.

Löfsjögård, M., Functional Properties of Concrete Roads - Development of an Optimisation Model and Studies on Road Lighting Design and Joint Performance. Doctoral Thesis 2003. Bulletin 73.

The bulletins enumerated above, with the exception for those which are out of print, may be purchased from the Department of Structural Engineering, The Royal Institute of Technology, SE-100 44 Stockholm, Sweden.

The department also publishes other series. For full information see our homepage http://www.byv.kth.se

Tryck: Universitetsservice US AB
Stockholm 2004
www.us-ab.com